University of Alberta

Ultrasonic wave dispersion and attenuation in cancellous bone

by

Yifu Qiu ©

A thesis submitted to the Faculty of Graduate Studies and Research in partial fulfillment of the requirements for the degree of **Master of Science**

Department of Physics

Edmonton, Alberta

Spring 2006

Library and Archives Canada

Published Heritage Branch

395 Wellington Street
Ottawa ON K1A 0N4
Canada

Bibliothèque et Archives Canada

Direction du Patrimoine de l'édition

395, rue Wellington
Ottawa ON K1A 0N4
Canada

Your file Votre référence
ISBN: 0-494-13877-7
Our file Notre référence
ISBN: 0-494-13877-7

NOTICE:
The author has granted a non-exclusive license allowing Library and Archives Canada to reproduce, publish, archive, preserve, conserve, communicate to the public by telecommunication or on the Internet, loan, distribute and sell theses worldwide, for commercial or non-commercial purposes, in microform, paper, electronic and/or any other formats.

The author retains copyright ownership and moral rights in this thesis. Neither the thesis nor substantial extracts from it may be printed or otherwise reproduced without the author's permission.

AVIS:
L'auteur a accordé une licence non exclusive permettant à la Bibliothèque et Archives Canada de reproduire, publier, archiver, sauvegarder, conserver, transmettre au public par télécommunication ou par l'Internet, prêter, distribuer et vendre des thèses partout dans le monde, à des fins commerciales ou autres, sur support microforme, papier, électronique et/ou autres formats.

L'auteur conserve la propriété du droit d'auteur et des droits moraux qui protège cette thèse. Ni la thèse ni des extraits substantiels de celle-ci ne doivent être imprimés ou autrement reproduits sans son autorisation.

In compliance with the Canadian Privacy Act some supporting forms may have been removed from this thesis.

While these forms may be included in the document page count, their removal does not represent any loss of content from the thesis.

Conformément à la loi canadienne sur la protection de la vie privée, quelques formulaires secondaires ont été enlevés de cette thèse.

Bien que ces formulaires aient inclus dans la pagination, il n'y aura aucun contenu manquant.

Canada

University of Alberta

Library Release Form

Name of Author: Yifu Qiu

Title of Thesis: Ultrasonic wave dispersion and attenuation in cancellous bone

Degree: Master of Science

Year this Degree: 2006

Permission is hereby granted to the University of Alberta Library to reproduce single copies of this thesis and to lend or sell such copies for private, scholarly or science research purposes only.

The author reserves all other publication and other rights in association with the copyright in the thesis, and except as herein before provided, neither the thesis nor any substantial portion thereof may be printed or otherwise reproduced in any material form whatsoever without the author's prior written permission.

_____

Signature

Abstract

Speed of Sound and Broadband Ultrasound Attenuation are two discriminating parameters for good and oesteoporotic bones. A cross-correlation based method is used to calculate phase velocity and attenuation. The method applies a window in correlation lag instead of in time domain and is more robust than the Fourier-based method. Transmission decay is also derived and corrected using the reflection signal upon bone-water interface.

Bone samples are cut into four thicknesses and measured. Bone groups of the thinnest thickness for both bovine and pig bone are more likely to show negative dispersion. BUA in the bovine transverse direction is obviously higher than that in axial direction. However, the linear dependence of BUA on thickness is not obvious. Transmission losses in bovine bones obtained using echo signal is comparable with those obtained using acoustic impedance.

Acknowledgement

I would like to thank my supervisors Dr. Lawrence Le and Dr. Mauricio Sacchi for the supervision and thesis revision. I would also like to express my gratitude to my supervisor Dr. Mauricio Sacchi for his suggestions on my future.

Thanks to the members of my examining committee for their valuable suggestions and for agreeing to read my thesis. Thank Rui Zheng for taking some pictures for my thesis.

Thank Department of Physics and Capital Health for financial support. I extend my thanks to the staff of the Physics Department, especially Dr. Doug Schmitt, Dr. Jeff Gu, Sarah Derr, Dr. Richard Marchand for their help. I also want to thank Mary Lou for correcting my pronunciation and office work.

Finally, special thanks to my family for their encouragement during my study at the University of Alberta

TABLE OF CONTENTS

CHAPTER 1 INTRODUCTION 1

1.1 BONE AND OSTEOPOROSIS 1

1.2 CURRENT TECHNIQUES FOR BONE RESEARCH 5

1.2.1 X-Ray Techniques 5

1.2.2 MRI Techniques 7

1.2.3 Quantitative Ultrasound Techniques 7

1.3 ULTRASOUND TECHNIQUES IN BONE RESEARCH 8

1.4 OBJECTIVE AND ORGANIZATION OF THE THESIS 11

CHAPTER 2 IN VITRO ULTRASONIC MEASUREMENT OF BONE SAMPLES 12

2.1 EXPERIMENTAL SETUP 12

2.2 BONE SAMPLE PREPARATION 14

2.3 DISCUSSION OF EXPERIMENT DATA 16

2.3.1 Data for Experiment 1 17

2.3.2 Data for experiment 2 27

CHAPTER 3 ESTIMATION OF DISPERSION CURVES USING CROSS-CORRELATION METHOD 31

3.1 INTRODUCTION 31

3.2 METHODS OF VELOCITY MEASUREMENT 31

3.2.1 Time-Domain Methods 31

3.2.2 The Phase Spectral Analysis Method 34

3.3 CROSS-CORRELATION TECHNIQUE FOR THE ESTIMATION OF PHASE VELOCITY 40

3.4 DISCUSSION OF RESULTS 50

CHAPTER 4 ESTIMATION OF BROADBAND ULTRASOUND ATTENUATION (BUA) 57

4.1 INTRODUCTION 57

4.2 POWER SPECTRUM ESTIMATION TECHNIQUE 58

4.2.1 Periodogram Technique....58
4.2.2 Indirect Estimation from Autocorrelation Function....59
4.2.3 Sinusoidal data fitting....59
4.3 REFLECTION POWER LOSS AND ATTENUATION....60
4.4 DISCUSSION OF RESULTS....64

CHAPTER 5 CONCLUSION AND FUTURE WORK....86

REFERENCE 88

APPENDIX A CROSS CORRELATION FUNCTION AND CROSS SPECTRUM 95

APPENDIX B ZERO PADDING AND FREQUENCY RESOLUTION.... 98

APPENDIX C MEASUREMENT OF SPEED OF SOUND IN WATER....99

APPENDIX D PHASE CORRECTION OF UNWRAPPED PHASE DIFFERENCE....101

TABLE OF FIGURES

Figure 1.1 Microstructure of cortical bone 4

Figure 1.2 A typical experimental setup to measure bone in-vitro 10

Figure 2.1 Experimental Setup 12

Figure 2.2 Experimental Setup (transducers mounted on water tank) 13

Figure 2.3 Illustration of bone orientation 14

Figure 2.4 Typical bone samples of four different sizes 15

Figure 2.5 Measurement area of bone sample 16

Figure 2.6 Water pulse (A) and its spectrum (B) 17

Figure 2.7 Signal of bovine trabecular bones of different thickness in transverse direction (Un-normalized) 20

Figure 2.8 Signal of bovine trabecular bone in transverse direction (Normalized by itself) 21

Figure 2.9 Signal of bovine trabecular bone in axial direction (Un-normalized) 22

Figure 2.10 Signal of bovine trabecular bone in axial direction (Normalized by itself) 23

Figure2.11 Signal of pig trabecular bone (Un-normalized) 24

Figure2.12 Signal of pig trabecular bone (Normalized by itself) 25

Figure 2.13 (A) water reference signal and echo signals from three typical bone samples 26

Figure 2.14 Experimental Setup for phantom in big water tank 27

Figure 2.15 Phantoms and two kinds of material 28

Figure 2.16 Structures of four phantoms 29

Figure 2.17 Ultrasound signals through four phantoms 30

Figure 3.1 The time responses of (A) a water pulse and (B) a pulse through a bone-mimic phantom 36

Figure 3.2 The magnitude spectra of the water pulse (A) and the phantom signal truncated at 538 data points 37

Figure 3.3 Windowing the signal pulse of Figure 3.1 (B). Numbers indicate the box window length starting from the origin, sampling interval is 0.025 38

Figure 3.4 Dispersion curves of the windowed pulse displayed in Figure 3.3 39

Figure 3.5 The cross-correlation between two signals given in Figure 3.2 42

Figure 3.8 The phase velocity of a pulse through a bone-mimic phantom in Figure 3.1(B) with same fixed length 400 data points but different tapering ratio 45

Figure 3.9 The phase velocity of a pulse through a bone-mimic phantom in Figure 3.1(B) with fixed tapering ratio r = 0.6 but of different length 46

Figure 3.10 A bone sample signal and water pulse 48

Figure 3.11 Effect of window length and window shape on dispersion 49

Figure 3.12 Phase velocity of bovine trabecular bone of d 51

Figure 3.13 Phase velocity of bovine tr 52

Figure 3.14 Phase veloc 53

Figure 3.15 Phase velocity of corresponding phantoms in figure 2.17 55

Figure 3.16 Magnitude Spectra of corresponding phantoms in figure 2.17 56

Figure 4.1 The power spectra of bovine bone signals of different thi 66

Figure 4.2 The BUA of bovine bone sample signals of different thickness in transverse 67

Figure 4.3 The BUA of bovine b 68

Figure 4.4 The transmission loss of one bovine bone sample 70

Figure 4.5 The power spectrum of pig bone signals of different thickness in mixed directions 72

Figure 4.6 The BUA of pig bone sample signals of different thickness in mixed directions 73

Figure 4.7 The BUA of pig bone sample signals of different thickness in mixed directions (transmission loss corrected) 75

Figure 4.8 The transmission loss of one pig bone sample 76

Figure 4.9 The power spectrum of bovine bone signals of different thickne 78

Figure 4.10 The BUA of bovine bone sample signals of different thickness in axial direction 79

Figure 4.11 The BUA of bovine bone sample signals of different thickness` in axial direction (transmission loss corrected) 82

Figure 4.12 The transmission loss of one bovine bone sample in axial direction 83

Figure 4.13 The BUA of phantom signal without transmission loss correction 85

Chapter 1

Introduction

1.1 Bone and Osteoporosis

Major part of the skeleton is bone, which provides structural support for muscles, protects vital organs, and makes movement possible. Although bone is strong and hard, it is dynamic and constantly changing tissue. The mineral content should be balanced by resorption and rebuilding procedure. Otherwise disease such as osteoporosis will occur.

The shape and function of bone varies from sites to sites, but bone from different sites share some similarity. All bone is built by the matrix of collagen fibers and mineral crystals, and contains four types of cells: osteoprogenitor cells, osteoblasts, osteocytes, and osteoclasts. Osteoprogenitor cells are unspecialized cells and can develop into osteoblasts (Tortora et al, 1993). Osteoblasts are bone-forming cells and can secrete collagen and other organic components needed to build bone. Usually they are found on the surfaces of bone. When they are surrounded with matrix materials, they become osteocytes and lost the forming ability. Osteocytes are the principal cells of bone tissue, and maintain daily cellular activities of bone tissue. Osteoclasts settle on the surfaces of bone and function in bone resorption (Tortora et al, 1993).

There are many small spaces between hard components of bone. Depending on the size and distribution of the spaces, the region of a bone can be categorized as compact or spongy (Tortora et al, 1993). Compact bone tissue (also called cortical bone) contains few spaces and forms the external layer of all bones. Spongy bone (also called trabecular bone) is the interior of bone and consists of a three dimensional lattice of branching spicules or

plates. The space between the bone mineral is bigger in spongy bone than that in compact bones, shown in figure 1.1. The thickness of trabeculae varies from 0.03 mm to 0.21 mm and the separation ranges from 0.21 mm to 1.17 mm, as reported by Müller et al. (1997).

There is a Haversian system called osteon inside the compact bone, providing the routes for nutrients and oxygen to reach the osteocytes and wastes to diffuse away. However, in spongy bone tissue, there is no osteon. The spaces between trabeculae are filled with marrow and blood vessels, from which osteocytes not deeply buried in trabeculae have access to nutriments directly (Tortora et al, 1993). Woven bone is another kind of bone, which only occurs if bone has to be formed rapidly, such as fracture healing, bone tumors, and tumor-like lesions (Hahn et al, 1997).

During the life of bone, all changes in bone tissue are based on four cell mechanisms: modeling, remodeling (Khan et al, 2001) perforation (Tortora et al, 1993; Hahn et al, 1997) and microcallus formations (Hahn et al, 1997). Both the formation of new bone tissue without prior resorption and resorption without subsequent bone formation are termed modeling; Remodeling includes the resorption followed by bone formation. The difference between modeling and remodeling is that, in the growing skeleton, modeling is dominant while in the non-growing skeleton, remodeling is dominant. Perforation refers to the complete separation of rod-like trabeculae or the perforation of plate-like structures of cancellous bone; Microcallus formations consist of immature woven bone and are formed at locally stressed sites in the bone tissue. Although it is an indication of the relative instability of trabecular bone, the establishment of microcallus formation is by no means a negative process. It is a physiological repair

mechanism of the bone tissue to stabilize and renew old and brittle bone (Hahn et. al, 1997).

The most common disease of bone is osteoporosis, defined as a systemic skeletal disease characterized by low bone mass and micro-architectural deterioration of bone tissue, with a consequent increase in bone fragility and susceptibility to fracture (Christiansen, 1993). Osteoporosis is often known as "the silent thief" because bone loss occurs without symptoms. Osteoporosis has long been viewed as a disturbance of the bone metabolism due to osteoblast insufficiency, which leads to a negative bone balance in the normally functioning relationship between formation and decomposition. However, Parfitt et al. (1983) thought the perforation of supporting structure rather than the decrease of trabeculae width causes the problem.

Osteoporosis has obvious physical and functional consequences such as kyphosis, restricted range of motion, and pain. What are not so obvious are the psychosocial sufferings that result from this metabolic bone disease. Many patients in the initial phases of the disease express substantial anxiety, especially about the possibility of future fractures and physical deformity. In sum, osteoporosis and related fractures are devastating psychologically, socially, and economically (Gold, 1996 and Khan et. al, 2001). Ray et al. (1997) proved with data that osteoporosis was an important public health problem that contributes to a significant proportion of fractures and associated health expenditures in USA. Health care expenditures attributable to osteoporotic fractures in 1995 were estimated at US $13.8 billion, of which US $10.3 billion (75.1%) was for the treatment of white women, US $2.5 billion (18.4%) for white men, US $0.7 billion (5.3%) for nonwhite women, and US $0.2 billion (1.3%) for nonwhite men. The results of their

study suggest that, once a fracture occurs, substantial health care expenditures be incurred. In Canada, the prevalence osteoporosis in women over 50 years was 12.1% at the lumbar spine and 7.9% at the femoral neck in 2000, while that in men over 50 years was 2.9% at the lumbar and 4.8% at the femoral neck (Tenenhouse et al, 2000). Therefore, evaluation of screening programs and interventions used to prevent osteoporotic fractures are warranted.

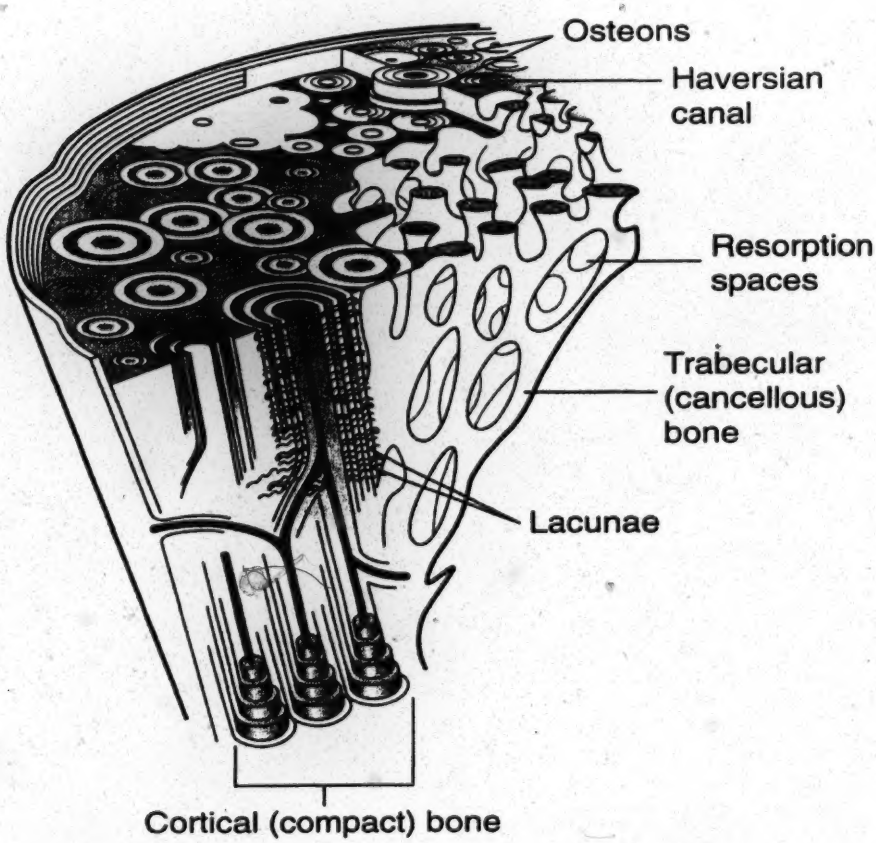

Figure 1.1 Microstructure of cortical bone (Khan et al, 2001).

1.2 Current techniques in bone research

Current techniques in bone research can be classified into three major categories: X-ray techniques, MRI techniques and ultrasound techniques, according to their principle, advantage, disadvantage and application.

1.2.1 X-Ray Techniques

The techniques adopt X-ray emitting device and take advantage of the x-ray absorption property of different material. The results usually are 2D or 3D imaging of the bone, through which information such as density or architecture parameters are further analyzed. The drawbacks of those techniques are the radiation effect, the unavailability of the expensive setup and high request for operator (Sievänen et. al, 1996). These techniques can be subcategorized into following classes:

Dual-Energy X-Ray Absorptiometry (DEXA/DXA)

Most quantitative diagnostic methods for bone mechanical integrity used nowadays are based on estimates of bone density measured by this 2D technique. The average Bone Mineral Density (BMD) value was determined for a rectangular region of interest. This is the only material property that can now be clinically measured non-invasively. Although bone mass correlates significantly with fracture risk, its predictive value is poor, and cannot be used as a reliable diagnostic tool by itself for the prediction of osteoporotic fractures (van Rietbergen et al, 2002).

DEXA measurement is conducted under the simple assumption that the geometry and structure of the bone is simple, therefore, the accuracy is compromised. Improvement can be made by combination of using tomographic 3D data on geometry and using 2D

DEXA on mass distribution of a bone at properly selected sites data on the entire bone (Sievänen, 1996).

Quantitative Computed Tomography (QCT)

The fundamental strength of quantitative computed tomography is its ability to three dimensionally measure BMD and geometry at any skeletal site. Lang et al. (1997) described a novel application for three dimensionally measuring the integral and trabecular bone mineral density in anatomically fixed subregions in the femoral neck and trochanter in their article. The results showed that the BMD measures are highly correlated with bone strength in vitro and the trabecular BMD measurements in vivo are highly reproducible, indicating that the method is suitable for longitudinal evaluation of the progression of metabolic bone disease (Lang et al.1997).

Micro-Computed Tomography (μCT)

This technique is similar to QCT, but with higher spatial resolution. Higher resolution can be achieved by two ways. One is through improved acquisition setup combined with a cone-beam reconstruction algorithm, as was pioneered by Feldkamp et al (1989). The resolution of this method was 50 μm, while another method μCT using synchrotron radiation can get a spatial resolution of 1 μm to 2 μm (Godzins, 1983; Müller et al, 1997; Salomé et al, 1999). The findings of Stenstroöm et al. (2000) indicated that in cancellous bone, bone strength is influenced not only by the trabecular structure but also by the cortical bone surrounding this structure. Micro-CT gives basic information of both cortical and cancellous structures, and may be useful to predict the risk of fracture (Stenstroöm et al, 2000).

1.2.2 MRI Techniques

MRI technique obtains a 2D or 3D image of the bone architecture, and similar analysis can be done as mentioned above. The principle of those techniques based on the different content of ^{1}H in marrow and trabecular bone, which lead to high image intensity for marrow and low image intensity for bone in MR images (Majumdar and Genant, 1997; Toffanina et al, 2001). There are drawbacks. They are not suitable when some metallic implants exist in the object body. Also they are expensive and hard to weigh several parameters in acquisition to obtain optimum results (Majumdar et al., 1995; Majumdar and Genant, 1997; Majumdar et al., 1998).

Based on the 3D image from μCT or MRI, imaging processing techniques can be used to quantify trabecular thickness, trabecular separation, bone volume density etc... (Hildebrand et al, 1996; Müller et al, 1997; Kothari et al, 1999). Other processing techniques are developed to quantify the orientation of trabeculae (Kinney et al, 2005) and to investigate the relationship between mechanical property and bone architecture (Uchiyama et al, 1999; Follet et al, 2005). Usually the elastic modulus in the craniocaudal direction was significantly higher than in the other two directions: mediolateral and anteroposterior (Uchiyama et al, 1999)

1.2.3 Quantitative Ultrasound Techniques (QUS)

Transducer is used to transmit and receive a broadband ultrasound signal, with the outcome measurement including ultrasound speed and broadband ultrasound attenuation (BUA). QUS techniques have the potential to obtain the information of bone micro-architecture. Furthermore, they are cheap and available for field test. Most importantly, they are free of radiation. The application of QUS techniques, however, is

limited by the fact that a number of inconsistencies in measurement exist and exactly what ultrasound measures remains a puzzle (Khan et al, 2001). In other words, the physical meaning of the measurement is not clear. More details and recent progress will be discussed in a separated section.

1.3 Ultrasound techniques in bone research

Ultrasound techniques have been adopted in the characterization of bone tissue for about half a century. The first application can be traced back to 1949 and was conducted by Tesismann and Pfander (Ji, 1998). They measured ultrasonic attenuation and propagation speed in the skull. While the application of ultrasonic techniques in clinical diagnosis of osteoporosis was not conducted until 1984, Langton (1984) proposed BUA as an indicator of bone quality. Since then, there has been an increasing trend of ultrasound study.

Compared with other techniques, ultrasound technique has many advantages. Usually, a broadband ultrasound pulse is generated by a transducer and travels through the bone, then the signal is received by a receiver transducer (transmission mode, as shown in Figure 1.2) or is reflected and received by the same transceiver (reflection mode). Through the interaction with bone structure, the pulse carries information of the bone density and microstructure. The advantage can be summarized as following: (1) Ultrasound is a mechanical disturbance of supra-audible frequency, therefore it involves no ionizing radiation; (2) Ultrasound field through bone tissue is affected by the acoustic properties such as bone density, architecture, so it has the potential to obtain more information of bone; (3) The ultrasound equipment is easy to operate and comfortable for the patient; (4) The cost is low.

Ultrasound technique, however, has its disadvantages: (1) The mechanisms of ultrasound propagation and interaction with bone structure are poorly understood (Tavakoli and Evans, 1992). (2) The measured quantities are not very consistent with the bone parameters, which limit the clinical application of this technique (Ji, 1998; Khan et al. 2001). (3) The interpretation of some ultrasound quantities remain uncertain (Langton, 1984). (4) The reproducibility varies in different system and usually is poor. Nicholson et al. showed that the standard deviation of repeated SOS (Speed of Sound) measurement was 28 m/s corresponding to a CV (Coefficient of Variation) of 1.6% and that of BUA was 0.16dB/MHz/cm corresponding to a CV of 1.2% (1994).

To overcome the above disadvantages, ultrasonic studies of cancellous bone have been focused on two major directions: (1) Comparison between ultrasound qualities and bone parameters obtained by other techniques. Nicholson et al. (1994) investigated the dependence of ultrasonic properties on orientation in human vertebral bone and found strong linear correlation existed between SOS and apparent density, as well as between BUA and apparent density in AP and LT direction, while in CC direction, the correlation was poor. Hans et al. (1999) found that the SOS was explained mostly by density and to a small extent by elasticity, micro-architecture, and measurement orientation. Nicholson et al. (2002) firstly demonstrated that bone marrow profoundly affected the acoustic properties of cancellous bone from the human heel using BUA and backscatter measurement. (2) Phantom or model studies aim to simulate and understand the relationship between ultrasound qualities and controllable bone parameters (Clark et al. 1994; Hughes et al. 1999; Wear 2001).

The final goal of these works is to find a "diagnostic index" that can provide a sensitive measure to discriminate a disease bone from competent bone. Unfortunately, this aim is still far from achieved, although in some cases, those techniques show some comparable indicator of bone quality.

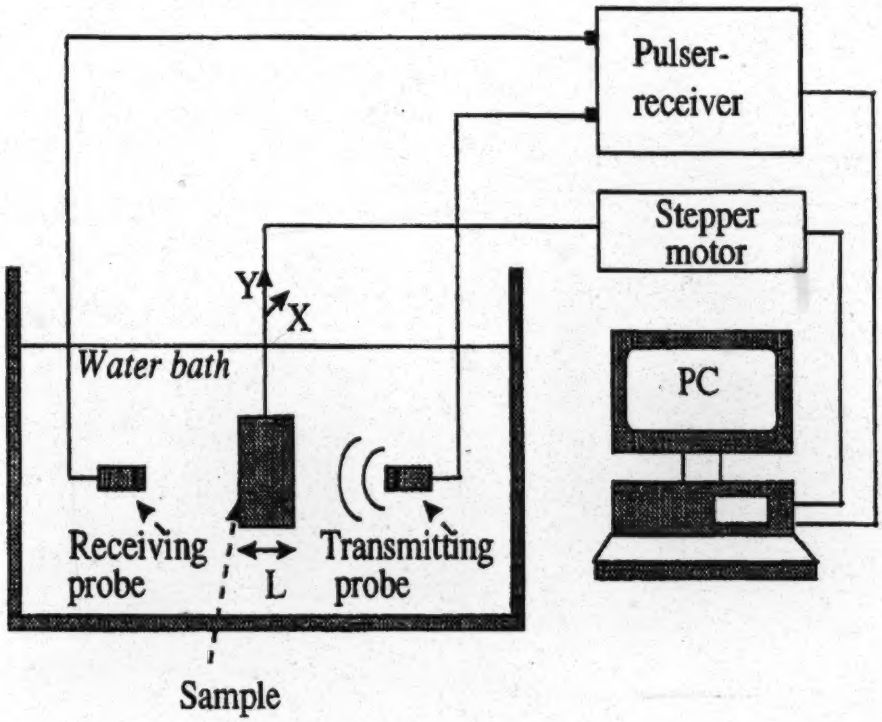

Figure 1.2 A typical experimental setup to measure bone in-vitro (taken from Fig. 1, Droin et al, 1998).

The bovine trabecular bone is often used in-vitro research. Wu et al.(1995) studied the impact of bone size on BUA using bovine bone. They measured the BUA of 9 pieces of bovine trabecular bone, then cut them in half and repeated the measurement on 18 pieces of cut bones. The nonlinear results, BUA of 70 dB/MHz for thickness of 1.2 cm and BUA of 98 dB/MHz for thickness of 2.4 cm suggested the device they used didn't work

well at higher BUA levels. Töyräs et al. (1999) measured BUA at 60-100 dB/MHz and SOS at 1541-1686 m/s in bovine femur bone. They found that BUA increase in a highly linear manner with bovine bone thickness of up to 2.5 cm. Lee et al. (2003) measured SOS and BUA in three center frequencies and have the results as follow: for center frequency 1 MHz, SOS was 1694 ± 43 m/s, BUA was 26.0 dB/cm/MHz; for center frequency 2.25 MHz, SOS was 1690 ± 44 m/s, BUA was 25.5 dB/cm/MHz; for center frequency 3.5 MHz, SOS was 1673 ± 43 m/s, BUA was 19.6 dB/cm/MHz.

1.4 Objective and Organization of the Thesis

The objective of the thesis is to investigate dispersion and attenuation of the ultrasound through cancellous bone samples. To calculate the phase velocity, a method based on cross-correlation is applied to replace a common Fourier Transform-based method.

Chapter 1 introduces briefly the bone structure, function and malfunction, then the current techniques in the bone studies are summarized, and finally the objective and the outline are given. Chapter 2 discusses the experimental setup and bone sample preparation. The structure of the phantom will be discussed. All data will be displayed. Chapter 3 reviews the methods used in calculating the velocity or phase velocity, then a method based on cross-correlation is applied to calculate the phase velocity in place of the common FFT based method. Discussion of the results follows at the end. Chapter 4 first summaries three power spectrum estimation methods briefly, then the equations calculating the attenuation as well as the transmission loss are derived. The data processing results using these equations are then discussed. Chapter 5 gives a summary of the thesis and indicates direction of future research in this area.

Chapter 2

In Vitro Ultrasonic Measurement of Bone Samples

2.1 Experimental Setup

The experimental setup includes ultrasound pulser/receiver, oscilloscope, ultrasound preamplifier, water tank, transducers. Figure 2.1 displays the pulser/receiver and oscilloscope. The model of computer controlled pulser/receiver is a Panametrics Model 5800, and the model of mixed signal oscilloscope is HP Hewlett Packard 54645D. A preamplifier is necessary for the measurement when the signals are too weak. The preamplifier is a small apparatus shown in Figure 2.1, and its model is Panametrics 5662.

Figure 2.1 Experimental Setup (pulser/receiver and oscilloscope).

Figure 2.2 displays the water tank with transducers mounted on the opposite sides. The water tank is 63x63 mm inside, and the transducers are 63 mm apart. The diameter of the transducer produced by Panametrics is ¾ inch in diameter and the center frequency is 1.0 MHz. The ruler attached to the bottom of water tank is used to locate the bone samples, and the two lines inside the scale are used to assure the bone sample block the ultrasound beam. If the bone sample straddles both lines at the same time, the ultrasound beam can not bypass the bone sample. A slab of iron is placed at the bottom to support the bone sample, so that

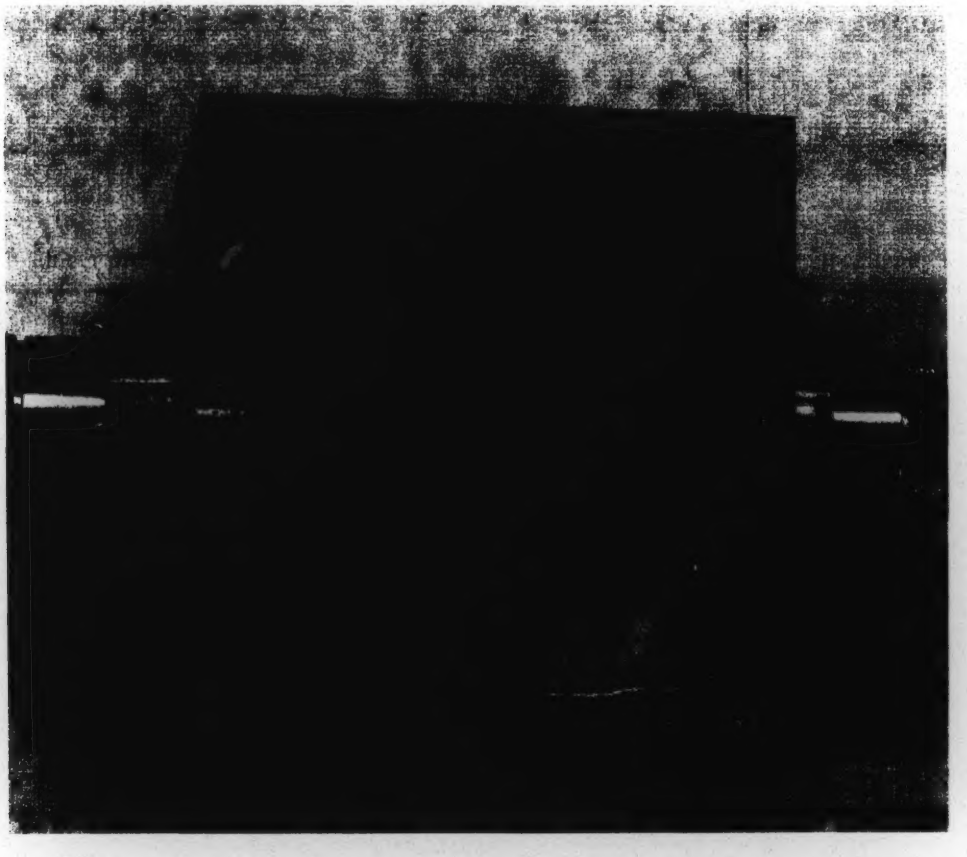

Figure 2.2 Experimental Setup (transducers mounted on water tank).

the ultrasound beam will pass through the center of the bone sample. By keeping two surfaces of the iron slab adjacent to the water tank and keeping the bone measurement surface even with the iron edge surface, we are able to keep the bone sample in the same place.

2.2 Bone Sample Preparation

In this thesis, we used cow bones and pig bones for samples. All bone samples are harvested from femur head, and two bone directions are investigated, that is, transverse and axial directions. Figure 2.3 illustrates the two directions. Axial direction is along the weight bearing direction as illustrated by black arrow and transverse direction is perpendicular to the axial direction and usually perpendicular to the surface of cortical bone layer, as illustrated by the dash line.

Figure 2.3 Illustration of bone orientation.

Band saw was used to cut the femur bones into slabs of different thickness. The slabs have two parallel surfaces and 4 different thicknesses between the two parallel surfaces, 0.5cm, 1.0cm, 1.5cm, 2.0cm, were cut and investigated. Bone samples of these four sizes are displayed in figure 2.4.

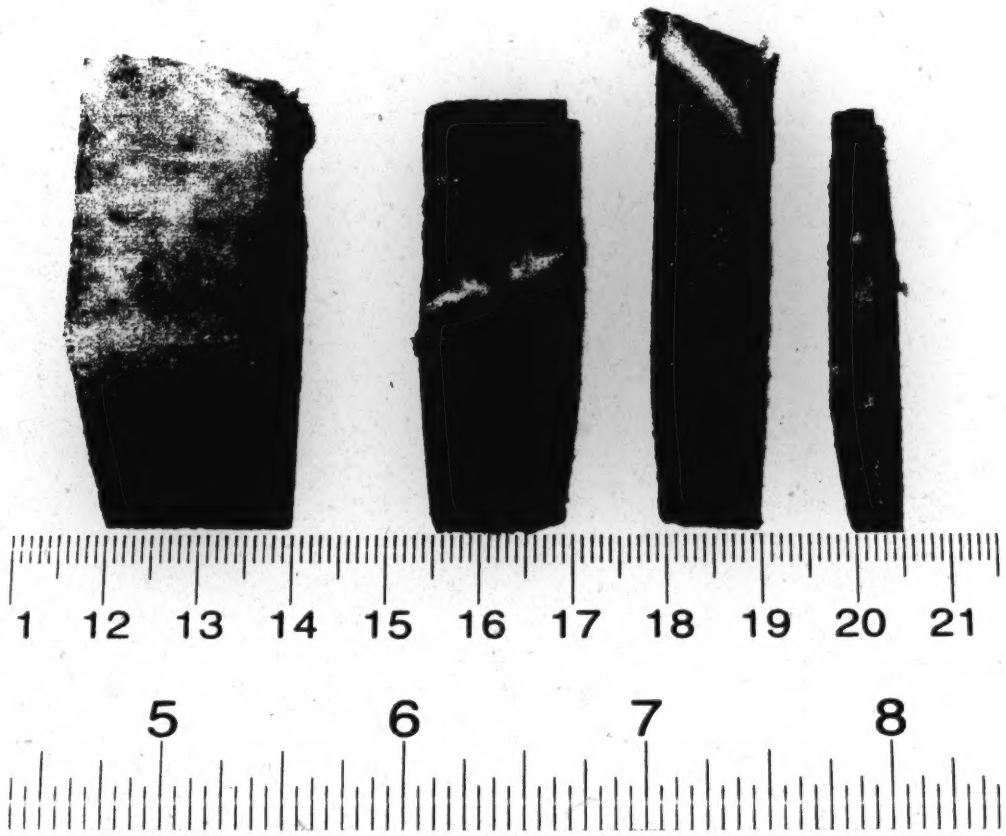

Figure 2.4 Typical bone samples of four different sizes, from left to right, the thickness are separately: 2 cm; 1.5 cm; 1.0 cm; 0.5 cm.

Figure 2.5 shows the bone sample surface perpendicular to the ultrasound beam. The white circle indicates the area that the ultrasound beam transmits through and is the measurement area. The parallel surfaces must be perpendicular to the ultrasound beam, and

so is the measurement area. During the experiment, the measurement area is selected to avoid the complex structure inside the trabecular bone, that is, to make the measured area as homogenous as possible.

Figure 2.5 Measurement area of bone sample.

2.3 Discussion of Experiment Data

The experiments were divided into two groups: Experiment 1 includes 48 bone samples. Twenty-five of them are bovine bones in transverse direction, 11 of them are bovine bones in axial direction, 12 of them are pig bones in axial/transverse direction. Experiment 2 involves some stratified phantoms simulating trabecular bone. Figure 2.6

displays the water reference pulse and its spectrum. The waveform is clear, with the center frequency at about 0.9 MHz. No scattering or reflection signal is present in the water pulse.

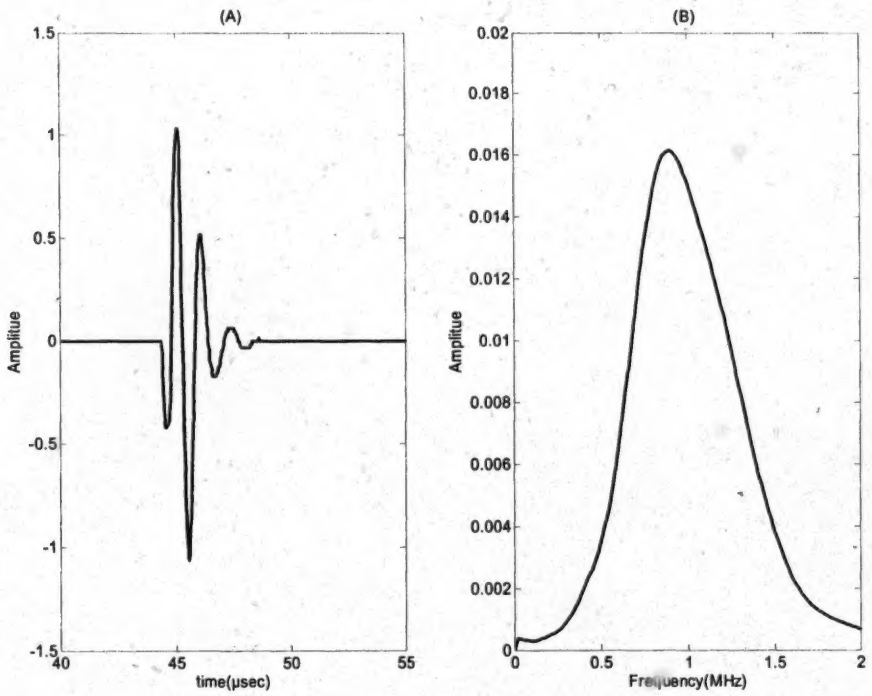

Figure 2.6 Water pulse (A) and its spectrum (B).

2.3.1 Data for Experiment 1

Figure 2.7 shows the waveforms of 20 bovine bone samples. The measurement surface is in the transverse direction. Figure 2.8 shows the same waveforms with normalization by its maximum amplitude value. The waveform is normalized by its own maximum amplitude. From Figure 2.7, the amplitude of the waveform decreases dramatically with increase thickness of the bone. From Figure 2.8, we can see that the waveform becomes more distorted with the thickness of the bone sample and one thing in common among the distortion is the pulse broadening.

Figure 2.9 shows the waveforms of 11 bovine bone samples, the measurement surface is in the axial direction. Figure 2.10 shows the same waveforms but are normalized by their own maximum amplitude. From Figure 2.9, the amplitude of the waveform decreases dramatically with increase thickness of the bone. Again, Figure 2.10 show both waveform distortion and pulse broadening.

By comparing Figure 2.8 and Figure 2.10, it is easy to find out that in the axial direction the waveform is more complicated, for the case of thickness 0.5 cm and 1.0 cm. In Figure 2.10, two of five axial direction samples (first and third one) of thickness of 0.5 cm show so called 'fast wave', which is often characterized by low amplitude 'waveform' prior to a high amplitude "waveform". However, among 10 transverse samples of thickness of 0.5 cm in the figure 2.8, none of them show similar phenomenon and all show a relatively clear pulse similar to the reference pulse through water. The bone samples of thickness of 1.0 cm show similar results. All of two axial 1.0 cm samples in the figure 2.10 show a low amplitude 'waveform' before a high amplitude 'waveform', but only one of five 1.0 cm transverse samples in the figure 2.8 show this kind of waveform.

It have been reported that cancellous bone displays highly oriented structure in load -bearing bones, showing anisotropic mechanical and ultrasonic properties (Nicholson et al. 1994; Hosokawa and Otani,1998). The above mentioned phenomenon seems to be connected to the anisotropic mechanical and ultrasonic properties. The low amplitude 'waveform' looks like so called fast wave as predicted by Biot's theory, based on the character of low amplitude and earlier arrival time. However, it can be more straightforwardly explained in a way other than using Biot's theory, as follows: since there is a highly oriented structure (axial direction) in load-bearing bones, part of the ultrasound

will travel mostly through the marrow while other will travel mostly through the trabecular rod or plate, thus causing the separation of fast wave from slow wave. On the other hand, there is no highly oriented structure in the transverse directions, all ray paths go through the bone with same portion between marrow and trabecular. This explanation agrees well with the result using a stratified model (Hughes et al, 1999).

Figure 2.11 shows the waveforms of 12 pig bone sample. Since they are the first bone samples we cut, we don't realize the need of recording the orientation, those measurement surfaces can be in either axial or transverse direction. Figure 2.12 shows the normalized waveforms. The waveform is normalized by its own maximum amplitude. From figure 2.11 we can see the amplitude of the waveform decreasing dramatically with the thickness. From figure 2.12 we can see that the waveform distortion and pulse broadening again, but it is not as severe as that in bovine bone samples.

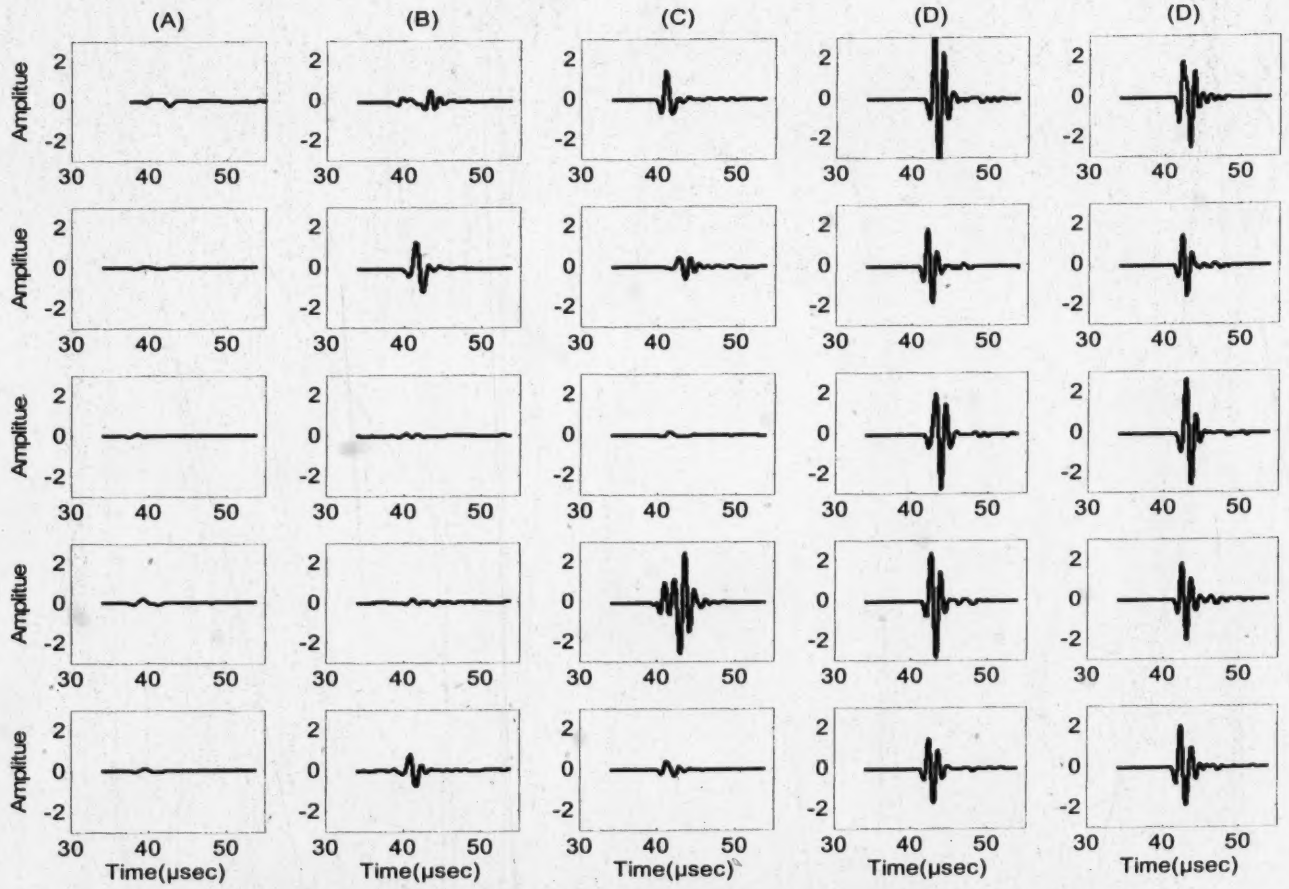

Figure 2.7 Signal of bovine trabecular bones of different thickness in transverse direction (Un-normalized): (A) 2.0 cm. (B) 1.5 cm. (C) 1.0 cm. (D) 0.5 cm

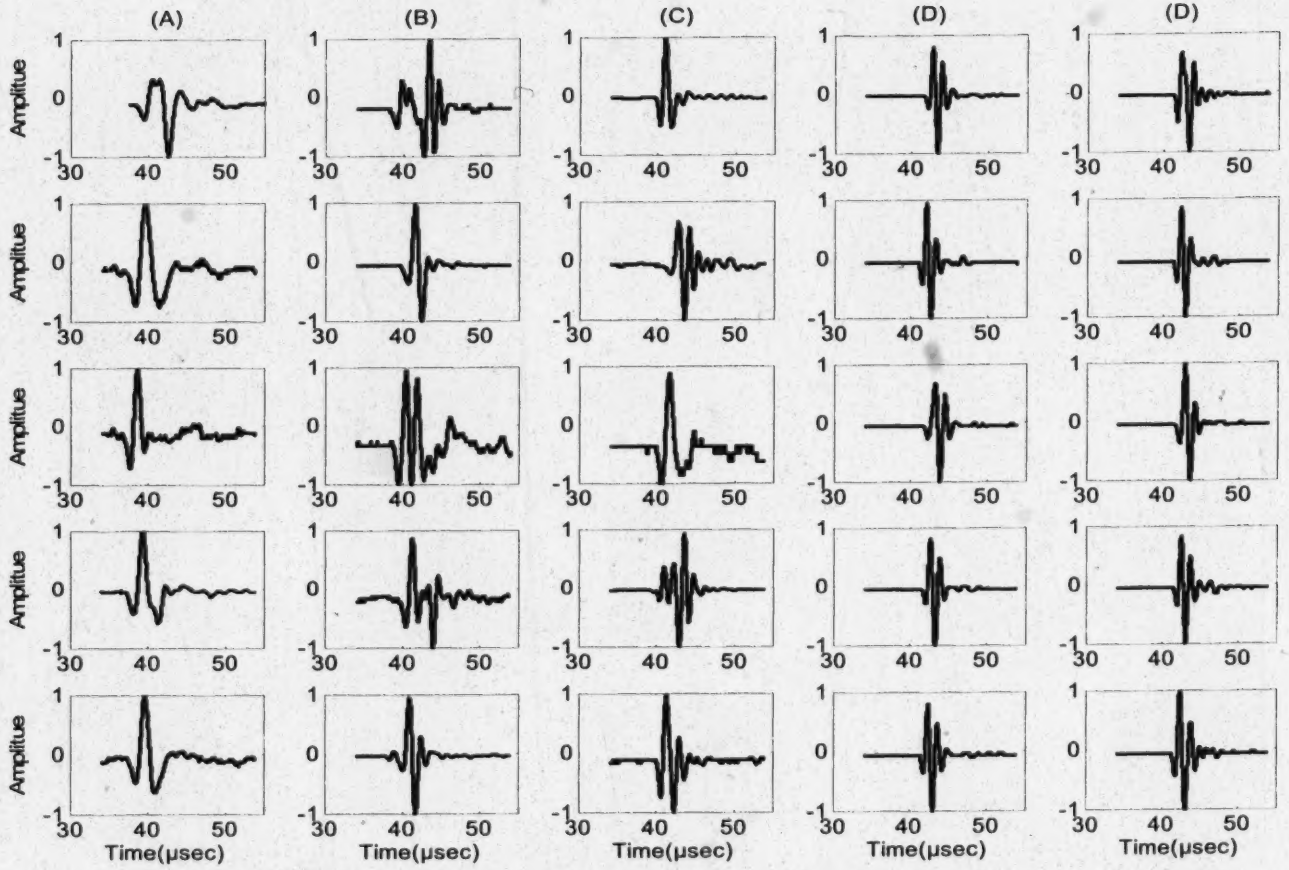

Figure 2.8 Signal of bovine trabecular bone in transverse direction (Normalized by itself): (A) 2.0 cm. (B) 1.5 cm. (C) 1.0 cm. (D) 0.5 cm.

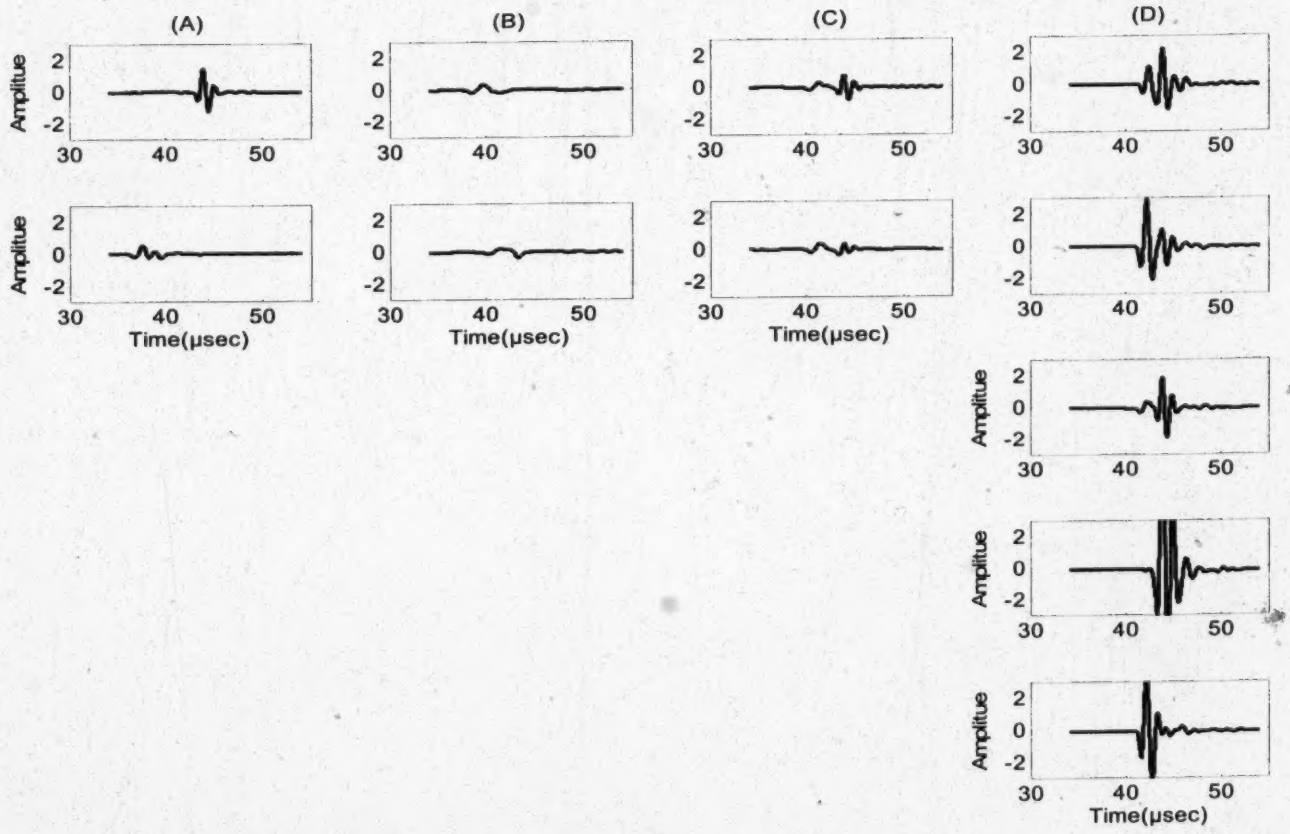

Figure 2.9 Signal of bovine trabecular bone in axial direction (Un-normalized): (A) 2.0 cm. (B) 1.5 cm. (C) 1.0 cm. (D) 0.5 cm.

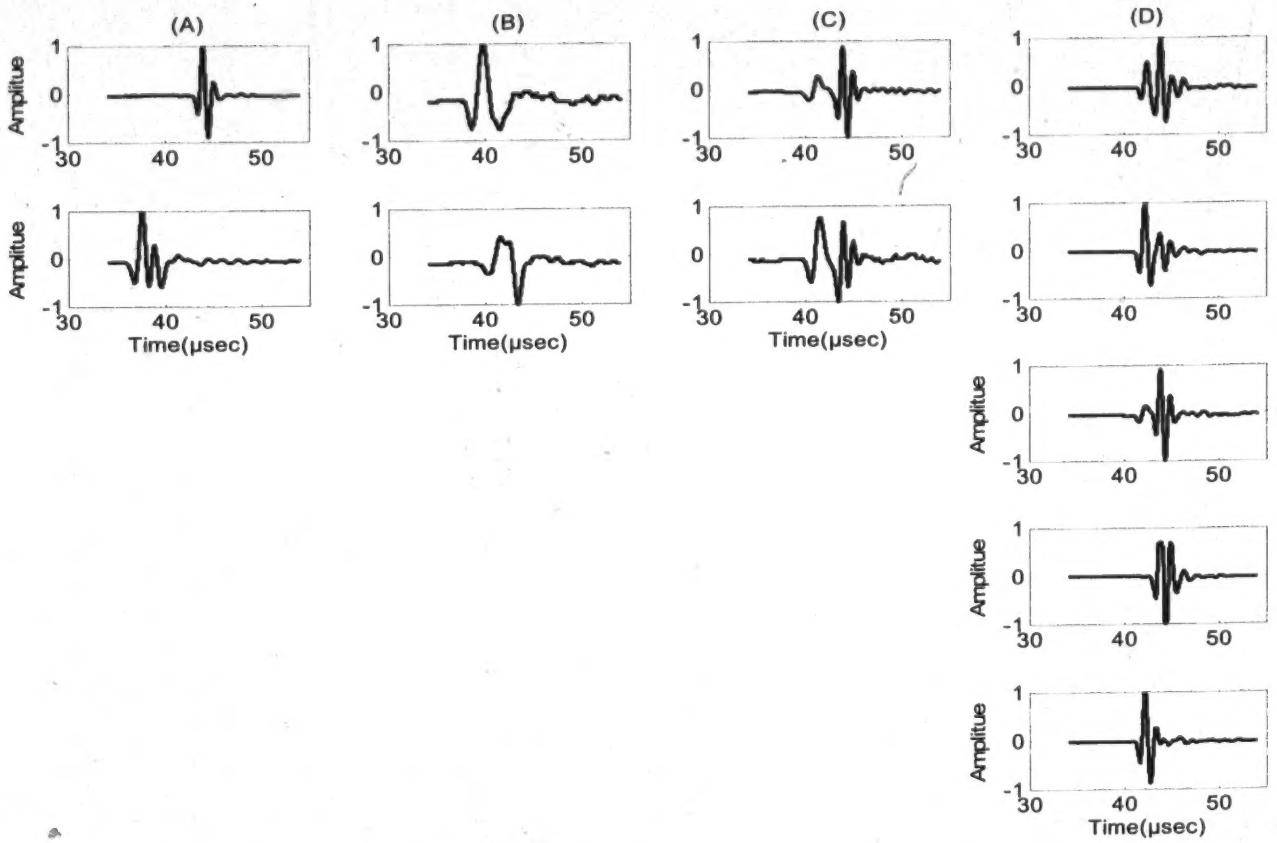

Figure 2.10 Signal of bovine trabecular bone in axial direction (Normalized by itself): (A) 2.0 cm. (B) 1.5 cm. (C) 1.0 cm. (D) 0.5 cm.

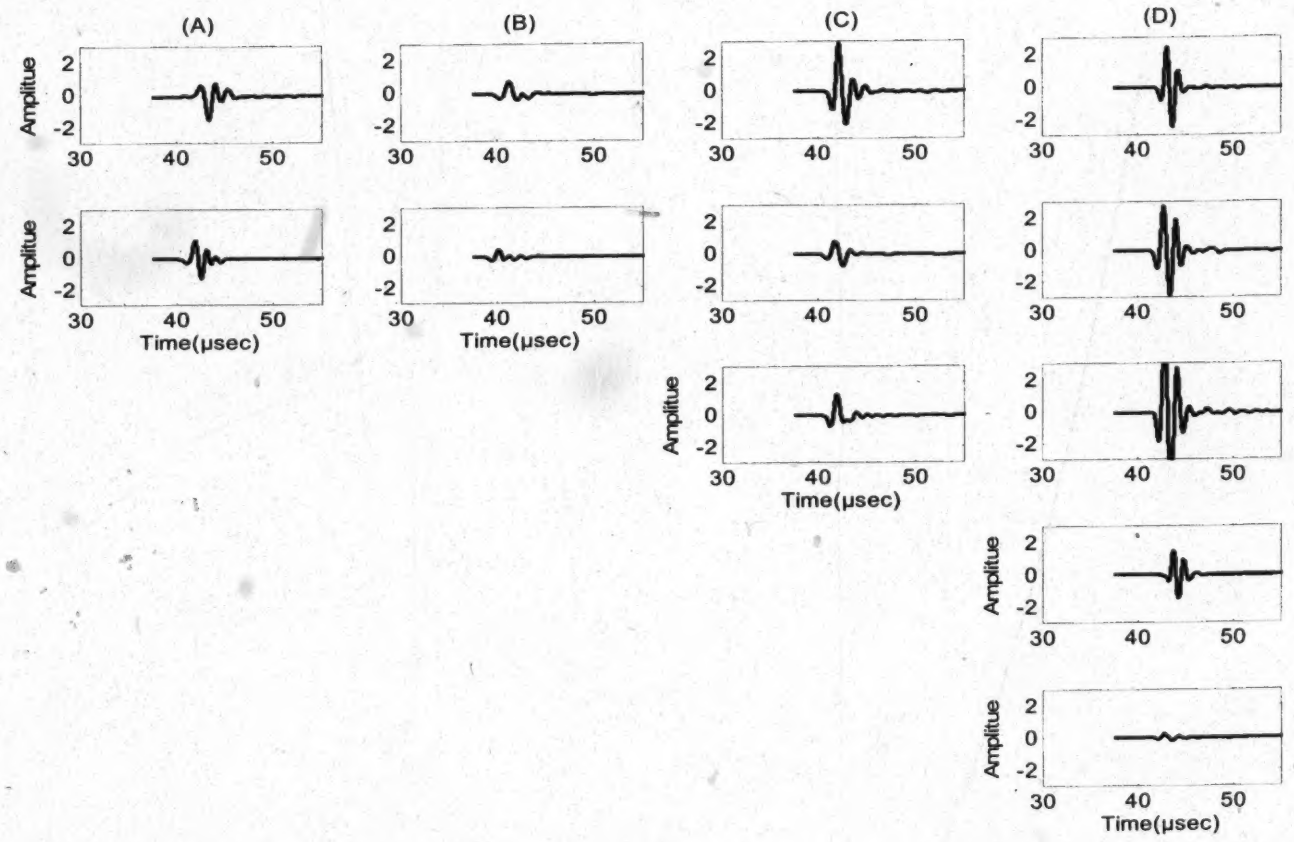

Figure2.11 Signal of pig trabecular bone (Un-normalized): (A) 2.0 cm. (B) 1.5 cm. (C) 1.0 cm. (D) 0.5 cm.

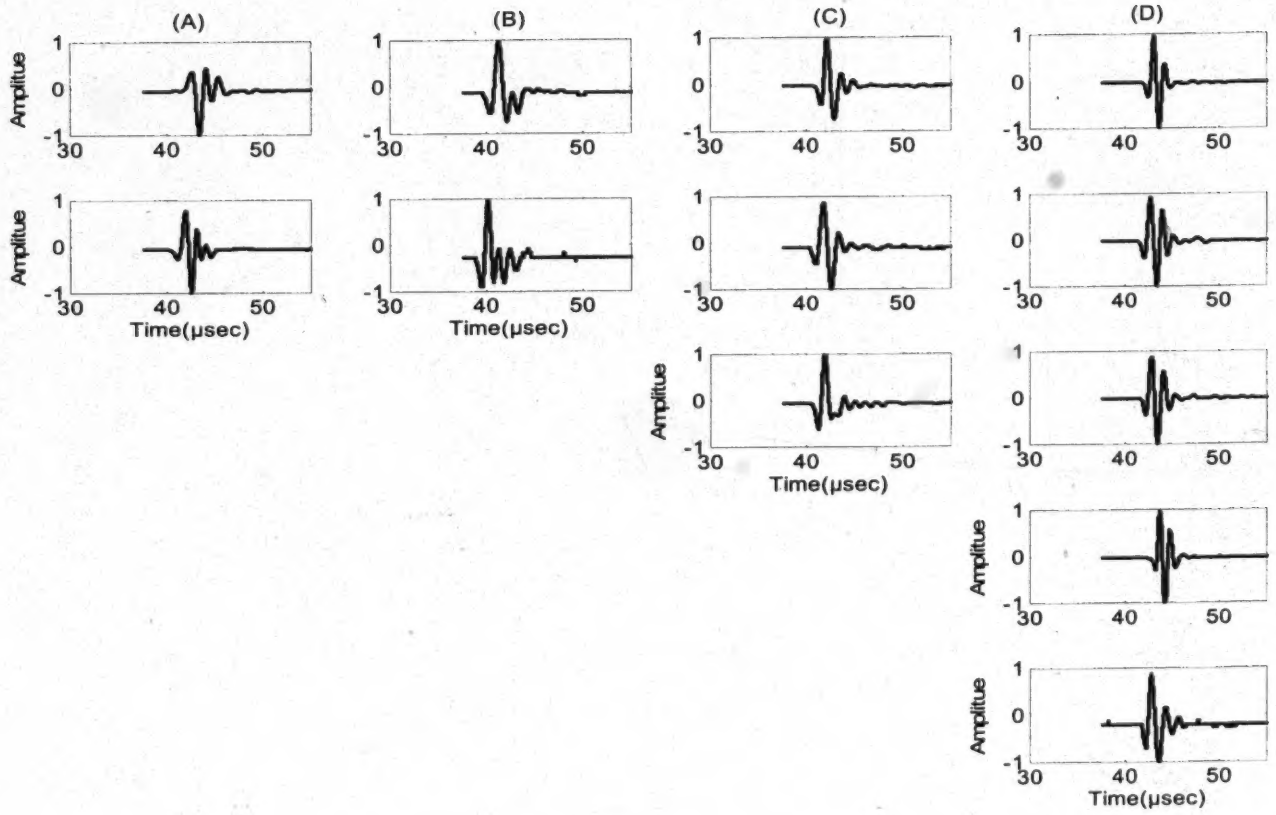

Figure2.12 Signal of pig trabecular bone (Normalized by itself) : (A) 2.0 cm. (B) 1.5 cm. (C) 1.0 cm. (D) 0.5 cm.

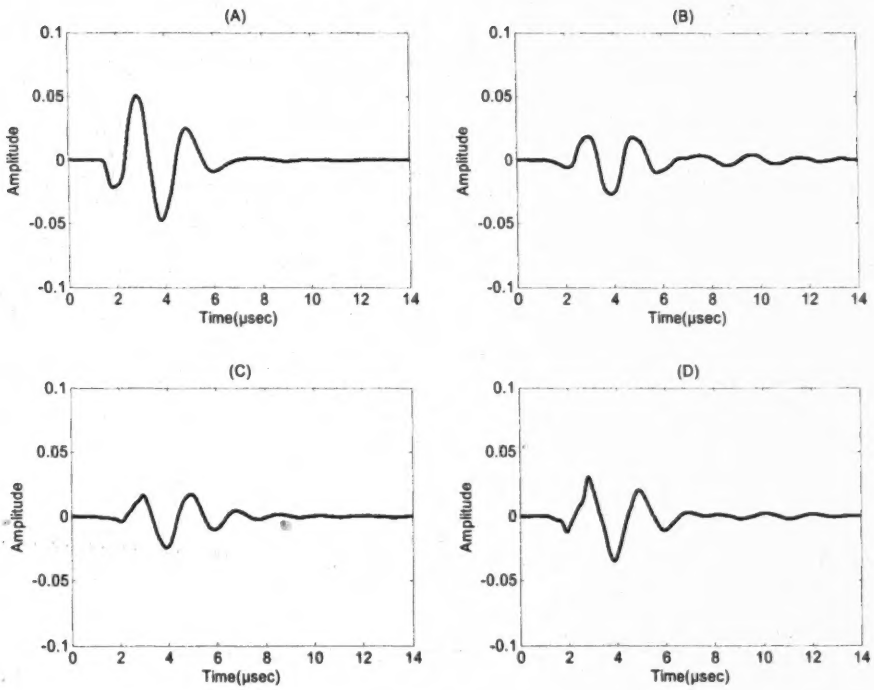

Figure 2.13 (A) water reference signal and echo signals from three typical bone samples: (B) Bovine bone sample in axial direction surface. (C) Bovine bone sample in transverse direction surface. (D) Pig bone sample.

Figure 2.13 shows the waveforms of the water reference signal (A), the echo waveform from the axial direction surface of bovine bone sample (B), the echo waveform from the transverse direction surface of bovine bone sample (C), the echo waveform from surface of pig bone sample (D). Those four signals are used to calculate the transmission loss of the ultrasound propagation in chapter 4.

2.3.2 Data for experiment 2

Experiment 2 includes 4 stratified phantoms, with the same experiment setup as experiment 1, except that the phantom is put in a bigger water tank as shown in figure 2.14. The phantom is composed of sheets of two kinds of material and four kinds of thickness.

Distance between two transducers is fixed and is 14.2 cm. For the thin phantom, the distance of one boundary to the receiver is 6.6 cm, while the distance of another boundary to the transmitter is 2.7 cm. For the thick phantom, the distance of one boundary to the receiver is 6.8 cm, and the distance of another boundary to the transmitter is 2.8 cm.

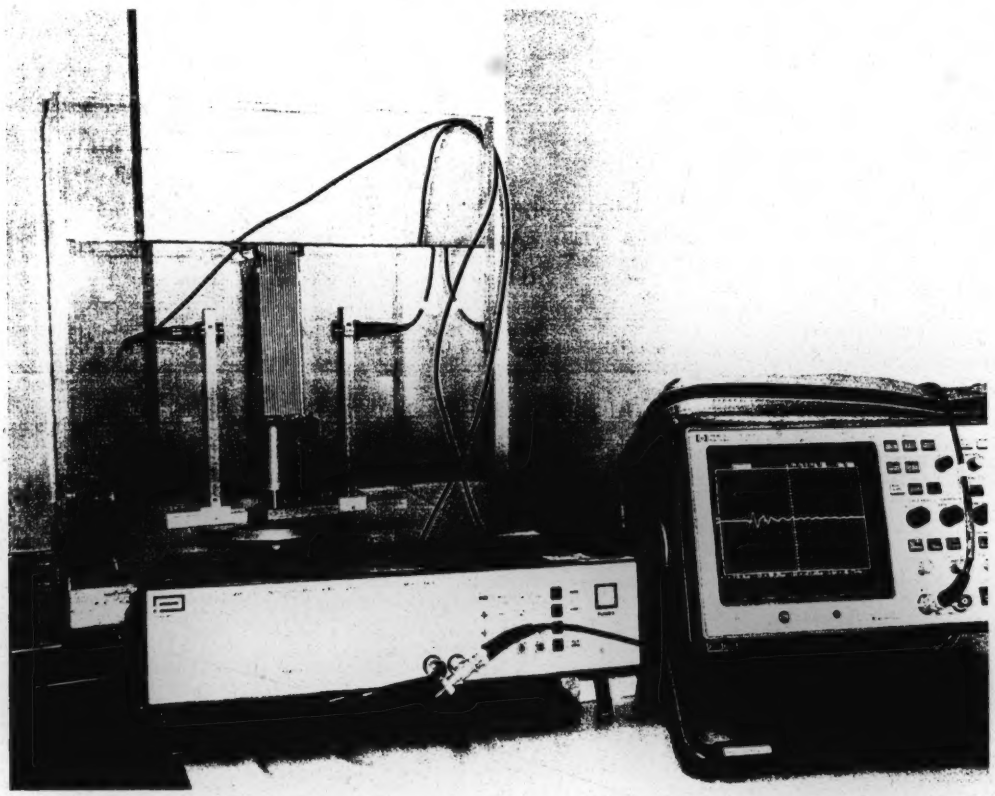

Figure 2.14 Experimental Setup for phantom in big water tank.

A frame is used to hold the sheets in place. There are two kinds of frame: one frame has thinner slots with total thickness of 4.9 cm and the other has thicker slots with total

thickness of 4.6 cm, as shown in figure 2.15. White sheet is made of polystyrene and thicknesses for thinner and thicker sheets are 0.75 cm and 1.55 cm respectively. The transparent sheet is made of polycarbonate and thicknesses for thinner and thicker sheets are 0.8 cm and 1.45 cm respectively.

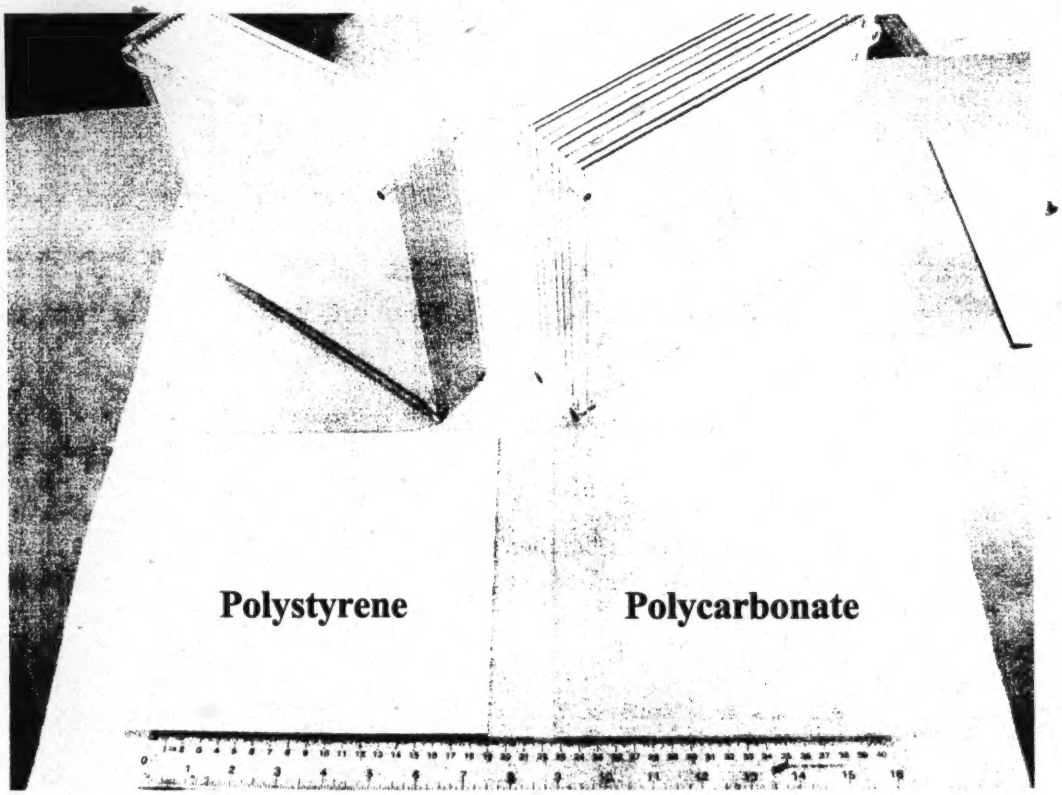

Figure 2.15 Phantoms and two kinds of material.

Figure 2.16 shows the structure of the four phantoms. In the figure, the white represents the water, grey represents polystyrene and dark represents polycarbonate. Figure 2.17 shows the corresponding signals for the four phantoms. All signals are not normalized and show the true amplitude.

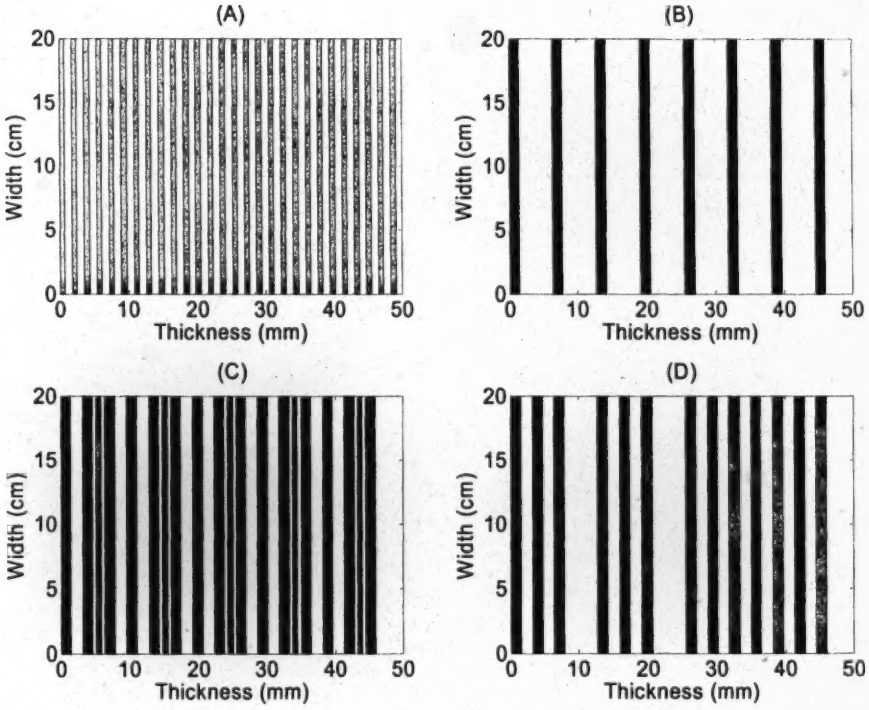

Figure 2.16 Structures of four phantoms.

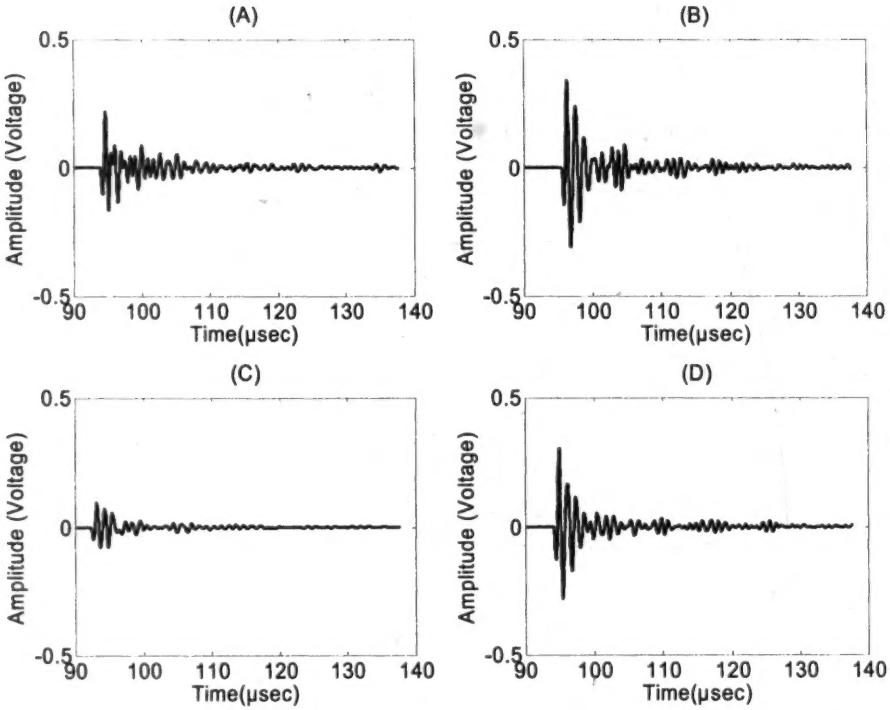

Figure 2.17 Ultrasound signals through four phantoms.

Chapter 3

Estimation of Dispersion Curves Using Cross-Correlation Method

3.1 Introduction

In-vitro studies of bone characterization using ultrasound have showed that speed of sound (SOS) and broadband ultrasound attenuation (BUA) are two important parameters (Langton, 1984; Strelitzki, 1996). Studies have shown that elastic moduli calculated from SOS and density correlate well with mechanically-determined elastic moduli in both cortical and cancellous bone (Ashman *et al* 1984). In this chapter, we will focus on retrieving information about velocity dispersion from the data. Several methods have been used in the literature (Ashman et al, 1984; Ashman et al, 1987; Jeong and Hsu, 1995; Strelitzki et al 1996; Le, 1998; Droin et al, 1998; Hughes et. al.1999; Wear, 2001) and can basically be categorized into time-based method and frequency-based method.

The outline of this chapter is as follows. First, we will give a brief summary of the techniques in estimating the ultrasound velocity in bone. Secondly, we will describe the cross correlation technique to estimate dispersion. Lastly, the technique will then be applied to phantom and bovine bone data and discussion of results will be provided.

3.2 Methods of Velocity Measurement

3.2.1 Time-Domain Methods

Ashman et al (1984) discussed a continuous wave technique (CW) to measure the elastic coefficients of human and canine cortical bone. The coefficients were determined by the velocity and density of the samples. The arrival time of the signal through samples of

small thickness was determined by measuring the phase shift of the signal required to align with the input signal. Ashman et al (1987) also used a 50 kHz CW technique to measure velocities in trabecular bone. The CW method was time consuming as one had to tune in the phase shift to estimate the time delay. If there were phase shift measurement errors due to reflections, mode conversions and other interfering signal, the results would be subject to errors (Fitting and Adler, 1981).

Among the time-domain methods, the pulse-transmission technique was most often used to determine SOS. Figure 1.2 shows a schematic diagram of a typical pulse-transmission experiment. The experiment involves transmitting and receiving a short pulse through water with and without the bone sample in the transmission path. The velocity of the bone sample is calculated by the substitution equation (Le, 1998):

$$v_s = \frac{d}{-\Delta t + \frac{d}{V_w}} \tag{3.1}$$

where d is the thickness of the bone sample, V_w is the ultrasound velocity in water, Δt is the time difference between the transit time without bone sample in water and the transit time with bone sample in water and can be written as

$$\Delta t = t_{water} - t_{sample} \tag{3.2}$$

Where t_{water} is the transit time of the pulse in water without bone sample in the transmission path and t_{sample} is the transit time of the pulse in water with bone sample in the transmission path.

Nicholson *et al* (1996) pointed out that measurement of velocity in trabecular bone was sensitive to the criteria used to determine the transit time. Three different criteria: first arrival, threshold and first zero-crossing, gave significant discrepancies in the derived

velocities. These differences could account for a difference of 260 m/s between first arrival and first zero-crossing. It was also pointed out that the change of the original pulse shape seemed to arise from a combination of different physical processes such as attenuation, dispersion and phase cancellation, given the fact that trabecular bone has a multiphase and anisotropic structure. These effects made transit time velocity measurements unreliable in trabecular bone and phase spectral analysis was suggested to provide better velocity information on dispersion.

Le (1998) suggested an envelope technique to overcome the above mentioned limitations. The method picked the peak of the envelope of a signal as a reference point to measure transit time difference. The numerical results indicated that the velocities thus obtained were more accurate and the technique was shown to be more robust in dealing with noisy signals. Strelitzki et al (1996) adopted a cross-correlation technique to estimate the transmit time. The time difference Δt between the two signals is the lag corresponding to the peak value of the cross-correlation function $R(\tau)$, calculated by the Inverse Fourier Transform (IFFT):

$$R(\tau) = F^{-1}[S^*(\omega)W(\omega)] \tag{3.3}$$

where F^{-1} means inverse Fourier Transform, $S^*(\omega)$ is the complex conjugate of the Fourier transformed signal in bone, and $W(\omega)$ is the Fourier transformed signal in water.

Time-domain methods are only reliable for non-dispersive or weakly dispersive medium. For absorptive medium, the pulse will be broadened due to selective removal of high frequencies. Pulse delay is also obvious and more serious for the later portion of the pulse. The delay will contribute to the uncertainty of the measurement.

3.2.2 The Phase Spectral Analysis Method

Let the signal through water be represented by $w(t)$ and the signal through bone sample by $s(t)$. Their Fourier representatives are respectively:

$$W(\omega) = \int_{-\infty}^{\infty} w(t) e^{-i\omega t} dt$$

and

$$S(\omega) = \int_{-\infty}^{\infty} s(t) e^{-i\omega t} dt \,. \tag{3.4}$$

In this method, the phase velocity can be calculated using the following formula (Sachse and Pao, 1978):

$$v_s(\omega) = \frac{\omega d}{-\Delta\phi(\omega) + \frac{\omega d}{V_w}} \tag{3.5}$$

where d is the thickness of the bone sample, V_w is the ultrasound velocity in water, $\Delta\phi(\omega)$ is the phase difference between the signal without bone sample in water and the signal with bone.

The phase difference $\Delta\phi(\omega)$ between the two signals is given by (Jeong and Hsu, 1995; Droin et al, 1998),

$$\Delta\phi(\omega) = \arctan\left\{\frac{\mathrm{Im}[W(\omega)/S(\omega)]}{\mathrm{Re}[W(\omega)/S(\omega)]}\right\} . \tag{3.6}$$

or (Hughes et. al.1999; Wear, 2001):

$$\Delta\phi(\omega) = \arctan\left\{\frac{\mathrm{Im}[W(\omega)]}{\mathrm{Re}[W(\omega)]}\right\} - \arctan\left\{\frac{\mathrm{Im}[S(\omega)]}{\mathrm{Re}[S(\omega)]}\right\} . \tag{3.7}$$

The above two equations are identical in theory, however, the former one should be avoided since the division of two signals will probably increase the uncertainty, especially when the denominator is very small.

Quite often with this method, great care is required to isolate the directly transmitted arrival for the analysis. This is not a trivial task as to decide where to truncate the data. Truncating too soon will misrepresent the main pulse, but truncating too further in time will include the latter reflection and scattering in the analysis.

Figure 3.1 shows a water pulse and a signal through a periodically layered phantom. The signals were sampled at 4×10^7 samples/sec. Figure 3.2 shows their corresponding spectra. Most of the signal energy lies within 0.7-1.1 MHz.

Figure 3.3 shows a series of truncated pulse with different window length. The window applied was a boxcar. Figure 3.4 shows the corresponding dispersion curves. When the signal is short, the dispersion is positive. As the signal length increase, the dispersion becomes negative as more scattering or reflection contributes to the signal.

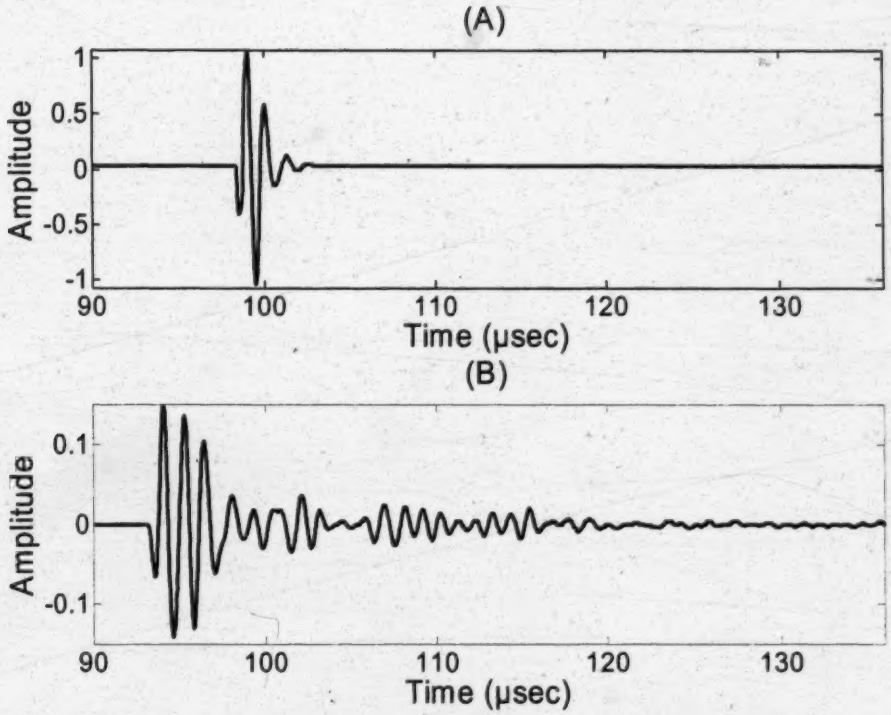

Figure 3.1 The time responses of (A) a water pulse and (B) a pulse through a bone-mimic phantom.

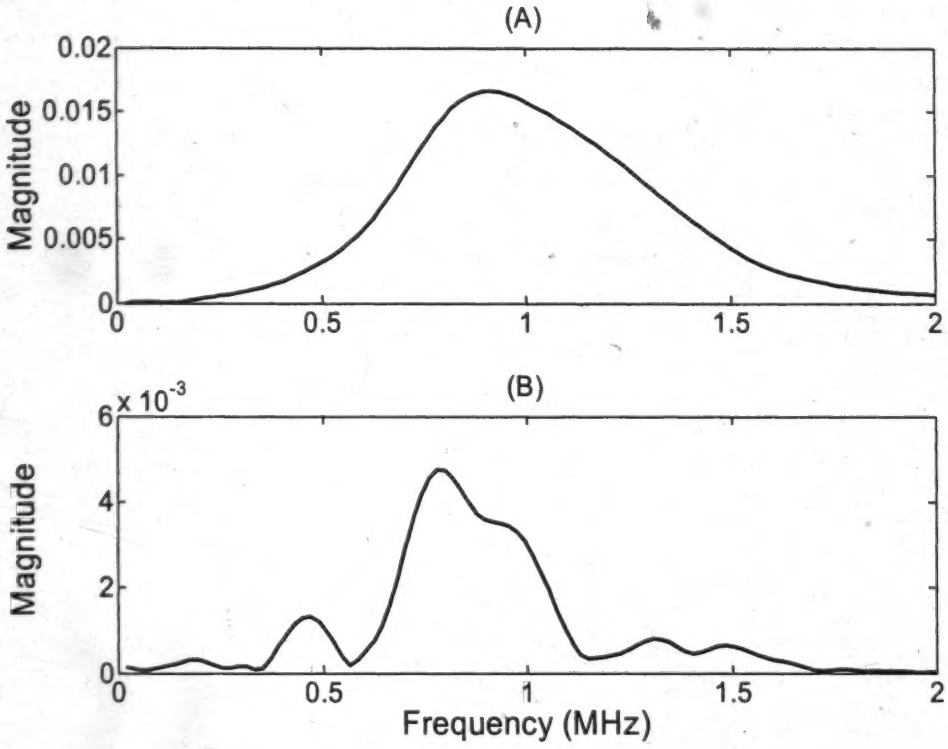

Figure 3.2 The magnitude spectra of the water pulse (A) and the phantom signal truncated at 538 data points (B) shown in Figure 3.1.

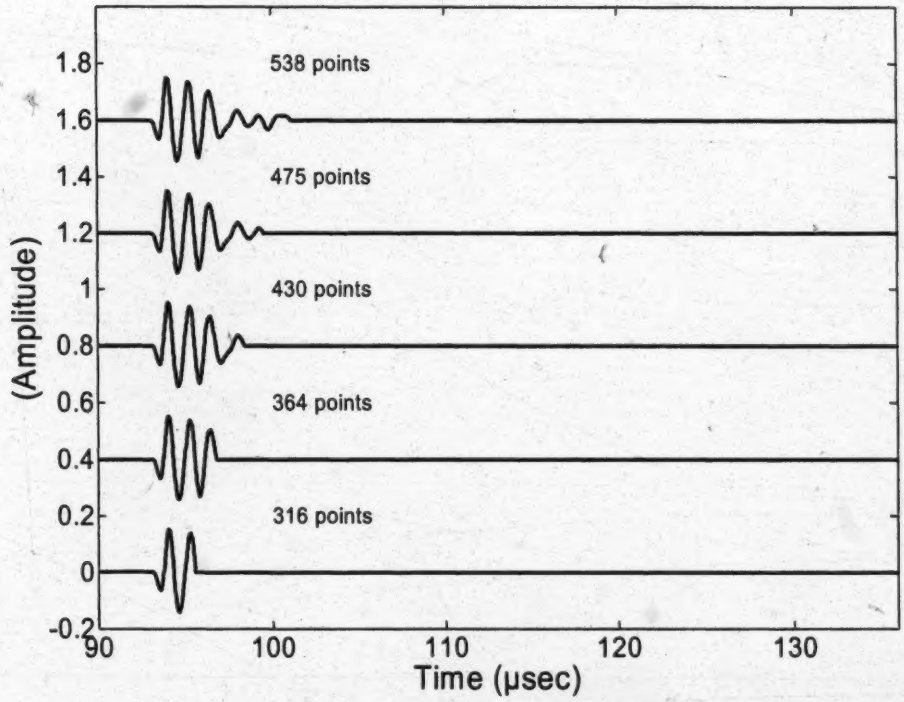

Figure 3.3 Windowing the signal pulse of Figure 3.1 (B). Numbers indicate the box window length starting from the origin, sampling interval is 0.025 μsec

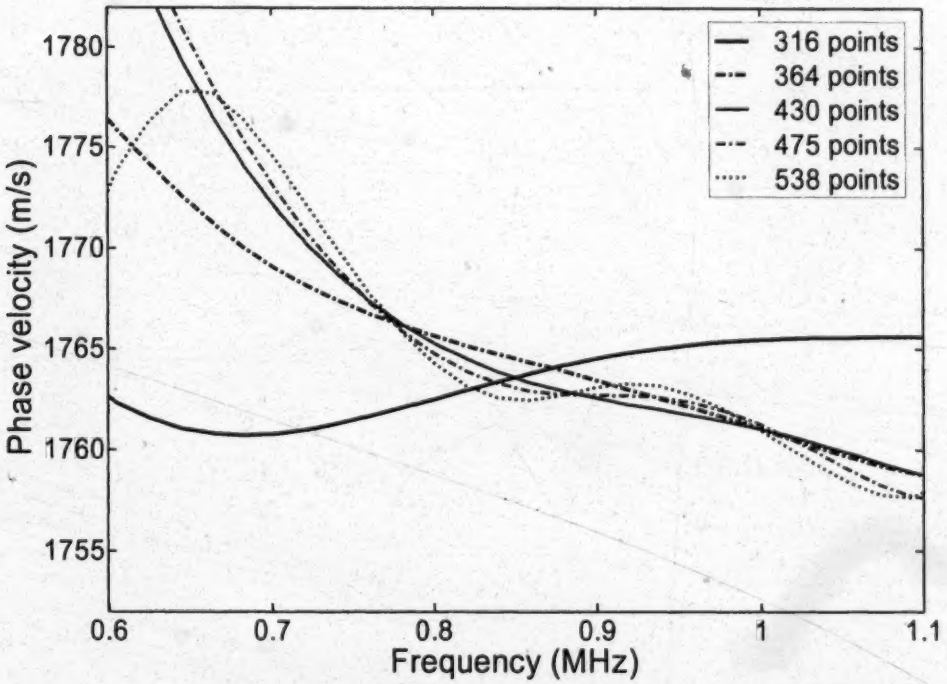

Figure 3.4 **Dispersion curves of the windowed pulse displayed in Figure 3.3.**

3.3 Cross-correlation Technique for the Estimation of Phase Velocity

The cross-correlation function between two zero-mean time signals $w(t)$ and $s(t)$ is

$$R_{ws}(\tau) = \int_0^\infty w(t)s(t+\tau)dt\,, \tag{3.8}$$

where τ is the time lag (Bendat and Piersol, 1971). Cross correlation-function is a standard technique of estimating the degree to which two time series are correlated. The cross correlation spectrum is given by

$$\Phi_{ws}(\omega) = \int_{-\infty}^{\infty} R_{ws}(\tau)e^{-j2\pi f\tau}d\tau\,. \tag{3.9}$$

It can be shown (see Appendix A) that the phase difference between these two signals is:

$$\Delta\phi(\omega) = \arctan\left(\frac{\mathrm{Im}(\Phi_{xy}(\omega))}{\mathrm{Re}(\Phi_{xy}(\omega))}\right). \tag{3.10}$$

Direct substitution of $\Delta\phi(\omega)$ into (3.5) will yield the dispersion curve. At this stage, it is equivalent to the FFT method discussed previously.

Figure 3.5 (A) shows the cross correlation of the two signals in Figure 3.1. The cross-correlation has the absolute maximum similarity at a non-zero lag. To facilitate the application of a window, it is more convenient to have the absolute maximum at zero lag (Rabiner and Gold, 1975). To do so, the phantom signal was shifted to align with the water pulse. Such a shift will introduce a phase shift of, say θ. Figure 3.5 (B) shows the cross-correlation of the shifted signal. Then the modified phase, $\Delta\phi_s(\omega)$ is given by

$$\Delta\phi_s(\omega) = \Delta\phi(\omega) + \theta(\omega)\,. \tag{3.11}$$

A taper window $w(t)$ is also considered to focus on the most correlated portion of the signals. Thus the windowed cross correlation is:

$$\hat{R}_{ws}(\tau) = R_{ws}(\tau) \cdot w_m(\tau), \tag{3.12}$$

where $w_m(\tau)$ is the lag window and m is the width of the lag window.

$$\begin{cases} w_m(\tau) = 0, & \tau < -(m-1)/2 \text{ or } \tau > (m-1)/2 \\ w_m(\tau), & -(m-1)/2 \le \tau \le (m-1)/2 \end{cases} \tag{3.13}$$

In our case, we adopted a Tukey window:

$$w_{N,r}(k) = \begin{cases} \frac{1}{2}[1+\cos(\frac{2\pi}{r}\frac{(k-1)}{N-1} - \pi)], & k < \frac{r}{2}(N-1)+1 \\ 1, & \frac{r}{2}(N-1)+1 \le k \le N - \frac{r}{2}(N-1), \\ \frac{1}{2}[1+\cos(\frac{2\pi}{r} - \frac{2\pi}{r}\frac{(k-1)}{N-1} - \pi)], & N - \frac{r}{2}(N-1) < k \end{cases} \tag{3.14}$$

where $k = 1$ *to* N, N is the window length, r is the ratio of taper to constant section and the value is between 0 and 1. A rectangular window is for r=0, and a Hann window is for r=1. The default value for r is 0.5. Figure 3.6 displays some windows with the same 128 points but of different taper ratio, r. Figure 3.7 shows how a certain window is applied to the cross-correlation of the shifted signal with the reference pulse.

The difference between cross-correlation method (CCM) estimating phase velocity and the phase spectral analysis method (PSAM) lies in the procedure of calculating the phase difference. The PSAM truncates the bone signal first, then applies Fourier Transform and compares two phases to get the phase difference. The CCM calculates the cross-correlation and applies windowing to the lag before further calculating the cross-correlation spectrum, from which the phase difference was obtained directly.

Figure 3.8 and Figure 3.9 compare the dispersion curves calculated from CCM with the result from PSAM. The solid lines represent the result of CCM with various window

length and tapering ratio and the dash line represent the result of PSAM without any windowing.

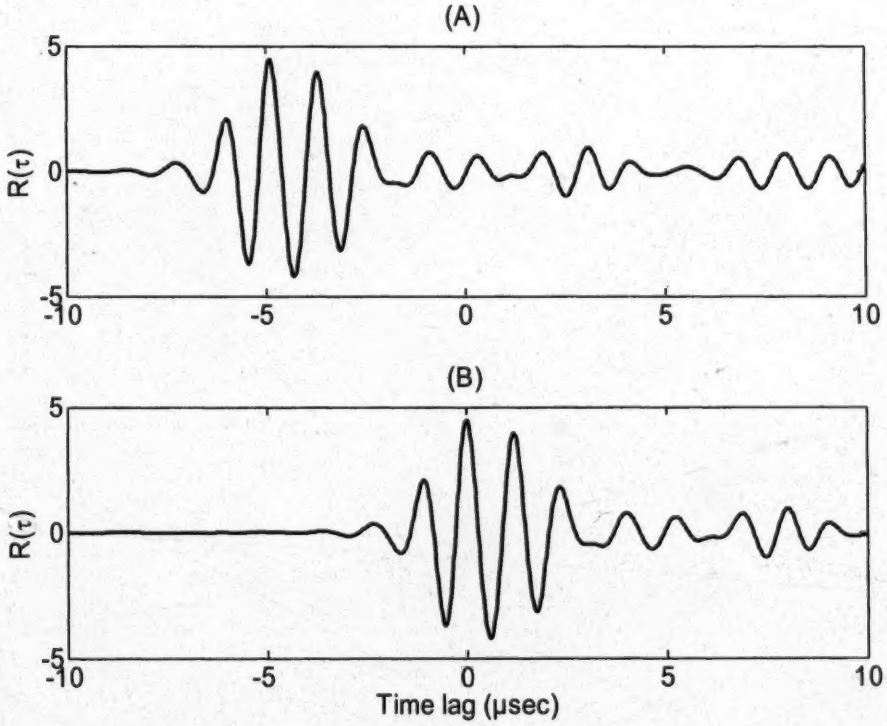

Figure 3.5 The cross-correlation between two signals given in Figure 3.2: (A) without shifting and (B) the pulse through phantom was delayed to align with the water pulse.

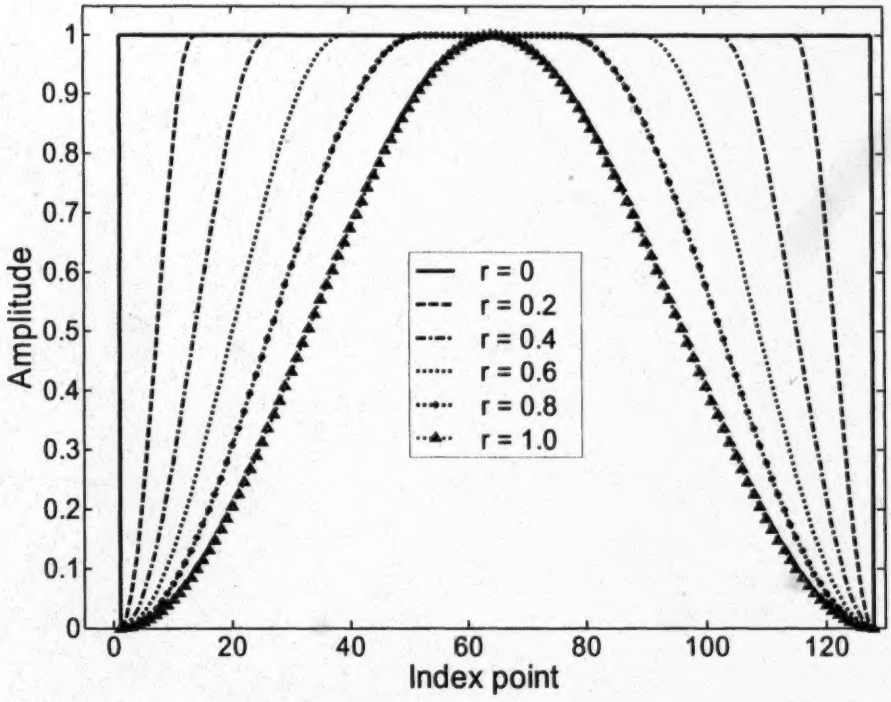

Figure 3.6 A 128-point Tukey taper for different r-values.

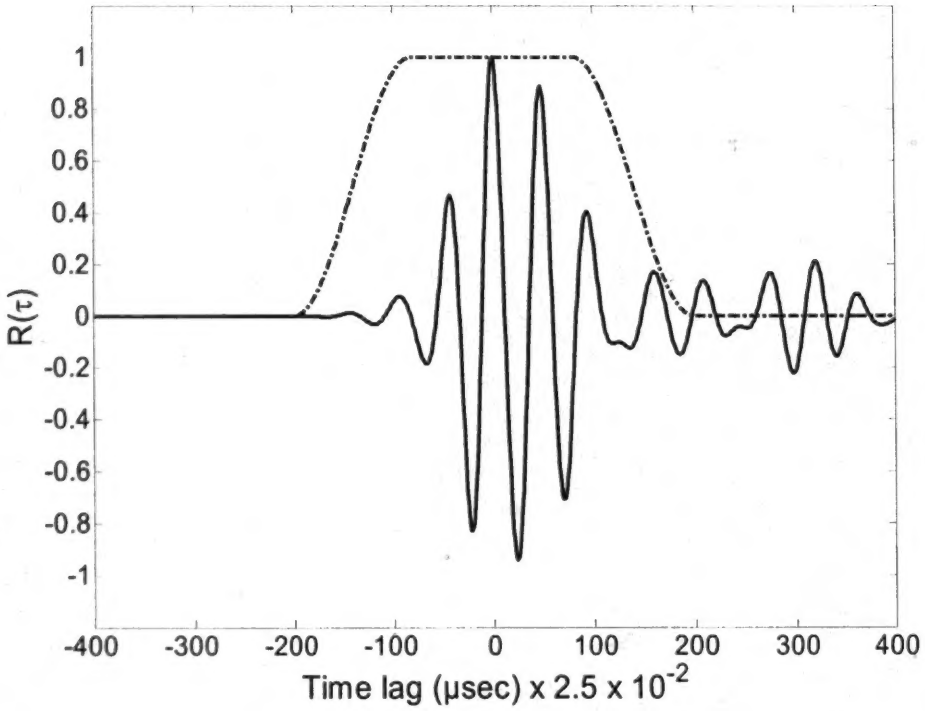

Figure 3.7 The cross-correlation of Figure 3.5(B) in solid line with a Tukey taper of 400 points (r = 0.6) in dash line.

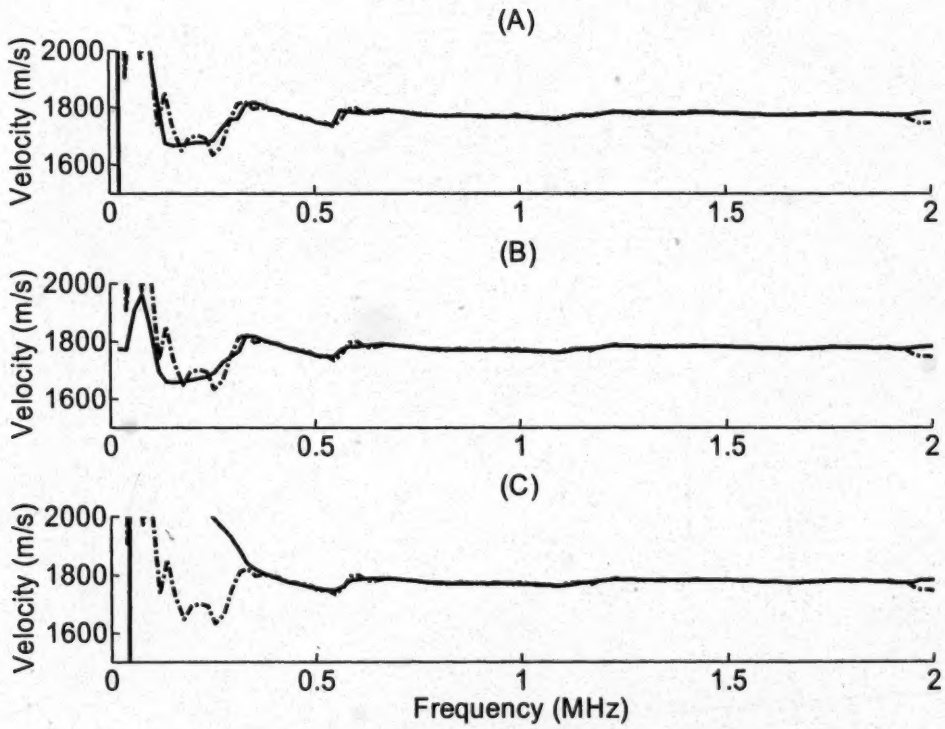

Figure 3.8 **The phase velocity of a pulse through a bone-mimic phantom in Figure 3.1(B) with same fixed length 400 data points but different tapering ratio: (A) $r = 0.5$; (B) $r = 0.6$ and (C) $r = 0.7$. Dash line represents the result of PSAM without any windowing.**

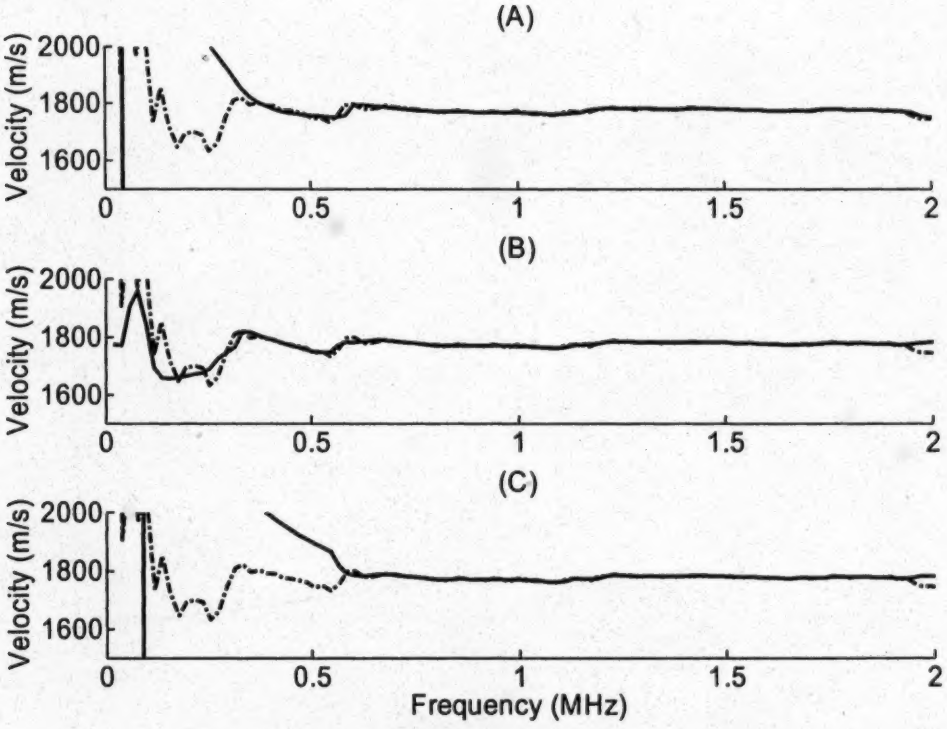

Figure 3.9 The phase velocity of a pulse through a bone-mimic phantom in Figure 3.1(B) with fixed tapering ratio r = 0.6 but of different length: (A) 300 data points; (B) 400 data points and (C) 500 data points. Dash line represents the result of PSAM without any windowing.

In the previous section, a phantom data was used to illustrate the cross-correlation method. Before we process the real bone sample data, here we use a typical bone data to choose a fixed window for all data processing. Figure 3.10 shows a data set of a 2 cm thick bone sample (B), also shown in Figure 2.8 (A1) and reference water pulse (A). The sample was cut in transverse direction. Both of the data contain 2000 data points, and sample interval Δt is 0.01 μsec. Figure 3.11 compares results using different windows length and taper ratio. The dash curve in Figure 3.11 is the dispersion result without windowing, and used here as a reference. Six window lengths were tested starting at 250 data points from the bottom and increase upward at interval of 250 data points. The results of the same window length are shown in the same row in the figure. Also five window ratio were used starting at r=0.2 from the left and increase at an interval of 0.2 to the right. From the figure 3.11, as the window length become short, the dispersion curve is smooth and flat; as the ratio increase, the dispersion curve become smooth and flat. In a word, the longer the window, the more information is used in calculation; the smaller the ratio, the more the information is unhampered in calculation. However, this doesn't mean the longer the window and the smaller the ratio, the better the results, there should be a trade-off between taper ratio and window length. The advantage of this CCM over the PSAM is, it is more robust and windowing in lag domain is more controllable than truncation in time domain.

In the analysis of all bone sample data, a window of 1000 data points length, which is equivalent to 400 points in phantom signal, and tapering ratio of 0.6 are adopted. Since the signal is longer in the phantom and the all data are acquired by 2000 points, to include more scattering, the phantom data were acquired by sample interval Δt of 0.025 μsec, while sample interval Δt for bone samples were 0.01 μsec.

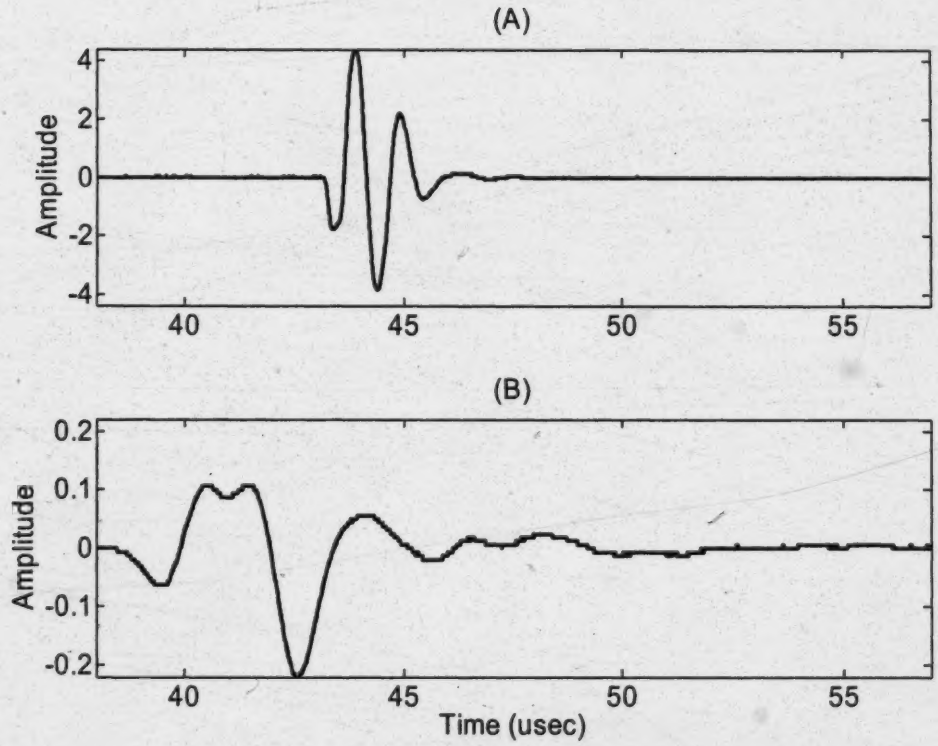

Figure 3.10 **A bone sample signal and water pulse: (A) water pulse through smaller tank and amplified by 34 dB. (B) Pulse through bone sample amplified by 54 dB.**

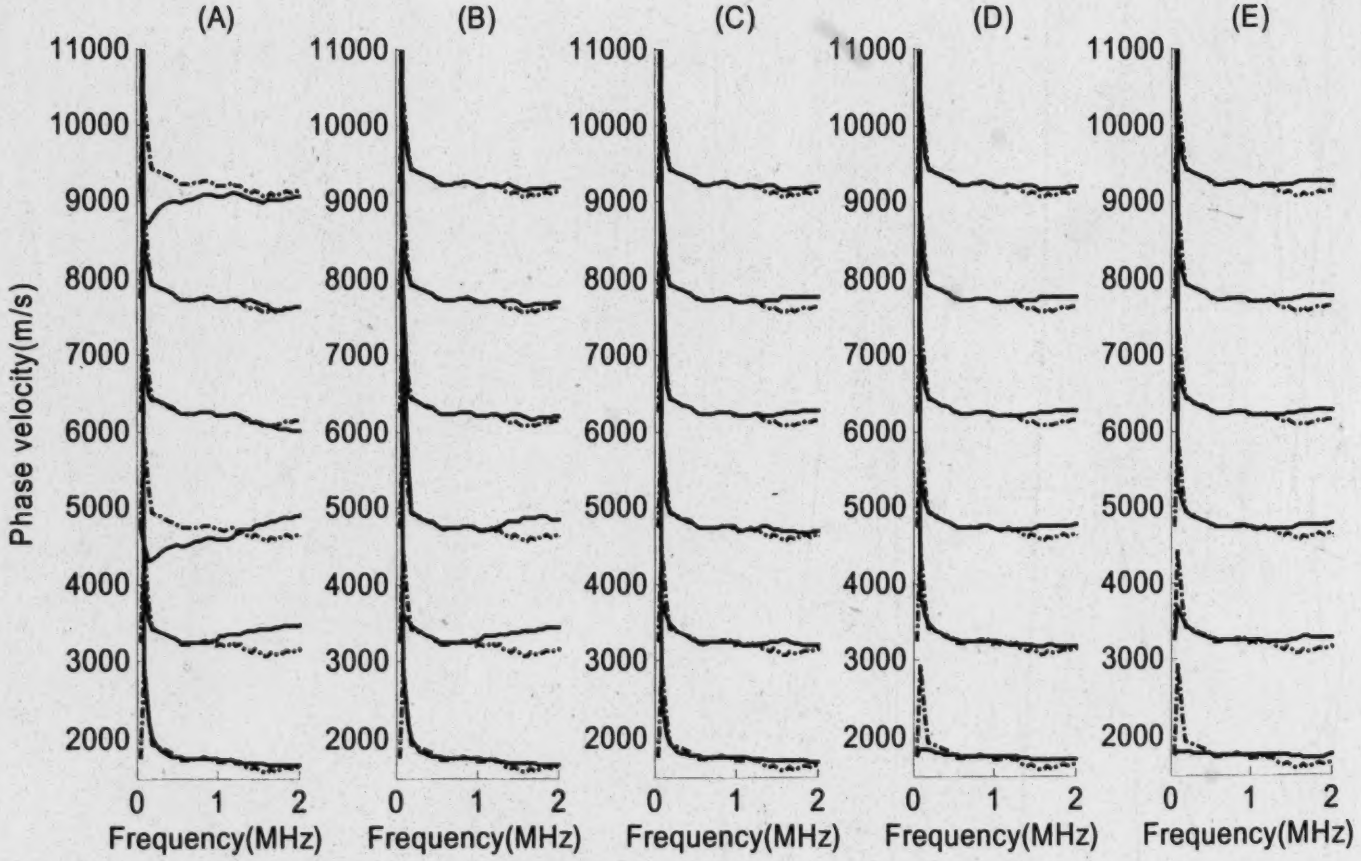

Figure 3.11 Effect of window length and window shape on dispersion: (A) ratio 0.2; (B) ratio 0.4; (C) ratio 0.6; (D) ratio 0.8; (E) ratio 1.0. Six window lengths were tested starting at 250 data points from the bottom and increase upward at interval of 250 data points.

3.4 Discussion of Results

In this section, the cross-correlation technique is applied to the bone data and the analysis results will be discussed. All bone sample data are discussed and displayed in chapter 2. The number in the figures in this section are slope of the dispersion curve in the effective frequency range, which is taken here as the range of frequency components having magnitude greater than 2/3 of the maximum magnitude in the magnitude spectrum. Magnitude spectrum of the corresponding bone samples are displayed in chapter 4. From the magnitude er spectrum, it can be found that the effective frequency range is very narrow for some signals.

The sold lines in those figures represent the portion of effective frequency range. The negative values represent negative dispersion, and positive values represent positive dispersion. For bovine trabecular bone in transverse direction (figure 3.12), three of the five 2.0 cm bone samples show negative dispersion, two of the five 1.5 cm bone samples show negative dispersion, two of the five 1.0 cm bone samples show negative dispersion, and seven of the ten 0.5 cm bone samples show negative dispersion. For bovine trabecular bone in axial direction (figure 3.13), none of the two 2.0 cm bone samples show negative dispersion, all two 1.5 cm bone samples show negative dispersion, none of the two 1.0 cm bone samples show negative dispersion, and two of the five 0.5 cm bone samples show negative dispersion. For pig trabecular bone in mixed direction (figure 3.14), all two 2.0 cm bone samples show negative dispersion, none of the two 1.5 cm bone samples show negative dispersion, one of the three 1.0 cm bone samples show negative dispersion, and four of the five 0.5 cm bone samples show negative dispersion.

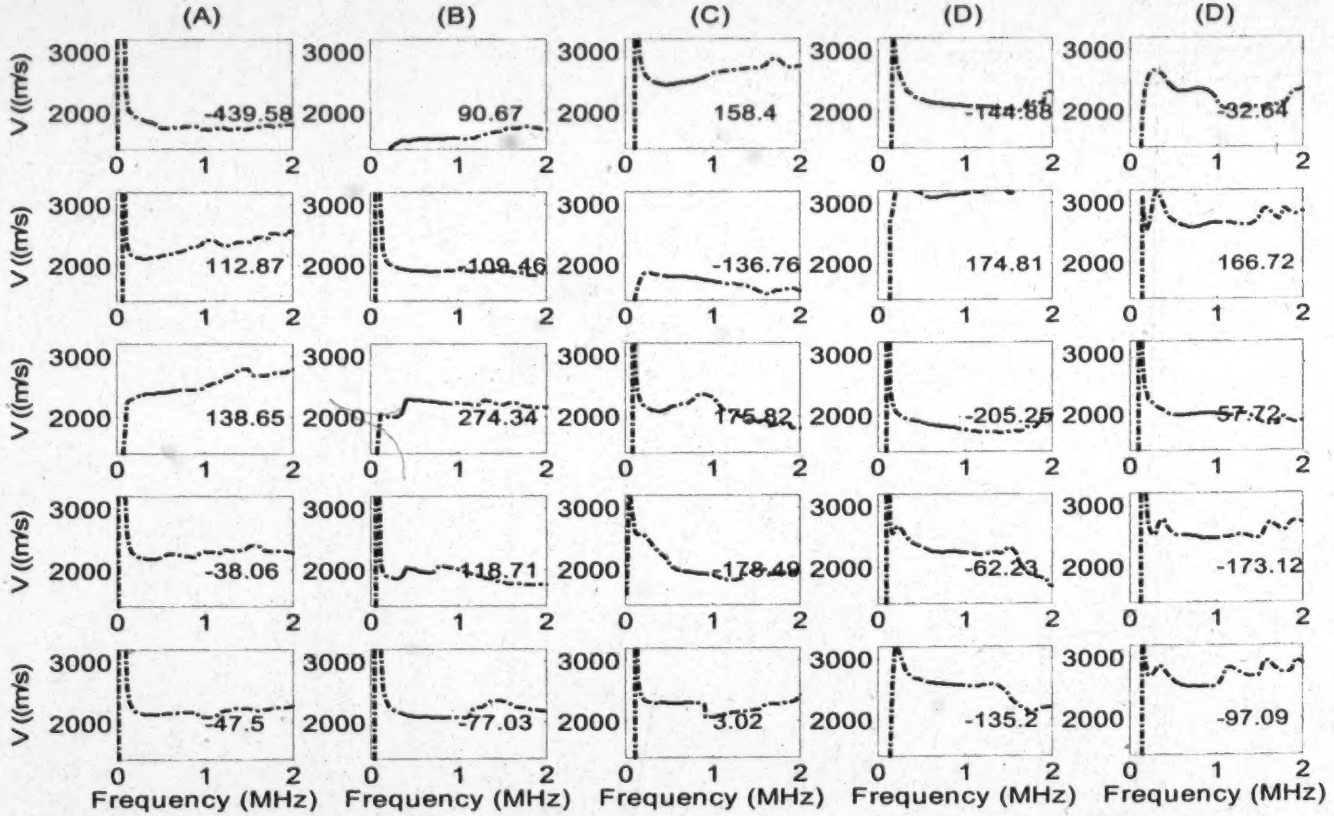

Figure 3.12 **Phase velocity of bovine trabecular bone of different thickness in transverse direction: (A) 2.0 cm. (B) 1.5 cm. (C) 1.0 cm. (D) 0.5 cm. The number in the figures indicates the slope of the dispersion curve in the effective frequency range.**

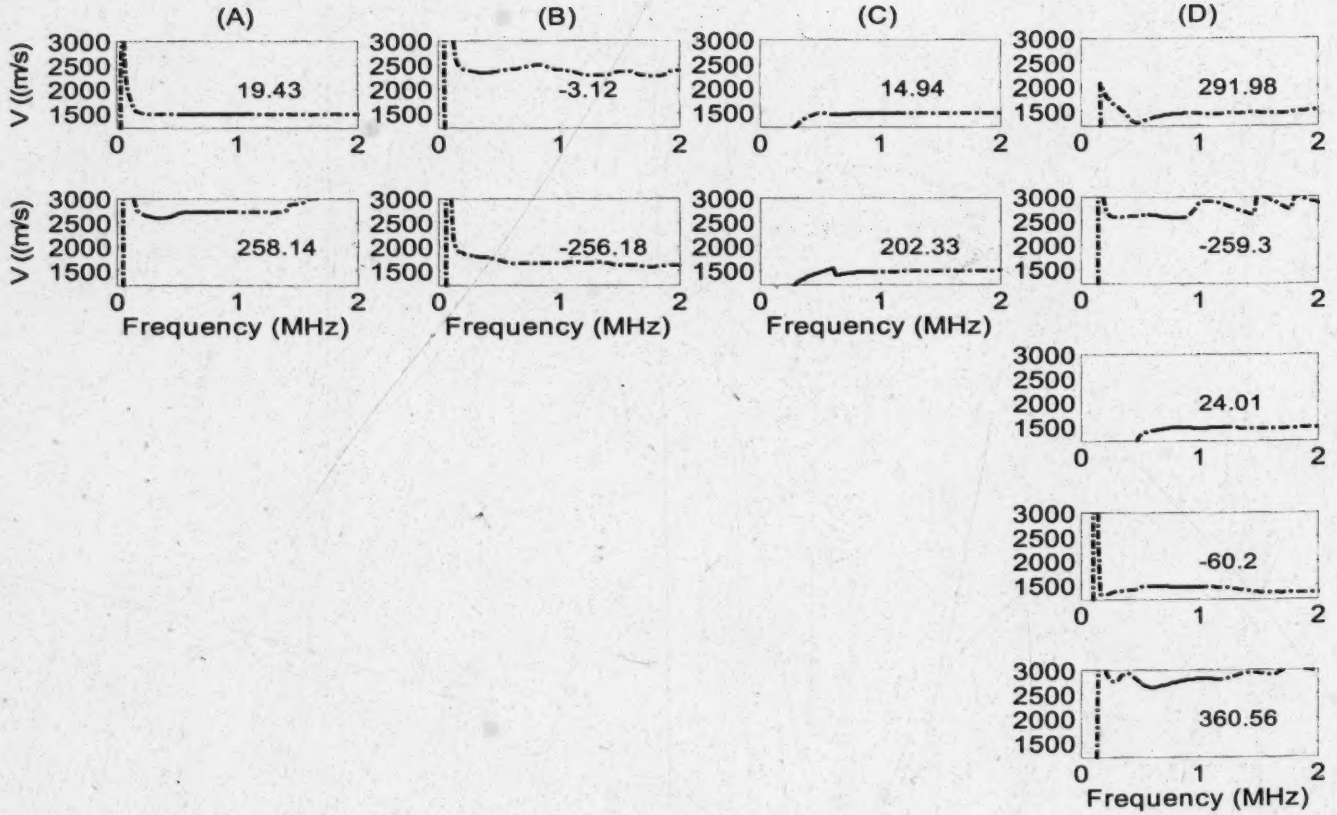

Figure 3.13 Phase velocity of bovine trabecular bone of different thickness in axial direction: (A) 2.0 cm. (B) 1.5 cm. (C) 1.0 cm. (D) 0.5 cm. The number in the figures indicates the slope of the dispersion curve in the effective frequency range.

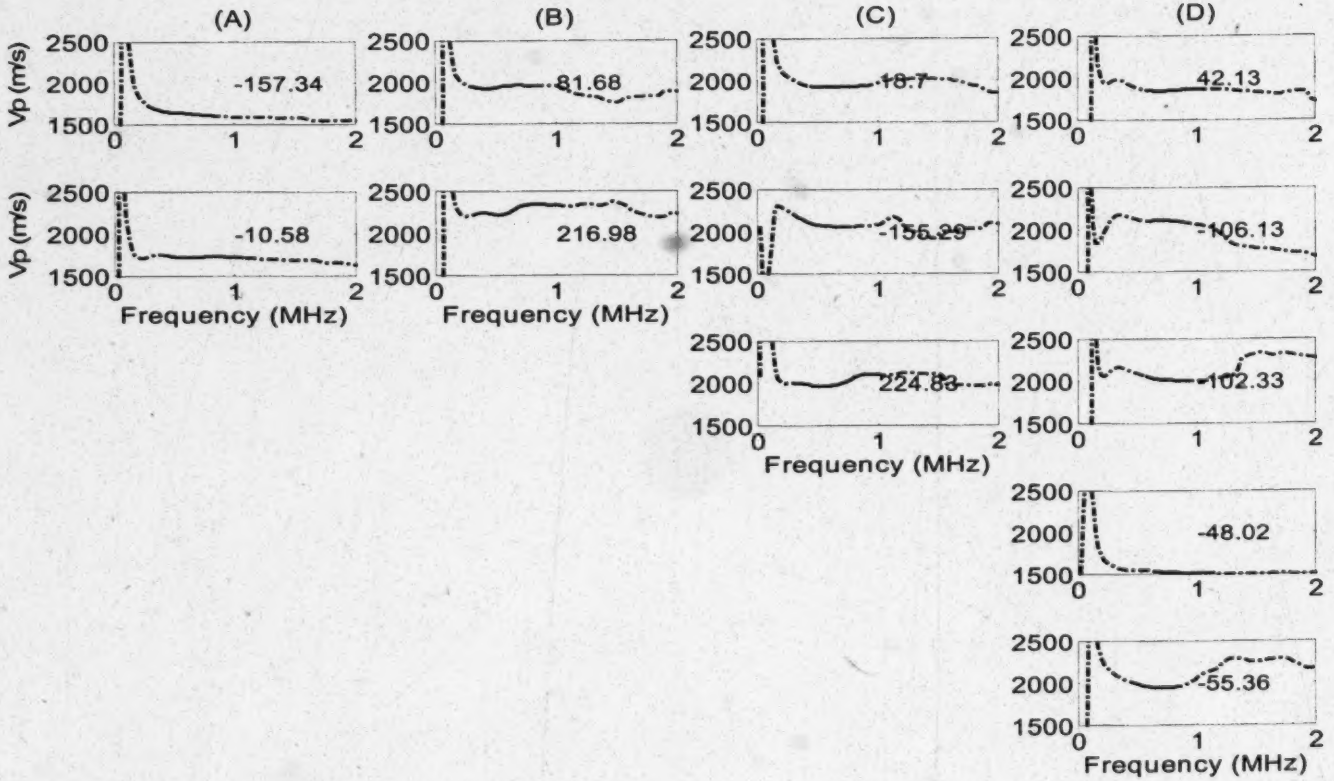

Figure 3.14 Phase velocity of pig trabecular bone of different thickness in mixed direction: (A) 2.0 cm. (B) 1.5 cm. (C) 1.0 cm. (D) 0.5 cm. The number in the figures indicates the slope of the dispersion curve in the effective frequency range.

It seems negative dispersion is more likely to happen when the thickness of bone sample becomes smaller in figure 3.12; however, no such trend exists for figures 3.13- figure 3.14. In these figures, the ratio of showing negative dispersion is high for larger thickness, then decreases when the thickness reduces, and increases again for the smallest thickness. Figure 3.15 shows the velocity of the four phantoms described in chapter 2. All 4 phantoms show negative dispersion. Figure 3.16 are their corresponding spectra.

The negative dispersion has been reported by many researchers and was assumed to relate to ultrasound scattering inside the trabeculae (Nicholson and Lower et al, 1996; Strelitzki and Evans, 1996; Droin and Uerger et al, 1998; Wear 2001). Dispersion has been summarized as the following categories (Sachse and Pao,1978): (1) geometric dispersion, caused by the presence of specimen boundaries, (2) material dispersion, caused by the frequency dependence of material constants, such as mass density, dielectric constants, elastic moduli, etc...(3) scattering dispersion, caused by the scattering of waves by densely distributed fine inhomogeneities in material; (4) dissipative dispersion, caused by the absorption or dissipation of wave energy into heat or other forms of energy in an irreversible process, (5) nonlinear dispersion, caused by the dependence of the wave speed on the wave amplitude. In fact, the dispersion of the bone samples is the combination of all these five sources of dispersion. Material dispersion, dissipative dispersion and nonlinear dispersion are common for almost all materials, and play important role in showing positive dispersion. Geometric dispersion and scattering dispersion are similar in mechanism and both are caused by the redirection of ultrasound energy by the inhomogeneities. The difference between the two is that the geometric dispersion is macroscopical and will result in coherence phase change, while the scattering dispersion is microscopical and will result in

random phase change. Therefore, the inhomogeneities contribute to the negative dispersions, with the plate-like trabeculae works like a specimen boundary.

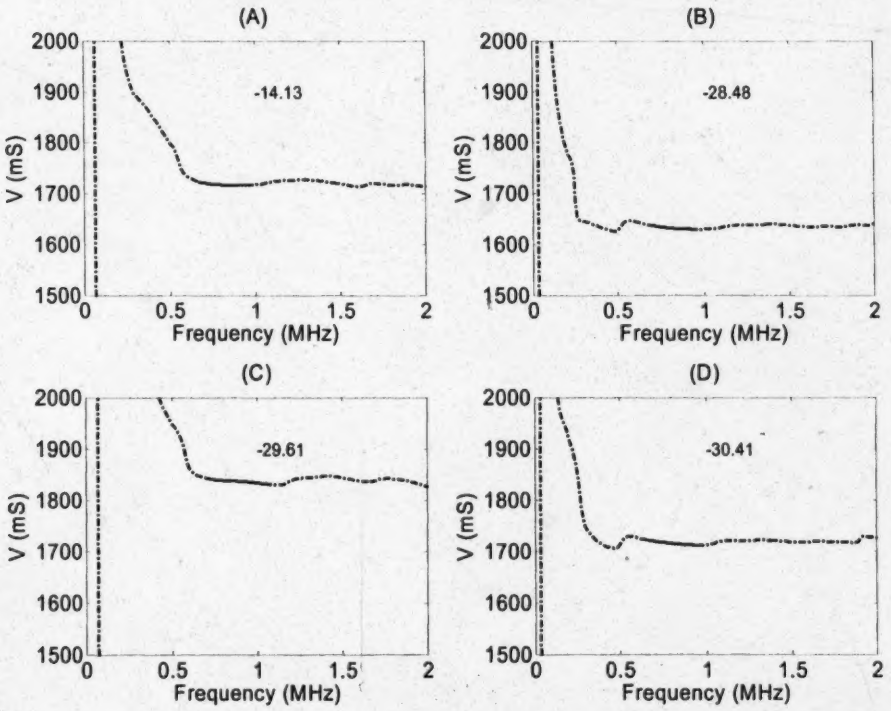

Figure 3.15 Phase velocity of corresponding phantoms in figure 2.17. Sample interval is 0.025 μsec, window length is 400 data points, and taper ratio is 0.6.

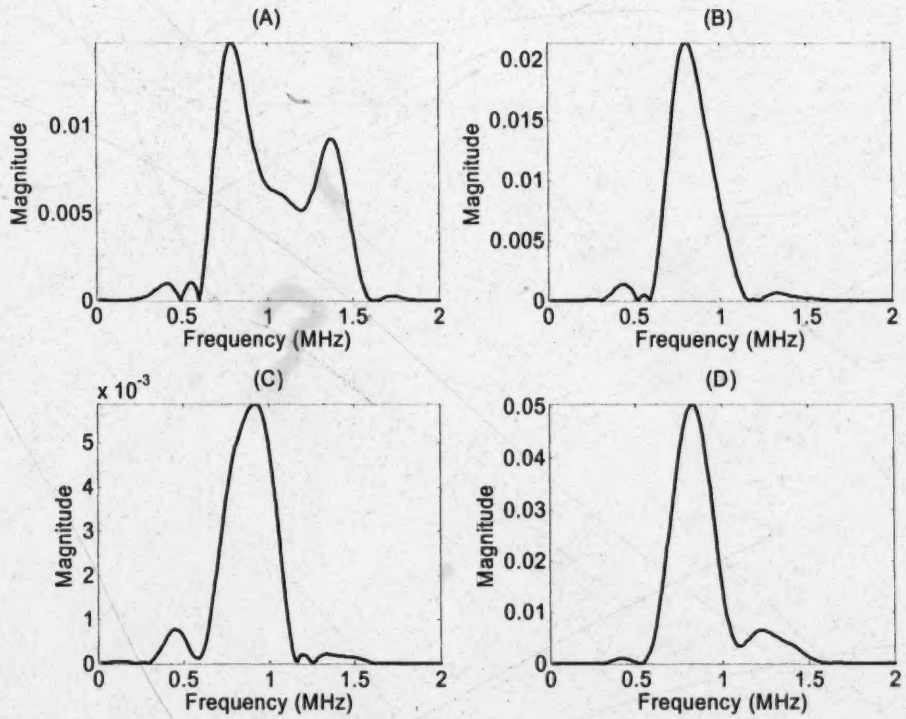

Figure 3.16 **Magnitude Spectra of corresponding phantoms in figure 2.17. Sample interval is 0.025 μsec, window length is 400 data points, and taper ratio is 0.6.**

Chapter 4

Estimation of Broadband ultrasound Attenuation (BUA)

4.1 Introduction

The energy loss of ultrasound beam through bone can be broadly categorized into two types: geometrical loss and intrinsic loss (Fitting and Adler, 1981). The first type includes reflection and refraction, wave guide effects, and beam spreading. In our experiment setup, the ultrasound beam is supposed to be perpendicular to the surface, so refraction and guide waves can be neglected. In addition, the distance that ultrasound travels within the bone sample is relatively short and the ultrasound beam is slightly divergent, so the beam spreading can also be neglected. The second type includes scattering and absorption. Both of these two energy loss mechanisms are inherent to the bone and contribute to the BUA discussed in this chapter. However, the first type of energy loss mechanisms, here mainly the reflection loss should be subtracted from the total energy loss in determining the absorption attenuation.

Scattering is due to the discontinuity inside the material and results in the redirection of ultrasound energy. This process in turn also results in extra chance of energy absorption, since the traveling length is increased. Absorption is the result of energy loss as heat, and can be caused by heat conduction in fluid or friction in solid. In heat conduction, Herzfeld and Litovitz (1959) provided the following explanation for a fluid. When a sound wave travels in the liquid, the liquid is subject to compression and expansion. At the moment of compression, the temperature will arise to one above the average, and due to the heat conduction, some of heat will diffuse into low temperature area. Accordingly, upon

re-expanding procedure, the compressed region will return less work than was expended on compressing them. A similar explanation applies to the recompression procedure of rarefaction regions. Thus, conduction of heat causes sound absorption in liquid.

4.2 Power Spectrum Estimation Technique

To estimate the attenuation of ultrasound in trabecualar bone, it is necessary estimate the power spectra of bone sample signal and reference signal. There are several methods to estimate the power spectrum. Some of the methods will be discussed briefly below.

4.2.1 Periodogram Technique

Assume $x(n)$ is N point signal, to calculate the energy that lies in any frequency band, we can isolate the portion of the signal within that frequency band by passing it through an ideal band-pass filter like

$$H(\omega)=\begin{cases}1, & \omega\in\Omega\\ 0, & \text{otherwise}\end{cases}. \tag{4.1}$$

Then, the energy of the filtered signal is the energy that the original signal contains in the frequency band Ω. If we repeat the computation for all frequency bands Ω, we will have an energy density function via the frequency variable ω.

The Fourier Transfer of the original signal can be expressed as

$$X(\omega)=\sum_{n=0}^{N-1}x(n)e^{-j\omega n}. \tag{4.2}$$

Then, an estimate of the energy spectrum density corresponding to the frequency band Ω can be obtained by

$$I=\int_{\Omega}\left|X(\omega)\right|^2 d\omega. \tag{4.3}$$

The energy spectrum density can also be scaled to obtain the power spectrum density by

$$\hat{S}(\omega) = \frac{1}{N}\left|X(e^{j\omega})\right|^2 . \tag{4.4}$$

The estimator is called periodgram (Roberts and Mull, 1987).

4.2.2 Indirect Estimation from Autocorrelation Function

If low order elements of the autocorrelation sequence of a signal are estimated independently, such as

$$\hat{r}(k) = \frac{1}{L}\sum_{l=0}^{L-1-k} y(k+l)y(l),\ 0 \le k \le N < L . \tag{4.5}$$

Then, the spectrum given by:

$$\hat{S}(\omega) = \sum_{k=-N}^{N} \hat{r}(k)e^{-jk\omega} \tag{4.6}$$

becomes the estimate of the power spectrum of signal $y(n)$, which is often called the Blackman-turkey estimate (Roberts and Mull, 1987).

4.2.3 Sinusoidal data fitting

If the spectrum of a signal is a linear spectrum, that is, in an extreme case that all signal power is concentrated on a finite set of the frequency components, it must consist of sinusoids at those frequencies. Then such a signal can be represented by

$$y(k) = \sum_{i=1}^{m} A_i \cos(k\omega_i + \phi_i) . \tag{4.7}$$

Each frequency component is characterized by 3 parameters: frequency, phase and amplitude. When those three parameters are known for all components, the power spectrum can be estimated by

$$\hat{S}(\omega) = \lim_{L\to\infty}\sum_{l=0}^{L-1} y(k+l)y(l) = \sum_{i=1}^{m}\frac{A_i^2}{2}\cos(k\omega_i) . \tag{4.8}$$

To obtain those parameters, the classical way is using Gaussian least-square method. For a signal $y[0,L-1]$ of m frequency components, set up a function

$$V(A_1, A_2 \cdots, A_m, \omega_1, \cdots \omega_m, \phi_1, \cdots \phi_m) = \sum_{k=0}^{L-1} \varepsilon(k)^2 , \tag{4.9}$$

where

$$\varepsilon(k) = y(k) - \sum_{i=1}^{m} A_i \cos(k\omega_i + \phi_i) . \tag{4.10}$$

When the function is minimum, the error is the smallest, and a best fitting of these parameter is obtained. The function V is not linear in the frequency and phase, which makes it difficult to minimize.

4.3 Reflection power loss and attenuation

When an ultrasound beam encounters the interface between bone sample and water, additional energy loss occurs due to transmission through the interfaces and this energy loss should be subtracted when calculating absorbed energy loss of the bone sample.

Since in our experiment setup, the ultrasound beam is perpendicular to the surface of bone sample, we only consider normal incidence in the plane interface. The two materials beside the interface are cancellous bone and water, whose density and ultrasound velocity are ρ_b, V_b and ρ_w, V_w respectively. Then the coefficients of reflection and transmission (incidence from water to cancellous bone) are defined as:

$$R = \frac{p_R}{p_I} = \frac{Z_b - Z_w}{Z_b + Z_w}, \tag{4.11}$$

$$T = \frac{p_T}{p_I} = \frac{2Z_b}{Z_b + Z_w} . \tag{4.12}$$

where $Z_b = \rho_b \cdot V_b$ is the acoustic impedance of cancellous bone, $Z_w = \rho_w \cdot V_w$ is the acoustic impedance of water; p_I is the sound pressure of incident wave, p_R is the sound pressure of reflected wave, p_T is the sound pressure of transmitted wave (Krautkämer and Krautkämer et. al, 1983).

Once the reflection and transmission coefficients are known, the decrease of the transmitted amplitude compared with the incident can be calculated. In our experimental setup, the ultrasound beam travels through two interfaces. In the first interface, ultrasound beam transits from water to cancellous bone, the corresponding decrease of the transmitted wave amplitude compared with incident wave amplitude is:

$$A_{wb} = 20\log\frac{p_T}{p_I} = 20\log\frac{2Z_b}{Z_b + Z_w} dB\,. \tag{4.13}$$

In the second interface, ultrasound beam travels from cancellous bone to water, the corresponding decrease of the transmitted wave amplitude compared with first transmitted wave amplitude is:

$$A_{bw} = 20\log\frac{p_{T_2}}{p_T} = 20\log\frac{2Z_w}{Z_b + Z_w} dB\,. \tag{4.14}$$

Therefore, the total decrease of the second transmitted wave amplitude compared with incident wave amplitude due to the transmission loss through the interface is:

$$A_{wb} + A_{bw} = 20\log\frac{2Z_b}{Z_b + Z_w} + 20\log\frac{2Z_w}{Z_b + Z_w} = 20\log\frac{4Z_wZ_b}{(Z_b + Z_w)^2} dB\,. \tag{4.15}$$

However, when we compare the bone sample signal and water reference signal, the attenuation include not only the above reflection loss but also the intrinsic absorption of the cancellous bone. The total decrease of the transmitted wave amplitude compared with the incident wave is:

$$A = A_{wb} + A_{bw} + A_{absorp} \tag{4.16}$$

where A_{absorp} is the attenuation of ultrasound through the bone sample. In the dispersive cancellous bone, the total decrease can be calculated using power density estimation technique given by

$$A(f) = 20\log(\frac{A_s(f)}{A_r(f)}), \tag{4.17}$$

where, $A_r(f)$ is the magnitude of corresponding frequency component of the reference signal, and $A_s(f)$ is the magnitude of corresponding frequency component in the bone sample signal.

Then what we want to get, A_{absorp} , corresponds to the Broadband Ultrasound Attenuation if divided by frequency, or corresponds to the normalized Broadband Ultrasound Attenuation if divided by frequency and sample width:

$$\begin{aligned} A_{absorp} &= A - (A_{wb} + A_{bw}) \\ &= 20\log(\frac{A_s(f)}{A_r(f)}) - 20\log\frac{4Z_wZ_b}{(Z_b + Z_w)^2}\, dB \end{aligned} \tag{4.18}$$

If we know the acoustic impedance of the cancellous bone and water, it is easy to calculate transmission loss. In the literature, density and velocity have been reported. Some of the values will be used to calculate BUA and compared with our experimental results. However, it is not easy to get the acoustic impedance of cancellous bone directly using our experimental setting, but luckily reflection coefficient can be obtained approximately from the experiment data.

Using the echo mode of acquisition, the signal reflected from the water/bone interface can be measured with a single transducer. By keeping the water/bone interface perpendicular to and in the middle of the two transducers, the ultrasound absorption in water

will be the same for the reference signal and echoed signal, since they travel the same distance in water. Then apply power density estimation technique on the echo signal and water reference signal, we can get the reflection decay

$$Atten_R(f) = 20\log(\frac{A_R(f)}{A_r(f)}), \tag{4.19}$$

where, $A_r(f)$ is the magnitude of corresponding frequency component of reference signal, and $A_R(f)$ is the magnitude of corresponding frequency component in bone sample echo signal.

At the boundary, according to the continuity of pressure, the following condition should be satisfied:

$$1+R=T. \tag{4.20}$$

Even the acoustic impedances of cancellous bone and water are unknown, as long as the reflection coefficient can be obtained in some way, the transmission coefficient can be calculated, vice versa. In this thesis, we care about only the transmission loss, which means the decay of signal due to reflections at two interface, although we can calculate transmission coefficient, it is not necessary, since we can obtain the transmission loss by

$$\begin{aligned} A_{wb} + A_{bw} &= 20\log\frac{4Z_wZ_b}{(Z_b+Z_w)^2} \\ &= 20\log\left[\frac{Z_b^2+2Z_wZ_b+Z_w^2}{(Z_b+Z_w)^2} - \frac{Z_b^2-2Z_wZ_b+Z_w^2}{(Z_b+Z_w)^2}\right]. \\ &= 20\log\left[1-\left(\frac{Z_b-Z_w}{Z_b+Z_w}\right)^2\right] = 20\log\left[1-R^2\right] \end{aligned} \tag{4.21}$$

Where R is the reflection coefficient at the interface between bone and water and can be calculated by

$$R = \frac{A_R(f)}{A_r(f)}. \tag{4.22}$$

Therefore, the final expression of absorption decay can be written as:

$$\begin{aligned} A_{absorp} &= 20\log(\frac{A_s(f)}{A_r(f)}) - 20\log\frac{4Z_wZ_b}{(Z_b+Z_w)^2} \\ &= 20\log(\frac{A_s(f)}{A_r(f)}) - 20\log(1-R^2) \\ &= 20\log(\frac{A_s(f)}{A_r(f)}) - 20\log\left[1-\left(\frac{A_R(f)}{A_r(f)}\right)^2\right]. \end{aligned} \tag{4.23}$$

To eliminate the water attenuation effect and get a correct reflection coefficient, the bone sample should be correctly positioned so that the echo interface is perpendicular to the ultrasound beam and in the exact middle of the two transducers. In this way, the ultrasound travels the same distance in the water for both echo signal and transmission water reference.

The density of solid trabeculae $\rho_{trabeculae}$, 1960kg/m^3, the density of marrow ρ_{marrow}, 930kg/m^3, and volume fraction, 0.17, 0.19, 0.25 have been used in research of Biot's theory (Hosokawa and Otani, 1996). The density of cancellous bone is here given by

$$\rho_{cancellous} = \rho_{trabeculae} \cdot \alpha_{trabeculae} + \rho_{marrow} \cdot (1-\alpha_{trabeculae}). \tag{4.24}$$

Then we use these parameters to approximately estimate the reflection coefficient and the transmission loss. Although these parameters are expected to vary from those of the bone samples being examined, we still hope the calculated results can provide some valuable comparison, in the case of lack of correct transmission loss.

4.4 Discussion of results

In our experiment, since the signal through bone sample is too weak, a preamplifier was used. Water pulses were amplified by 34 dB, while bone signals were amplified by 54 dB. Therefore, $54-34=20dB$ correction should be applied to the final BUA results.

Figure 4.1 display the power spectra of bovine bone signals in transverse direction, calculated using auto-correction technique. The tapering window is 1001 data point Tukey window with tapering portion $r= 0.6$. We can see from the figures that the dominant energy shifts to lower frequency as the bone sample thickness increase, showing rapid absorption in higher frequency. The same algorithm is used to remove the DC components, that is calculating the average of the time signal then subtracting this average from the whole signal.

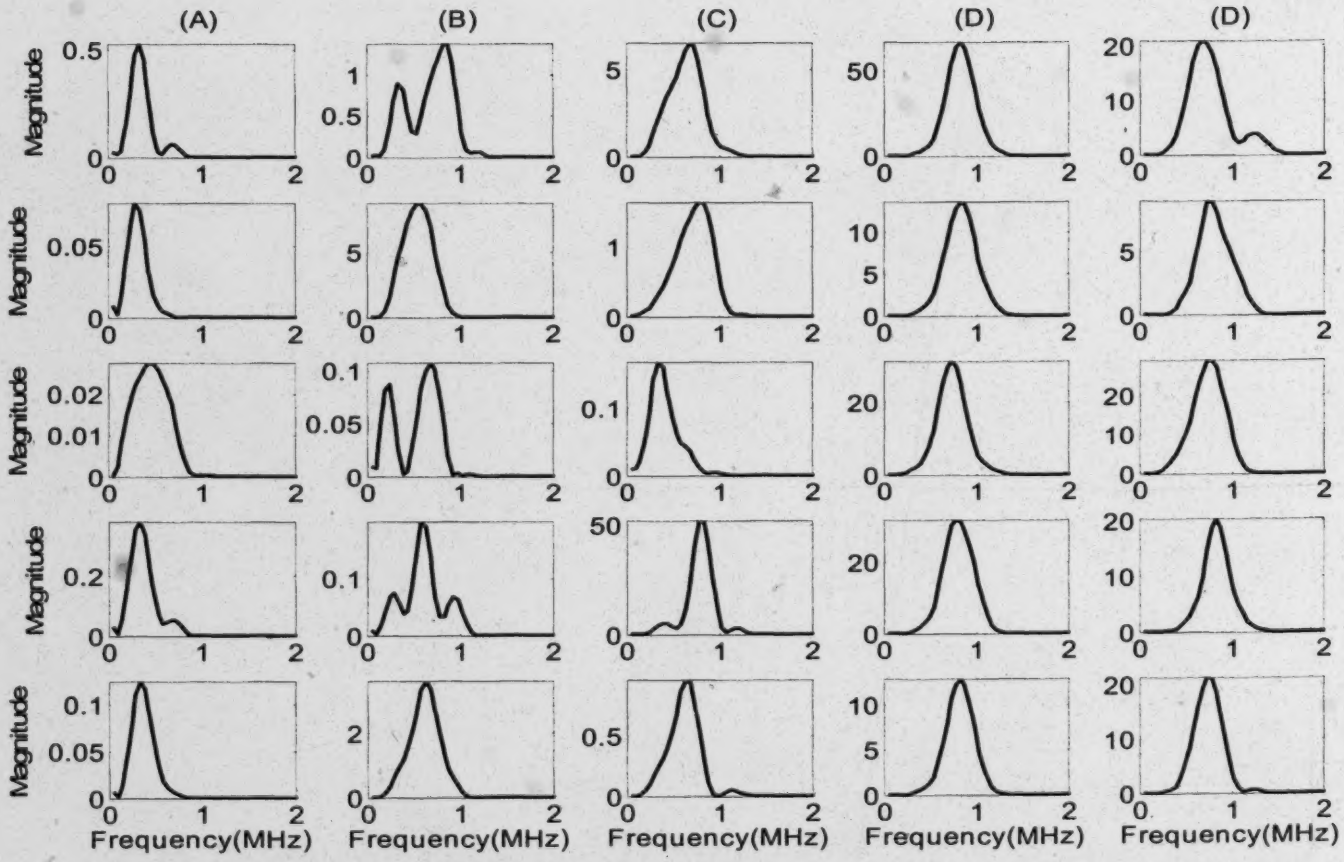

Figure 4.1 The power spectra of bovine bone signals of different thickness in transverse direction: (A) 2.0 cm. (B) 1.5 cm. (C) 1.0 cm. (D) 0.5 cm.

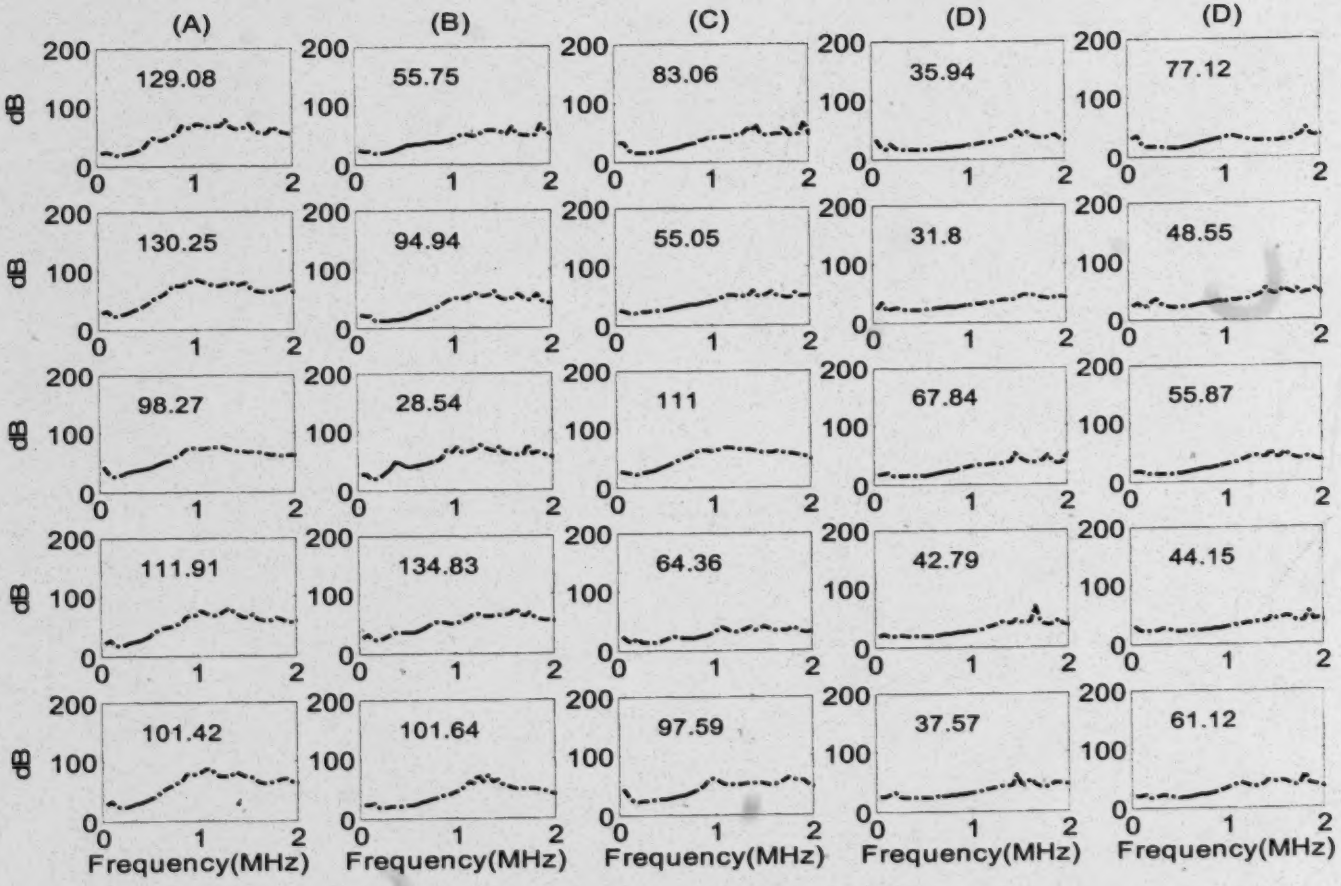

Figure 4.2 The BUA of bovine bone sample signals of different thickness in transverse direction: (A) 2.0 cm. (B) 1.5 cm. (C) 1.0 cm. (D) 0.5 cm.

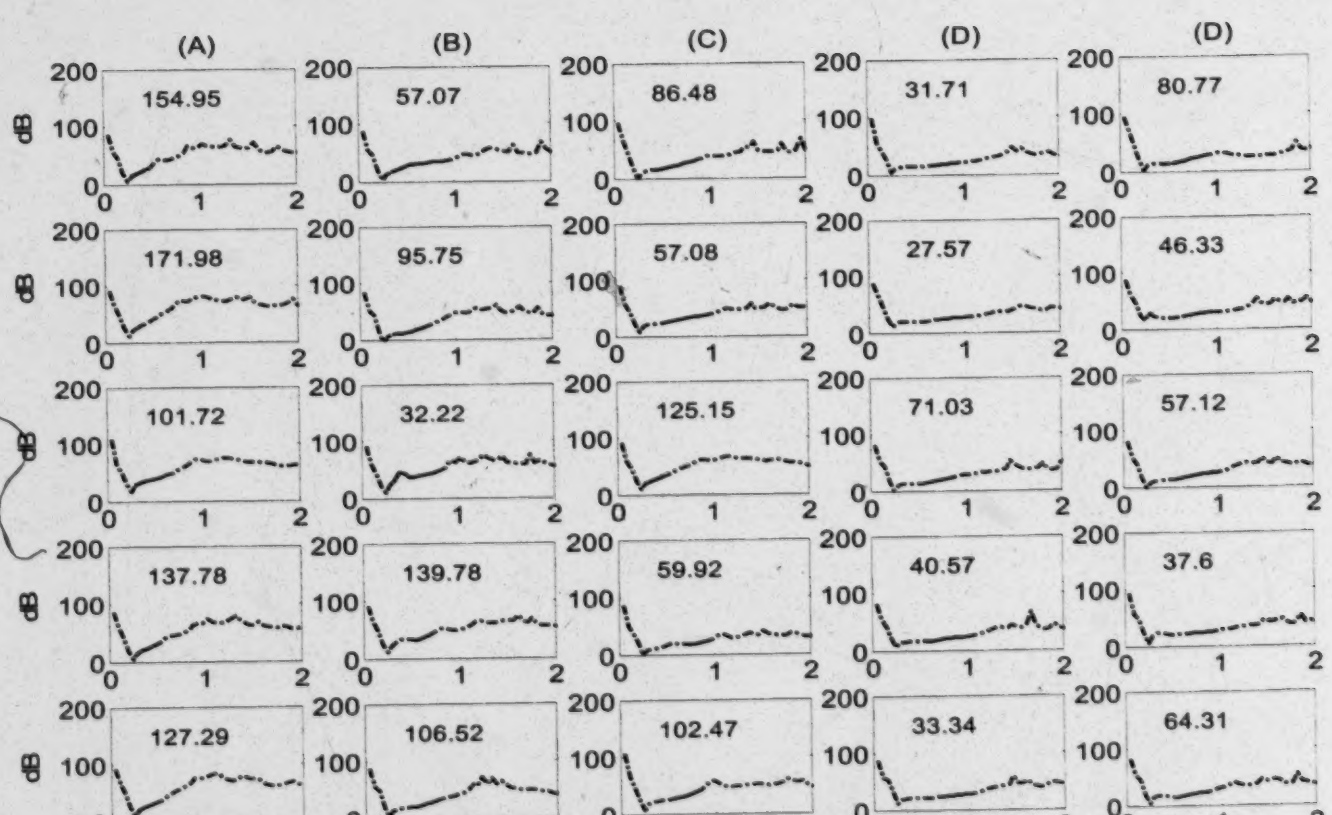

Figure 4.3 The BUA of bovine bone sample signals of different thickness in transverse direction (transmission loss corrected): (A) 2.0 cm. (B) 1.5 cm. (C) 1.0 cm. (D) 0.5 cm.

Figure 4.2 display the energy loss of bovine bone sample signals in transverse direction compared with water reference signal. The value in the figure is the slope, and the solid line is the portion used to do this calculation, which in turn depends on the effective frequency range. Equation (4.17) $A(f) = 20\log(\frac{A_s(f)}{A_r(f)})$ is used in this procedure, where, $A_r(f)$ is the magnitude of corresponding frequency component reference signal, and $A_s(f)$ is the magnitude of corresponding frequency component in bone sample signal. Therefore, the calculated energy loss includes the transmission loss and absorption. As the bone sample thickness increase, the linear portion of attenuation curve shift to lower frequency and at the same time become steeper. The 20dB amplification difference has been corrected.

Figure 4.3 displays the transmission loss corrected energy loss of bovine bone sample signals in transverse direction compared with water reference signal. The value in the figure is the slope, also BUA. The solid line is the portion used to do this calculation. The corrected energy loss is calculated using equation (4.23), with the second term in the right side representing transmission loss. Here we use only one bone sample to calculate the transmission loss and apply it to the whole group, hoping that interface of same kind of bone and same direction will produce same energy loss. The curves don't change much except some obvious change in the lower frequency. Compared with figure 4.2, some slopes increase while others decrease, depending on the effective frequency range used to calculate the slope.

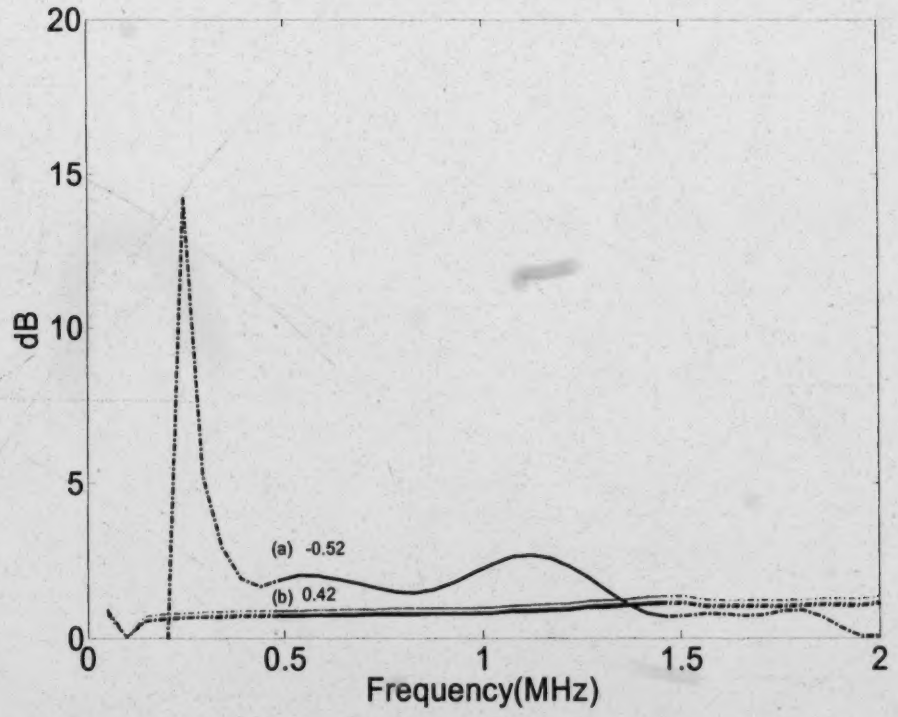

Figure 4.4 **The transmission loss of one bovine bone sample. (a) is obtained using the echo signal; (b) is the results calculated from literature parameter, using equation (4.15).**

Figure 4.4 displays the transmission loss of a bovine bone sample with thickness being 2.0 cm in transverse direction. To calculate the transmission loss, echo from the water/bone interface is acquired and isolated to do power density estimation, which is then compared to the power density estimation of water reference signal to obtain the reflection coefficient, which finally goes into equation (4.23) to calculate the transmission loss. The result is compared with results calculated from acoustic impedances. Density of bone is calculated for volume fraction, 0.17, 0.19, 0.25, the velocity is the phase velocity in those bone samples, and then equation (4.21) is used to calculate the transmission loss. Since the densities of three different combinations are similar, the three results are almost same and nearly coincident in the figure. As shown in the figure, the results calculated from acoustic impedances are smaller than that calculated from echo in the effective frequency range, and may indicate that the bone volume fraction should be larger.

Figure 4.5 displays the power spectrum of pig bone signals in mixed direction, calculated using auto-correction technique. The tapering window is 1001 data point Tukey window with tapering portion r=0.6. We can see from the figure that the dominant energy shift to lower frequency as the bone sample thickness increases, showing rapid absorption in higher frequency.

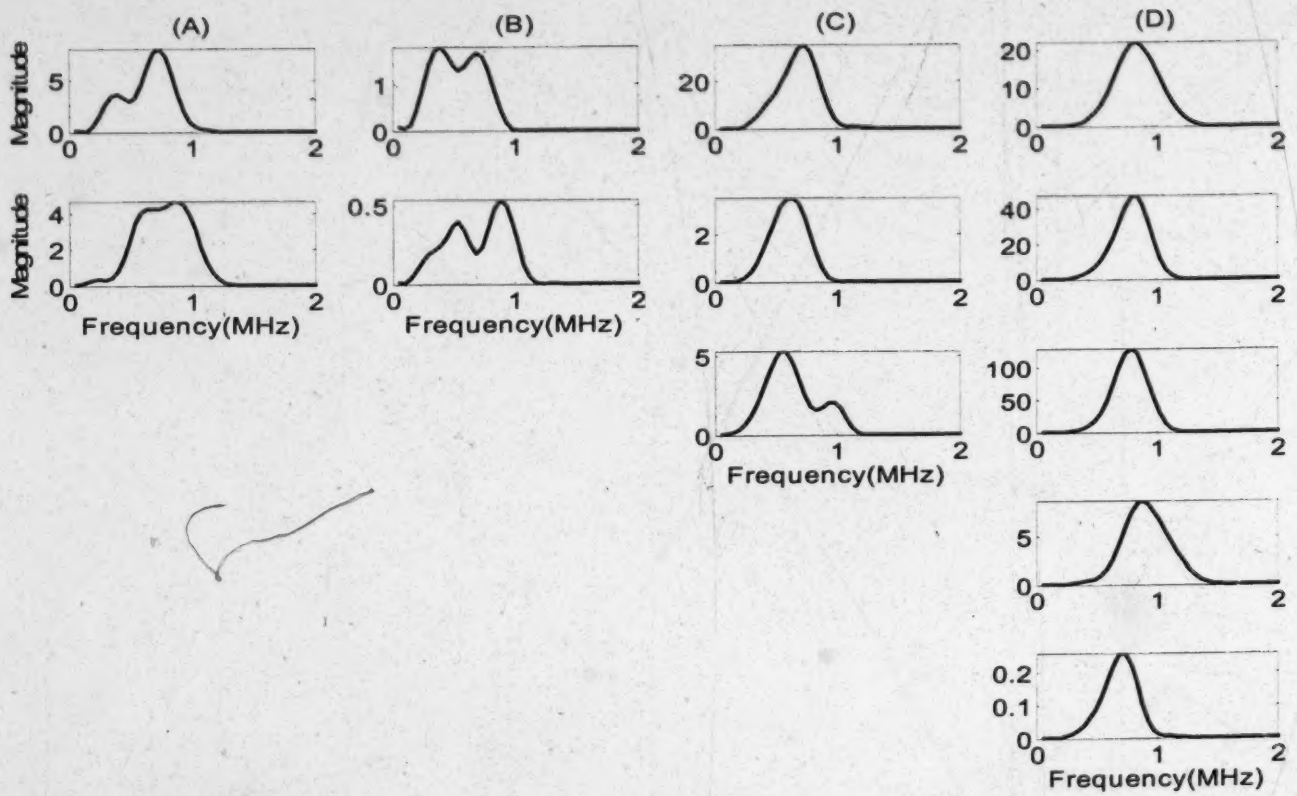

Figure 4.5 The power spectrum of pig bone signals of different thickness in mixed directions: (A) 2.0 cm. (B) 1.5 cm. (C) 1.0 cm. (D) 0.5 cm.

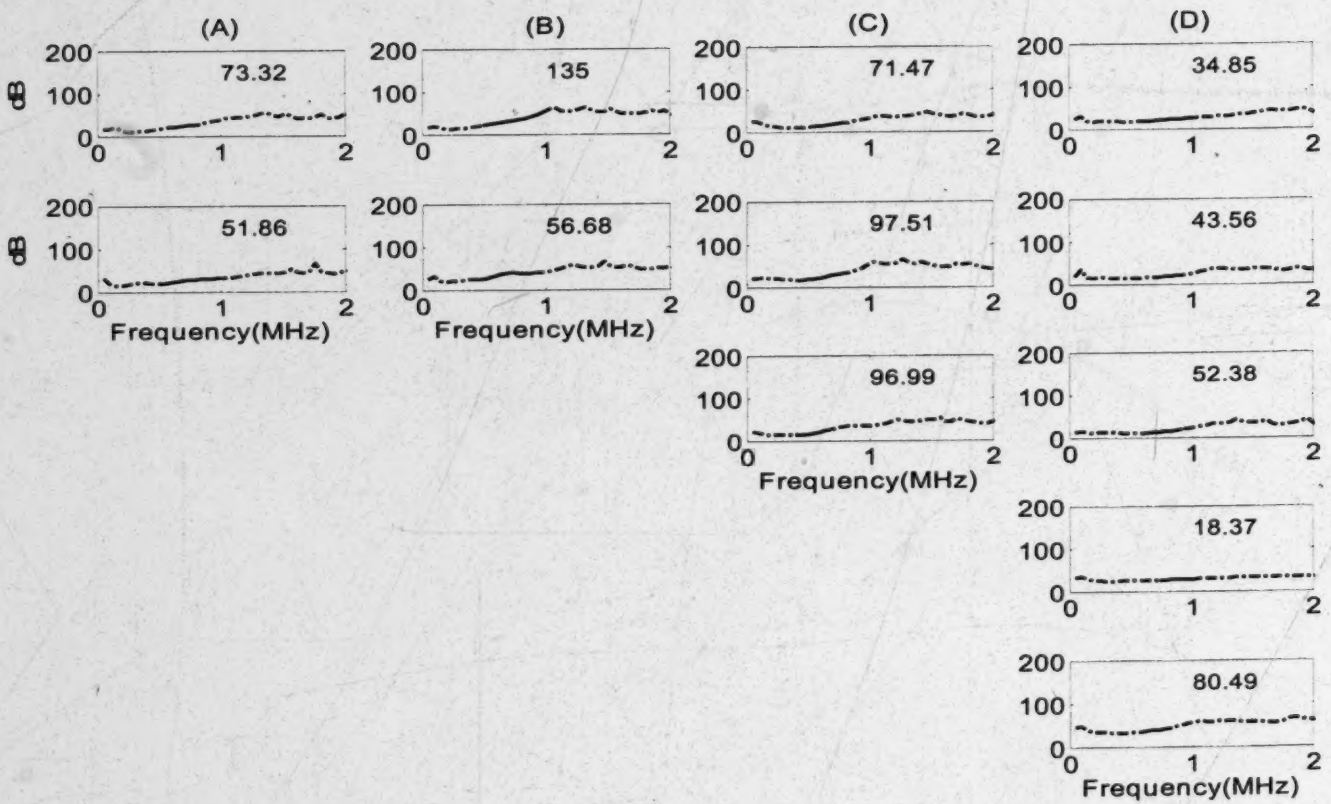

Figure 4.6 The BUA of pig bone sample signals of different thickness in mixed directions: (A) 2.0 cm. (B) 1.5 cm. (C) 1.0 cm. (D) 0.5 cm.

Figure 4.6 displays the energy loss of pig bone sample signals in mixed direction, compared with water reference signal. Equation (4.17) $A(f) = 20\log(\frac{A_s(f)}{A_r(f)})$ is used in this procedure, where, $A_r(f)$ is the magnitude of corresponding frequency component reference signal, and $A_s(f)$ is the magnitude of corresponding frequency component in bone sample signal. Therefore, the calculated energy loss includes the transmission loss and absorption. As the bone sample thickness increase, the linear portion of attenuation curve shift to lower frequency and at the same time become steeper. The 20dB amplification difference has been corrected.

Figure 4.7 displays the transmission loss corrected energy loss of pig bone sample signals in mixed direction compared with water reference signal. The corrected energy loss is calculated using equation (4.23), with the second term in the right side representing transmission loss. Here we use only one bone sample to calculate the transmission loss and apply it to the whole group, hoping that interface of same kind of bone and same direction will produce same energy loss. Compared with figure 4.6, some slopes increase while others decrease, depend on the effective frequency range used to calculate the slope.

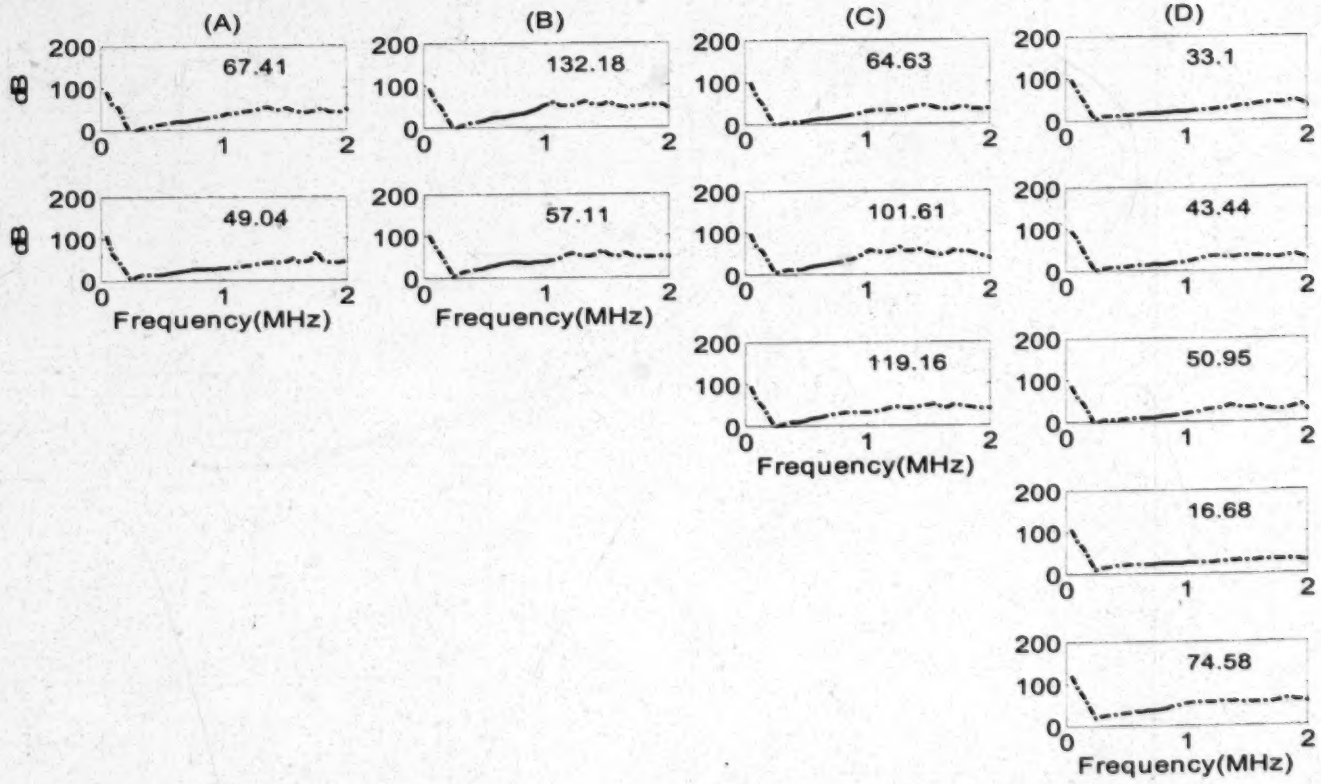

Figure 4.7 The BUA of pig bone sample signals of different thickness in mixed directions (transmission loss corrected): (A) 2.0 cm. (B) 1.5 cm. (C) 1.0 cm. (D) 0.5 cm.

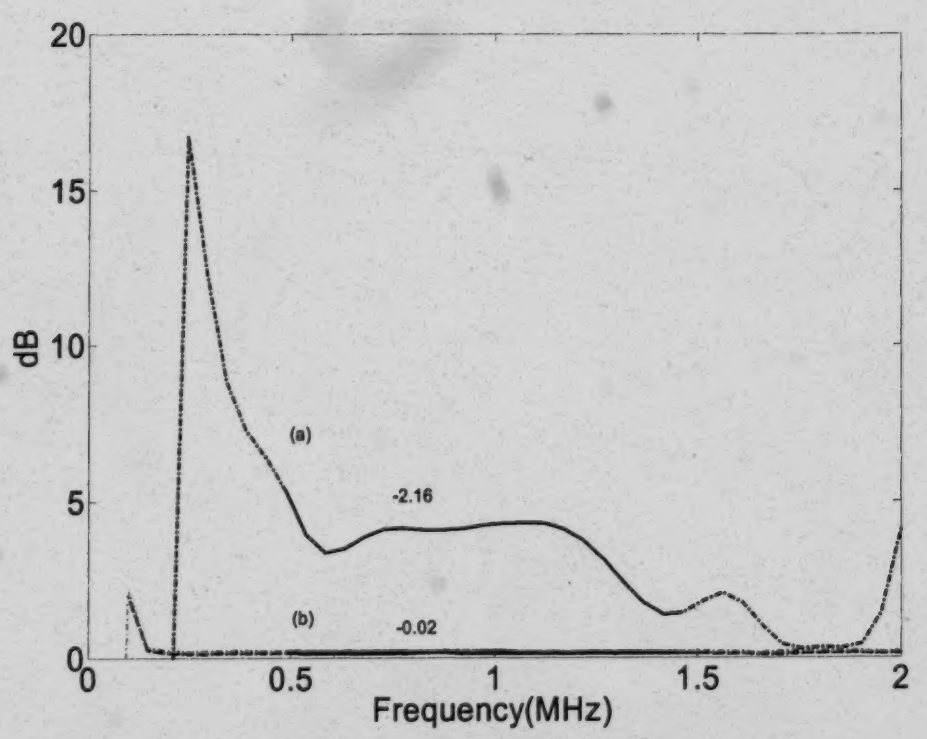

Figure 4.8 The transmission loss of one pig bone sample. (a) is obtained using the echo signal; (b) is the results calculated from literature parameter, using equation (4.15).

Figure 4.8 displays the transmission loss of one pig bone sample with thickness being 2.0 cm in mixed direction. To calculate the transmission loss, echo from the water/bone interface is acquired and isolated to do power density estimation, which is then compared to the power density estimation of water reference signal to obtain the reflection coefficient, which finally goes into equation (4.23) to calculate the transmission loss. . The result is compared with results calculated from acoustic impedances. Density of bone is calculated for volume fraction, 0.17, 0.19, 0.25, the velocity is the phase velocity in those bone samples, and then equation (4.21) is used to calculate the transmission loss. Since the densities of three different combinations are similar, the three results are almost same and nearly coincident in the figure. As shown in the figure, the results don't agree at all in the effective frequency range, basically it is because that the density and volume fraction is come from bovine bone and it is not comparable with that of pig bone.

Figure 4.9 displays the power spectrum of bovine bone signals in axial direction, calculated using auto-correction technique. The tapering window is 1001 data point Tukey window with tapering portion r= 0.6. We can see from the figure that the dominant energy shifts to lower frequency as the bone sample thickness increase, showing rapid absorption in higher frequency. There is DC component remain in the first figure, caused by the erratic waveform.

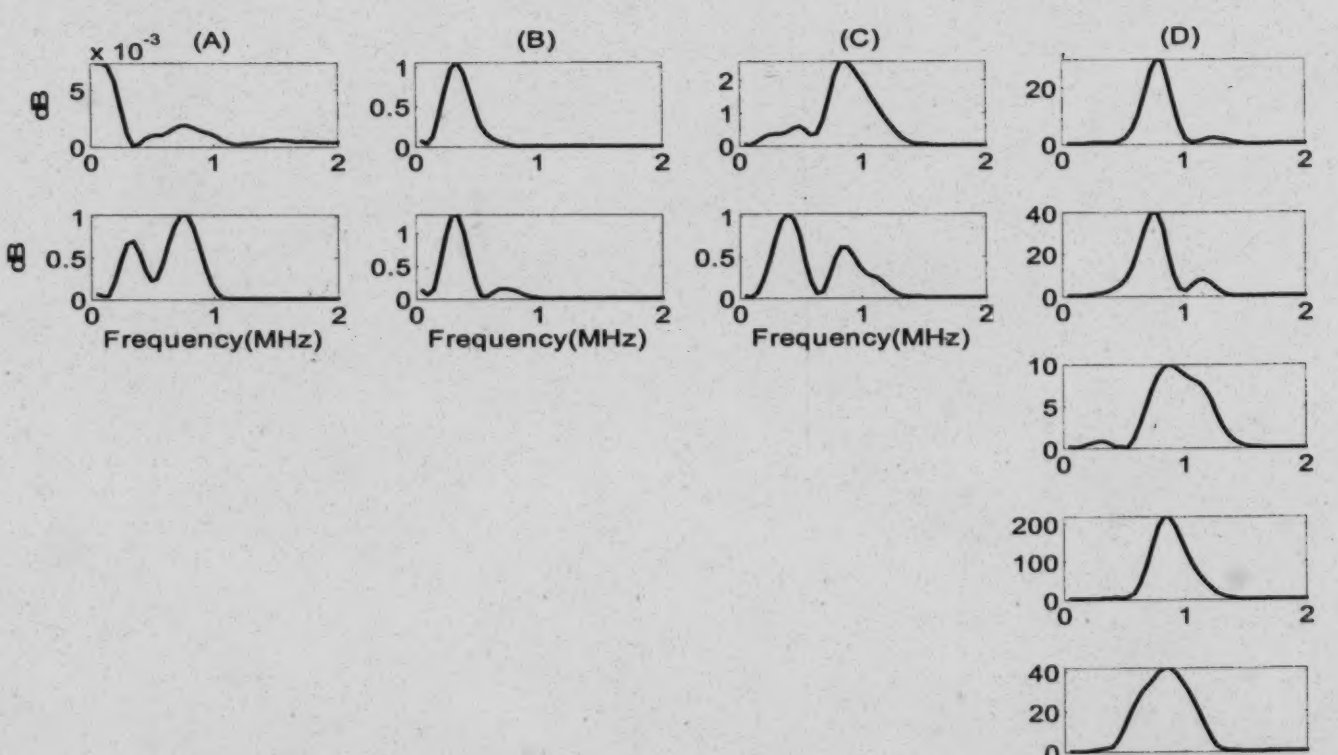

Figure 4.9 **The power spectrum of bovine bone signals of different thickness in axial direction:(A) 2.0 cm. (B) 1.5 cm. (C) 1.0 cm. (D) 0.5 cm.**

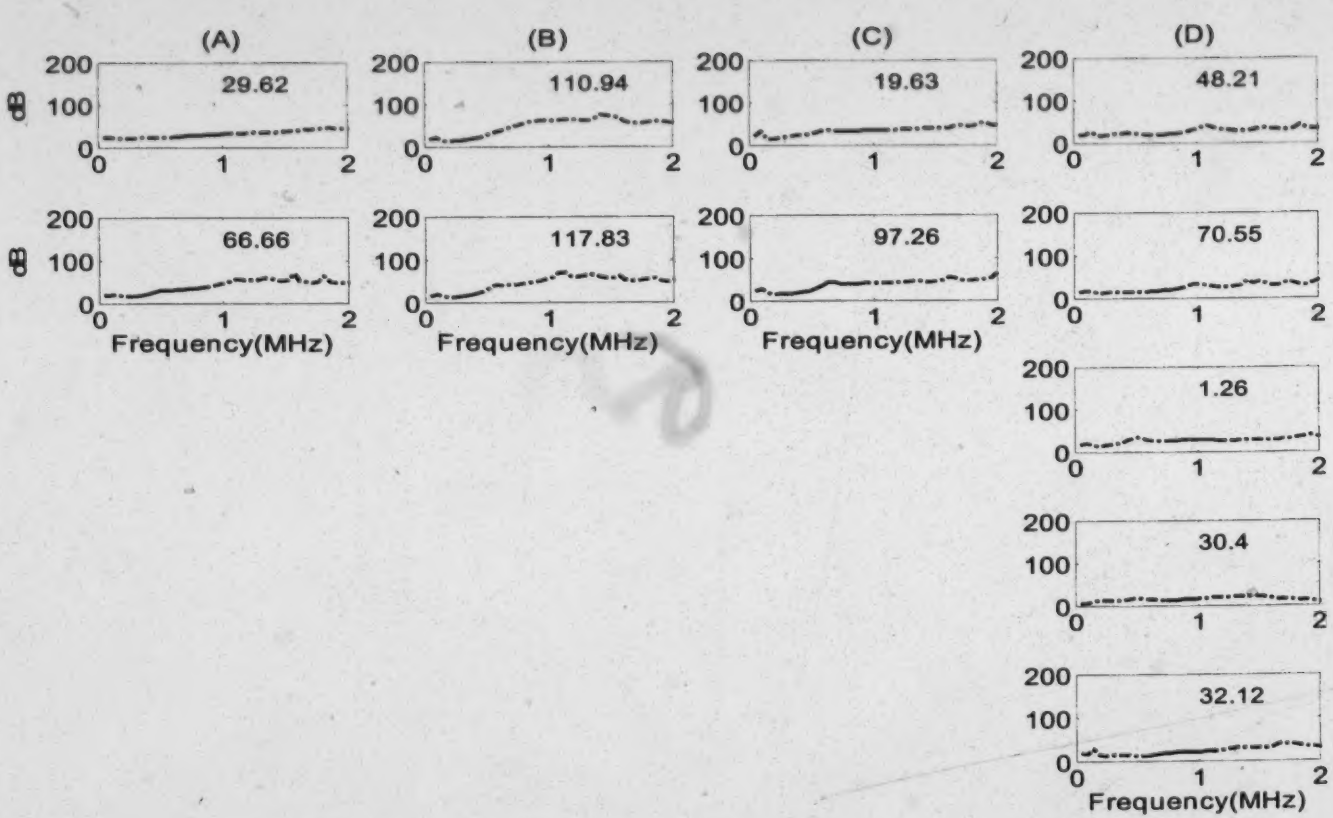

Figure 4.10 The BUA of bovine bone sample signals of different thickness in axial direction: (A) 2.0 cm. (B) 1.5 cm. (C) 1.0 cm. (D) 0.5 cm.

Figure 4.10 display the energy loss of bovine bone sample signals in axial direction compared with water reference signal. Equation (4.17) $A(f) = 20\log(\frac{A_s(f)}{A_r(f)})$ is used in this procedure, where, $A_r(f)$ is the magnitude of corresponding frequency component reference signal, and $A_s(f)$ is the magnitude of corresponding frequency component in bone sample signal. Therefore, the calculated energy loss includes the transmission loss and absorption. As the bone sample thickness increase, the linear portion of attenuation curve shift to lower frequency but do not become so constantly steeper as in bone sample axial direction. The 20dB amplification difference has been corrected.

Figure 4.11 displays the transmission loss corrected energy loss of bovine bone sample signals in axial direction compared with water reference signal. The corrected energy loss is calculated using equation (4.23), with the second term in the right side representing transmission loss. Here we use only one bone sample to calculate the transmission loss and apply it to the whole group, hoping that interface of same kind of bone and same direction will produce same energy loss. Compared with figure 4.10, some slopes increase while others decrease, depending on the effective frequency range used to calculate the slope.

Generally speaking, in the above three groups of bone samples, the slope of attenuation increases with the bone sample thickness. The phenomenon can be explained in the following simple way. Suppose the amplitude of one high frequency component can be represented as a function of travel distance L in the following way $A_h \exp^{-\alpha_h L}$. Here α_h represents the absorption coefficient, A_h represents its initial amplitude.; the amplitude of one low frequency component can be represented as a function of travel distance L in the

following way $A_l \exp^{-\alpha_l L}$, here α_l represents absorption coefficient of this low frequency component, A_l represents its initial amplitude. The attenuation of these two frequency components can be represented as:

$$Atten_h = 20\log(\frac{A_h e^{-\alpha_h L}}{A_h}) = -20\alpha_h L \log e, \tag{4.24}$$

$$Atten_l = 20\log(\frac{A_l e^{-\alpha_l L}}{A_l}) = -20\alpha_l L \log e. \tag{4.25}$$

Since attenuation is the function of travel distance for fixed frequency, it is clear to see that the attenuation increase with travel distance L. At the same time, the attenuation slope is calculated by:

$$\begin{aligned} Atten_{slope} &= \frac{Atten_h - Atten_l}{freq_h - freq_l} = \frac{-20\alpha_h \log e \cdot L - (-20\alpha_l \log e \cdot L)}{freq_h - freq_l} \\ &= \frac{-20(\alpha_h - \alpha_l)\log e}{freq_h - freq_l} L \end{aligned}, \tag{4.26}$$

where, the negative sign indicate the decrease and the fraction is constant for certain frequencies. Since higher frequency has bigger absorption coefficient, value in the bracket is positive, the attenuation slope is a linear function of L and increases with the travel distance. This also shows that, for the same bone quality, that is, absorption coefficient is constant for same frequency, the slope should be constant, agreeing with the results of Serpe and Rho (1996), who got a rate of approximately 3.6 dB MHz^{-1} mm^{-1}. However, based on our experiment results, dependence of the attenuation on frequency is not strongly linear. This may be caused by the non-homogeneity in the bone sample and the uncertainty of the thickness.

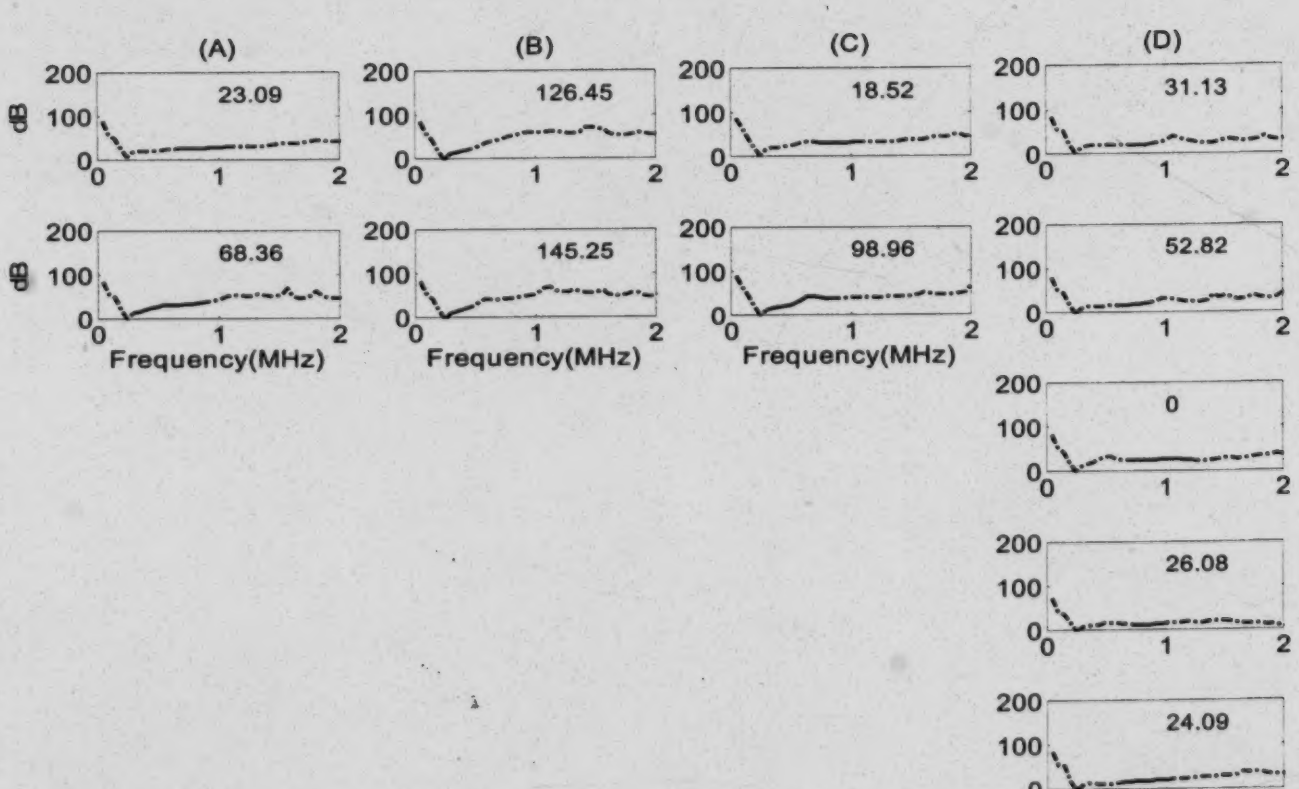

Figure 4.11 The BUA of bovine bone sample signals of different thickness` in axial direction (transmission loss corrected): (A) 2.0 cm. (B) 1.5 cm. (C) 1.0 cm. (D) 0.5 cm.

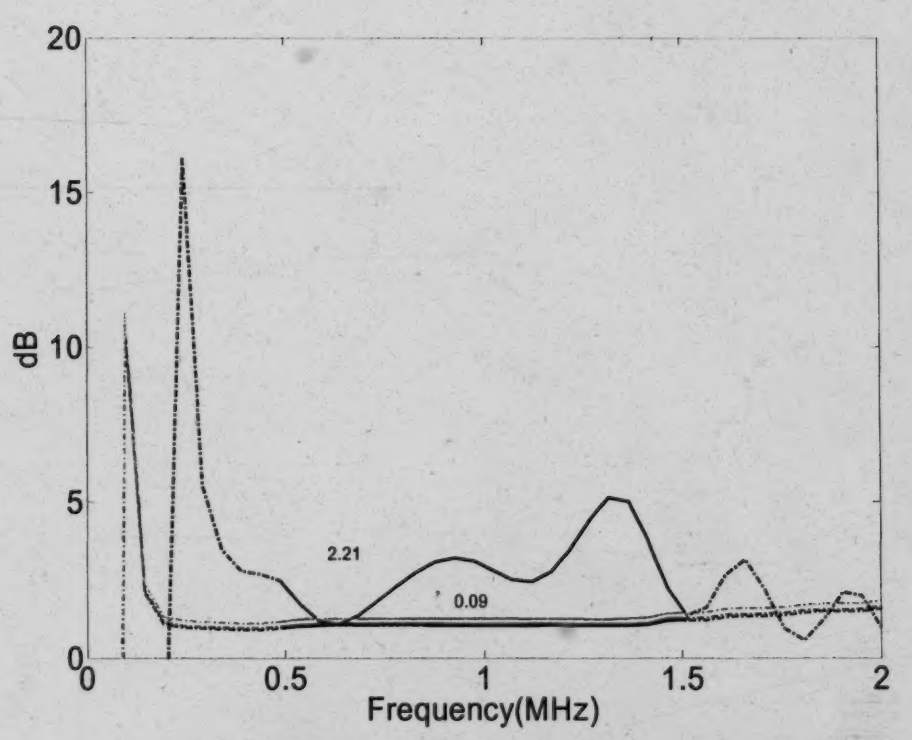

Figure 4.12 The transmission loss of one bovine bone sample in axial direction. The top one is obtained using the echo signal; the bottom lines are the results calculated from literature parameter, using equation (4.15).

Figure 4.12 displays the transmission loss of one bovine bone sample with thickness being 2.0 cm in axial direction. The result equation obtained using water pulse and reflected signal is compared with results calculated from acoustic impedances. Density of bone is calculated for volume fraction, 0.17, 0.19, 0.25, the velocity is the phase velocity in those bone samples, and then equation (4.15) is used to calculate the transmission loss. Since the densities of three different combinations are similar, the three results are almost same and nearly coincident in the figure. As shown in the figure, the results calculated from acoustic impedances are smaller than that calculated from echo in the effective frequency range, and may indicate that the bone volume fraction should be larger.

Figure 4.13 displays the energy loss of 4 phantom signals. This energy loss is not corrected by the transmission loss.

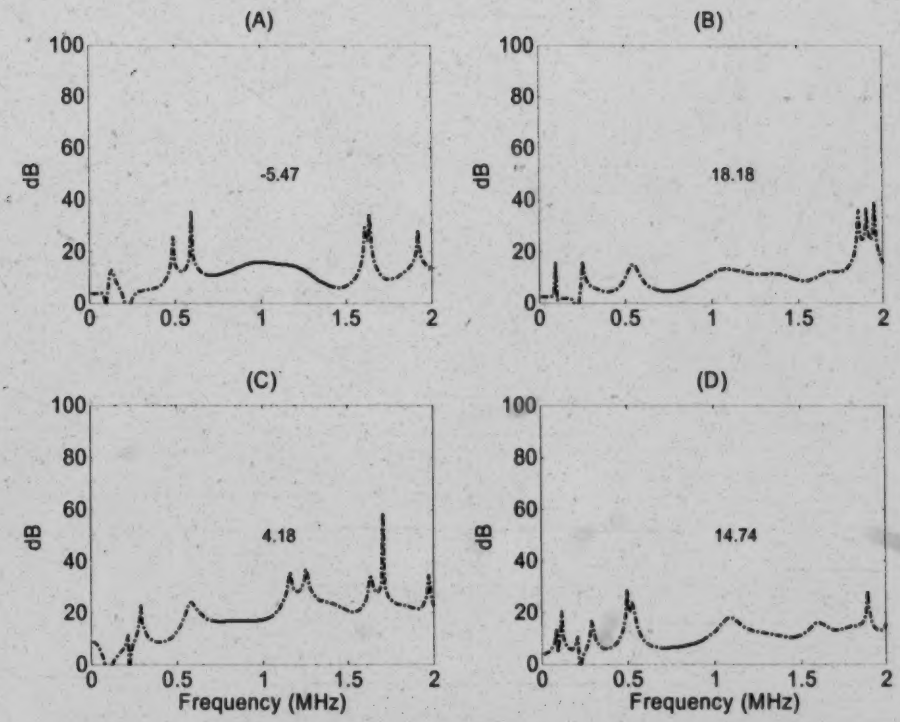

Figure 4.13 The BUA of phantom signal without transmission loss correction.

Chapter 5

Conclusions and Future Work

This thesis briefly introduced the bone structure and quality, followed by literature review of current research on bone characterization. However, the major part of this thesis is involved with the experiment and the data processing. The experiment is aimed to investigate the velocity and absorption of trabecular bone and phantom data. The bones were bovine and pig bone.

The trabecular bone consists of 3 dimensional network of trabeculae, but there is also some cartilage occasionally appearing inside the trabeculae. The existence of those cartilages will make the estimation of phase velocity and absorption biased from the actual results. The reason for this is that, the cartilage will redirect the energy and also cause the transmission loss, thus resulting in more severe attenuation. As for the phase velocity, the error is mainly caused by the waveform distortion due to the reflection in the cartilage surface, and is also related to the method we used to calculate the phase velocity.

As we can see in chapter 3, the equation of calculating the phase velocity is essentially based on the phase difference between water reference signal and bone sample signal. However, the phase difference is not only depending on the traveling time but also depending on the waveform, if the waveform is changed in a way other than due to different phase velocity, thus calculated phase difference is not correct, therefore, the final phase velocity is not accurate. Absorption will cause this kind of unexpected waveform distortion. In my opinion, however, pure absorption, here I mean the amplitude decrease of each frequency component, alone will not cause error in phase difference. If there is reflection

from cartilage surface, dramatic waveform distortion will occur, and it is this distortion that will cause the maximum error in phase velocity.

The velocity varies slightly with the thickness, with the uncertainty increasing with the decrease of the thickness. The reason for this trend is that when the thickness is smaller, the uncertainty of the thickness is increased by the error propagation law. On the other hand, the attenuation increases obviously with the thickness, the reason for this is easy to understand. Meanwhile, the slope of attenuation also increases with the bone sample thickness. However, based on our experiment results, dependence of the attenuation on frequency is not strongly linear.

Two methods were used to calcuate the transmission loss. One is based on power spectrum estimation of reflected signal and water reference signal. Another is based on acoustic impedances of water and cancellous bone. The transmission loss results using two methods are comparable for the bovine bone.

In future work, skeleton in particular portion, such as calcaneus, vertebra worth tested and to see whether they contain cartilage or not. Since tone burst or broadband ultrasound pulse is easily affected by the scattering or reflection, first cycle or half cycle of the broadband pulse, can be considered as the investigating tool. The advantage of this portion is that it is not so likely be affected by scatter or reflection.

Reference

Accardo, A., Candido, G., Jellúˇs, V. Toffanin, R, Vittur, F., *Ex vivo assessment of trabecular bone structure from three-dimensional projection reconstruction MR micro-Images*. IEEE transactions on biomedical engineering, Vol. 50, No. 8, pp. 967-977, Aug. 2003.

Ashman R. B., Cowin S C, van Buskirk, W C and Rice J C, *A continuous wave technique for the measurement of the elastic properties of cortical bone*, *J. Biomech.* **17**, pp. 349–61, 1984.

Bendat, Julius S. Piersol, Allan G., *Random data: Analysis and measurement procedures*, John Wiley & Sons, Inc, 1971.

Clark, A.J., Evans, J. A., Truscott, J. G., Milner, R., Smith, M. A., *A phantom for quantitative ultrasound of trabecular bone*, phys. Med. Biol., Vol. 39, pp. 1677-1687 1994.

Christiansen, C., *Consensus Development Conference: Diagnosis, Prophylaxis, and Treatment of Osteoporosis*, the American Journal of Medicine, Volume 94 pp. 646-650, Jun. 1993.

Droin, P., Berger, G. and Laugier, P., *Velocity dispersion of acoustic waves in cancellous bone*, IEEE Trans. Ultrason., Ferroelect., Freq. Contr., Vol. 45, pp. 581-592, May 1998.

Fitting, Dale W., Adler, L., *Ultrasonic spectral analysis for nondestructive evaluation*, Plenum press, New York and Londaon,pp.47, 1981.

Feldkamp, L. A., Goldstein, S. A., Parfitt, A. M., Jesion, G., Kleerekoper, M., *The direct examination of three-dimensional bone architecture in vitro by computed tomography*. J Bone Miner Res. Vol. 4 (1), pp:3-11,1989.

Follet, H., Bruye`re-Garnier, K., Peyrin, F., Roux, J. P., Arlot, M. E., Burt-Pichat, B., Rumelhart, C., Meunier, P. J., *Relationship between compressive properties of human os calcis cancellous bone and microarchitecture assessed from 2D and 3D synchrotron microtomography*. Bone, Vol. 36 pp. 340– 351, 2005.

Genant, H., *Evaluation of technical factors affecting the quantification of trabecular bone structure using magnetic resonance imaging, Bone*, Vol. 17, Issue 4, pp. 417-430, Oct.1995.

Gold, D. T., *The Clinical Impact of Vertebral Fractures: Quality of Life in Women With Osteoporosis*, Bone Vol. 18, No. 3, pp. 185-189, Supplement. Mar. 1996.

Grodzins, L., *Optimum energies for x-ray transmission tomography of small samples :Applications of synchrotron radiation to computerized tomography*. Nuclear Instruments and Methods, Vol. 206, pp: 541-545,1983.

Hahn, M., Vogel, M., Ritzel, H., and Delling, G., *The significant of histology in relation to non-invasive techniques in the evaluation of bone tissue*, Bone research in Biomechanics, G. Lowet ta al. (Eds.), IOS Press, 1997.

Hans, D., Wu, C., Njeh, C.F., Zhao, S., Augat, P., Newitt, D., Link, T., Lu, Y., Majumdar, S., Genant, H. K., *Ultrasound velocity of trabecular cubes reflects mainly bone density and elasticity*. Calcif. Tissue Int. Vol. 64, pp.18-23, 1999.

Herzfeld, Karl F., Litovitz, Theodore A., *Absorption and dispersion of ultrasonic waves*. Academic press, New York and London, pp.39, 1959.

Hildebrand, T., Rüegsegger, P., *A new method for the model-independent assessment of thickness in three-dimensional images*, Journal of Microscopy, Vol. 185, pp. 67–75, 1996.

Hosokawa, A. and Otani, T.,*Ultrasonic wave propagation in bovine cancellous bone. J Acoust Soc Am* 101, pp. 558–562. 1997.

Hosokawa, A. and Otani, T. *Acoustic anisotropy in bovine cancellous bone. J Acoust Soc Am* 103, pp. 2718–2722. 1998.

Hughes, E. R., Leighton, T. G., Petley, G. W., White, P. P., *Ultrasonic propagation in cancellous bone: A new stratified model*, Ultrasound in Med. & Biol. Vol 25. No. 5. Pp.811-821, 1999.

Jeong, H. and Hsu, D. K., *Experimental analysis of porosity-induced ultrasonic attenuation and velocity change in carbon composites*, Ultrasonic, Vol. 33, No.3, 1995.

Ji, Q., *A physical model for broadband ultrasonic studies of cancellous bone*, Ph. D., thesis, University of Alberta, Apr. 1998.

Khan, K., Mckay, H, Kannus, P., Bailey, D., Wark, J., Bennell, K., *Physical activity and bone health. Human Kinetics*, 2001.

Kinney J. H., Stölken,J. S., Smith, T.S., Ryaby, J. T., Lane, N. E., *An orientation distribution function for trabecular bone*. Bone, Vol. 36, pp. 193–201, 2005.

Kothari, M., Keaveny, T. M., Lin, J. C., Newitt, D. C., Majumdar, S., *Measurement of Intraspecimen Variations in Vertebral Cancellous Bone Architecture*, Bone, Vol. 25, No. 2, pp. 245–250, Aug. 1999.

Krautkämer, Josef and Krautkämer, Herbert et. al, *Ultrasonic testing of materials*, spring – Verlag Berlin Heidelberg New York, 1983.

Lang, T. F., Keyak, J. H., Heitz, M. W., Augat, P., Lu, Y., Mathur, A., Genant, H. K., *Volumetric quantitative computed tomography of the proximal femur: Precision and relation to bone strength*, Bone, Vol. 21, Issue 1, pp. 101-108, July 1997.

Langton, C.M., Palmer, S.B., and Porter, R.W., *The measurement of broadband ultrasonic attenuation in cancellous bone*, Eng Med, vol. 13, no. 2, pp.89-91, 1984.

Le, L. H, *An investigation of pulse-timing techniques for broadband ultrasonic velocity determination in cancellous bone: a simulation study*, Phys. Med. Biol. 43 2295–2308, 1998.

Lee, K. I., Roh, H., Yoon, S. W., *Correlations between acoustic properties and bone density in bovine cancellous bone from 0.5 to 1 MHz*, J.Acoust. Soc. Am. Vo.113, No.5, pp.2933-2938, 2003.

Majumdar, S., Newitt, D., Jergas, M., Gies, A., Chiu, E., Osman, D., Keltner, J., Keyak, J., Majumdar, S., and Genant H. K., *Assessment of trabecular structure using high-resolution magnetic resonance imaging*. G. Lowet et al. (Eds.), IOS Press, 1997.

Majumdar,S., Kothari, M., Augat, P., Newitt, D. C., Link, T. M., Lin, J. C., Lang, T., Lu, Y., Genant, H. K., *High-Resolution Magnetic Resonance Imaging: Three-Dimensional Trabecular Bone Architecture and Biomechanical Properties*, Bone, Vol. 22, No. 5, pp. 445-454, May 1998.

Müller, R. and Rüegsegger P., *Micro-tomographic imaging for the nondestructive evaluation of trabecular bone architecture*, Bone research in Biomechanics, G. Lowet et al. (Eds.), IOS Press, 1997.

Nicholson, P. H. F., Haddaway, M. J., and Davie, M. J., *The dependence of ultrasonic properties on orientation in human vertebral bone*, phys. Med. Biol., Vol. 39, pp. 1013-1024. 1994.

Nicholson, P H F, Lowet G, Langton C M, Dequeke J R and der Perre G Van, *A comparison of time-domain and frequency-domain approaches to ultrasonic velocity measurement in trabecular bone* ,Phys. Med. Biol. 412421–2435, 1996.

Nicholson, P.H.F., and Bouxsein, M. L., *Bone marrow infuence quantitative ultrasound measurements in human cacellous bone*. Ultrasound in Med. & Biol., Vol. 28, No. 3, pp. 39-375, 2002.

Parfitt, A. M., Mathews, C. H., Villanueva, A. R., Kleerekoper, M., Frame,B. and Rao, D. S., *Relationships between surface, volume, and thickness of iliac trabecular bone in aging and in osteoporosis: Implications for the microanatomic and cellular mechanisms of bone loss*. J Clin. Invest, Vol. 72, No, 4, pp.1396–1409, Oct.1983.

Pierce, A. D., *Acoustics: An introduction to its physical principles and applications*. New York: McGraw-Hill, 1981.

Press, William H., Teukolsky, Saul A., Vetterling, William T., Flannery, Brian P., *Numerical Recipes in Fortran*, second edition, Cambridge university press, pp. 630. 1992.

P Pollintine, Haddaway, M. J. and Davie, M. W. J., *The use of tonebursts as an alternative to broadband signals in the measurement of speed of sound in human cancellous bone*, Phys. Med. Biol. 45, pp. 1941–1951, 2000.

Rabiner, Lawrence R., Gold Bernard, *Theory and application of digital signal processing*. Bell telephone laboratories, Inc. and Lincoln Laboratory, pp: 410, 1975.

Ray, N. F., Chan, J. K., Thamer, M. and Melton, L. J., *Medical Expenditures for the Treatment of Osteoporotic Fractures in the United States in 1995: Report from the National Osteoporosis Foundation*. Journal of Bone and Mineral Research, Vol. 12, No.1, pp: 24-30, January 1997.

Roberts, Richard A., Mull Clifford T., *Digital signal processing*, Addison-Wesley publishing company, 1987.

Sachse Wolfgang and Pao, Yih-Hsing, *On the determination of phase and group velocities of dispersive waves in solids*. J. Appl. Phys, Vol. 49, pp. 4320, 1978.

Salomé, M., Peyrin, F., Cloetens, P, Odet, C., Laval-Jeantet, A., Baruchel, J., Spanne, p., *A synchrotron radiation microtomography system for the analysis of trabecular bone samples*, Med. Phys, Vol. 26, No. 10, pp.2194–204, 1999.

Serpe, Louie J. Rho, Jae-Y., *Broadband ultrasound attenuation value dependence on bone width in vitr.,* Phys. Med. Biol, Vol. 41, pp. 197–202, 1996.

Sievänen, H., Kannus, P., Nieminen, V., Heinonen, A., Oja, P., Vuori, I., *Estimation of various mechanical characteristics of human bones during dual energy x-ray absorptiometry: methodology and precision*, Bone, Vol. 18, No. 1, pp.17-27, Supplement Jan. 1996.

Stenstroöm, M, Olander, B., Lehto-Axtelius, D., Madsen, J. E., Nordsletten, L., Carlsson, G. A., *Bone mineral density and bone structure parameters as predictors of bone strength: an analysis using computerized microtomography and gastrectomy-induced osteopenia in the rat*, Journal of Biomechanics, Vol. 33, pp. 289-297, 2000.

Strelitzki, R, Evans, J.A. *On the measurement of the velocity of ultrasound in the os calcis using short pulses,* European Journal of Ultrasound 4, pp. 205-213, 1996.

Strelitzki, R. Clarke, A J and Evans, J A. *The measurement of the velocity of ultrasound in fixed trabecular bone using broadband pulses and single-frequency tone bursts*, Phys. Med. Biol. 41, pp. 743–753, 1996.

Tavakoli, M. B., Evans, J. A., T*he effect of bone structure on ultrasonic attenuation and velocity*, Ultrasonics, Vol. 30, No. 6, pp. 389-395. 1992.

Tenenhouse, A., Joseph, L., Kreiger, N., Poliquin, S., Murray, T. M., Blondeau, L., Berger, D., Hanley, D. A., Prior, J. C., and the CaMos Research Group, *Estimation of the prevalence of low bone density in Canadian women and men using population-specific DXA reference standard: the Canadian multicentre osteoporosis study (CaMos)*, Osteoporosis Int., Vol. 11, pp. 897-904, 2000.

Toffanina, R., Jellúš, V., Szomolányi, P., Vittur, F., *Short-TE projection reconstruction NMR microscopy of trabecular bone*, Magnetic Resonance Imaging, Vol. 19, pp. 485–486, 2001.

Tortora, G. J., Grabowski, S. R., *Principles of anatomy and physiology*, Harper Collins College Publishers, seventh edition, 1993.

Töyräs, J., Kröger, H., Jurvelin, J. S., *Bone properties as estimated by mineral density, ultrasound attenuation, and velocity*. Bone, Vol. 25, No.6, pp. 725-731, 1999.

Uchiyama, T., TanizawA, T. Muramatsu, H., Endo, N., Takahashi, H. E., Hara, T., *Three-Dimensional Microstructural Analysis of Human Trabecular Bone in Relation to Its Mechanical Properties*, Bone, Vol. 25, No. 4, pp. 487–491 Oct.1999.

Van Rietbergen, B., Majumdar, S., Newitt, D., MacDonal, B., *High-resolution MRI and micro-FE for the evaluation of changes in bone mechanical properties during longitudinal clinical trials:application to calcaneal bone in postmenopausal women afterone year of idoxifene treatment*, Clinical Biomechanics, Vol. 17, pp. 81–88, 2002.

Wear, K. A., *A stratified model to predict dispersion in trabecular bone*, IEEE transaction on ultrasonics, ferrlelectrics, and frequency control, vol. 48, No. 4, July 2001.

Wu, C. Y., Gluer, C. C., Jergas, M., Bendavid, E., Genant, H. K., *The impact of bone size on broadband ultrasound attenuation. Bone*, vol.16, No. 1, pp.137-141, 1995.

Appendix A

Cross Correlation Function and Cross Spectrum

The cross-correlation function between two zero-mean signals $x(t)$ and $y(t)$ is

$$R_{xy}(\tau) = \int_{-\infty}^{\infty} x(t)y(t+\tau)dt \tag{A.1}$$

and its Fourier Transform is

$$\Phi_{xy}(\omega) = \int_{-\infty}^{\infty} R_{xy}(\tau)e^{-j2\pi f\tau}d\tau\,. \tag{A.2}$$

Substituting (A.2) into (A.1) yields

$$\Phi_{xy}(\omega) = \int_{-\infty}^{\infty}\int_{-\infty}^{\infty} x(t)y(t+\tau)dt\; e^{-j2\pi f\tau}d\tau \tag{A.3}$$

or

$$\begin{aligned}\Phi_{xy}(\omega) &= \int_{-\infty}^{\infty}\int_{-\infty}^{\infty} x(t)y(t+\tau)\; e^{-j2\pi f\tau}d\tau dt \\ &= \int_{-\infty}^{\infty}\int_{-\infty}^{\infty} x(t)y(t+\tau)\; e^{j2\pi ft}e^{-j2\pi f(\tau+t)}d\tau dt\,. \\ &= \int_{-\infty}^{\infty}\int_{-\infty}^{\infty} y(t+\tau)\; e^{-j2\pi f(\tau+t)}d\tau\; x(t)e^{j2\pi ft}dt\end{aligned} \tag{A.4}$$

The inner integral is

$$\int_{-\infty}^{\infty} y(t+\tau)e^{-j2\pi f(\tau+t)}d(\tau) = \int_{-\infty}^{\infty} y(t+\tau)e^{-j2\pi f(\tau+t)}d(t+\tau) = Y(\omega) \quad \text{(A.5)}$$

Using (A.4), (A.5) becomes

$$\begin{aligned}\Phi_{xy}(\omega) &= \int_{-\infty}^{\infty} Y(\omega)\, x(t)e^{j2\pi ft}dt \\ &= Y(\omega)\int_{-\infty}^{\infty} x(t)e^{j2\pi ft}dt \\ &= Y(\omega)X^{*}(\omega)\end{aligned} \quad \text{(A.6)}$$

where $X^{*}(\omega)$ is the complex conjugate of $X(\omega)$. Writing (A-6) in terms of amplitude and phase, we have

$$X(\omega) = |X(\omega)|e^{i\theta x(\omega)} \quad \text{(A-7)}$$

and

$$X^{*}(\omega) = |X(\omega)|e^{-i\theta x(\omega)}. \quad \text{(A.8)}$$

Similarly, the $Y(\omega)$ can be expressed as

$$Y(\omega) = |Y(\omega)|e^{i\theta y(\omega)}. \quad \text{(A.9)}$$

Thus equation (A.6) can be written in the following form:

$$\begin{aligned}\Phi_{xy}(\omega) &= Y(\omega)X^{*}(\omega) \\ &= |Y(\omega)|e^{i\theta_y(\omega)}|X(\omega)|e^{-i\theta x(\omega)} \\ &= |Y(\omega)|\cdot|X(\omega)|e^{i[\theta_y(\omega)-\theta x(\omega)]}\end{aligned} \quad \text{(A.10)}$$

where

$$\theta_x = \arctan\{\frac{\mathrm{Im}[X(\omega)]}{\mathrm{Re}[X(\omega)]}\} \ , \tag{A.11}$$

$$\theta_y = \arctan\{\frac{\mathrm{Im}[Y(\omega)]}{\mathrm{Re}[Y(\omega)]}\} \ . \tag{A.12}$$

and *Im*() and *Re*() are the imaginary and real parts of a complex argument.

Appendix B

Zero Padding and Frequency Sampling

Zero padding is used frequently to improve frequency sampling. Consider a time series of N data points sampled at interval of Δt, the maximum frequency is given by:

$$f_{\max} = \frac{1}{2\Delta t} \tag{B.1}$$

with a frequency sampling:

$$\Delta f = \frac{f_{\max}}{N/2} = \frac{1/2\Delta t}{N/2} = \frac{1}{N\Delta t} \quad . \tag{B.2}$$

If the length of the time series is made longer to a total length of M data point by padding M-N zeros at the end of series, the frequency sampling will be improved by having a smaller Δf:

$$\Delta f = \frac{1}{M\Delta t} < \frac{1}{N\Delta t} \quad . \tag{B.3}$$

Appendix C

Measurement of Speed of Sound in Water

When calculating the phase or group velocity of ultrasound in bone samples, speed of sound in water V_w is needed as given by (3.7) and its accuracy will affect results for all bone samples. The accuracy of V_w is important as it will affect the calculated phase velocity of bone samples. V_w can be simply determined by:

$$V_w = \frac{L}{t} \tag{C.1}$$

where L is the distance ultrasound travels in water, and t is the time it takes in our experiments to travel such a distance.

However, SOS calculated using (C.1) in our experiments was around 1450 m/s in room temperature instead of the accepted velocity of 1490 m/s (Pierce, 1981; Wear, 2001). The distance L between those two transducers can be measured quite accurately with caliper and is subject to an error of no more than 1 mm, which does not account for the discrepancy. As for the time measurement, since water is a non-absorptive or perhaps slightly dispersive medium, the first detectable deviation from zero is taken as the arrival time t, which can be as accurate as to 0.01 μsec in our measurement. However, if there is a systematic delay Δt introduced by the acquisition system in timing departure of ultrasound off the transmitter surface and recording of the signal by another transducer, the arrival time t should be corrected by a subtraction of Δt. Thus (C.1) can be modified by

$$V_w = \frac{L}{t - \Delta t} > \frac{L}{t}. \tag{C.2}$$

The modified equation also explains why the ultrasound velocity using the simple equation (C.1) is always smaller than the accepted value. However, Δt is unknown in (C.2). To overcome this, we made two measurements, t_1 and t_2, for two distances L_1 and L_2. Then

$$V_w = \frac{L_1}{t_1 - \Delta t} = \frac{L_2}{t_2 - \Delta t}. \tag{C.3}$$

Since

$$\frac{L_1}{t_1 - \Delta t} = \frac{L_2}{t_2 - \Delta t},$$

$$\frac{L_2}{L_1} = \frac{t_2 - \Delta t}{t_1 - \Delta t},$$

$$\frac{L_2 - L_1}{L_1} = \frac{t_2 - t_1}{t_1 - \Delta t}$$

or

$$\frac{L_1}{t_1 - \Delta t} = \frac{L_2 - L_1}{t_2 - t_1}, \tag{C.4}$$

(C.3) becomes

$$V_w = \frac{L_2 - L_1}{t_2 - t_1}. \tag{C.5}$$

Using this procedure, we obtained a value of 1491m/s, which is quite close to the accepted value.

Appendix D

Phase Correction to Unwrapped Phase Difference

The speed of sound in bone sample is calculated by the substitution equation:

$$v_s(\omega) = \frac{\omega d}{-\Delta\phi(\omega) + \frac{\omega d}{V_w}}, \tag{D.1}$$

where $\Delta\phi(\omega)$ is the phase difference between the two signals. In our case, the two signals are the reference water pulse and the pulse through the sample. Phase difference can be calculated by equations (3.6), (3.7) or (3.10).

The phase difference must be unwrapped by adding or subtracting $2n\pi$ to any discontinuity bigger than π. After unwrapping procedure, let $\phi_0(\omega)$ be the phase of the source signals at time $t = 0$ The phase is frequency dependent as it is different for different frequency component, ω. For $t \neq 0$, the phase is $\phi_0(\omega) + \omega \cdot t$. For water pulse, the phase is $\phi_0(\omega) + \omega \cdot t_w$, where $t_w = d / V_w$ is the arrival time of the pulse, d is the distance traveled and V_w is the SOS of the water, which is constant. For signal through sample, the phase is $\phi_0(\omega) + \omega \cdot t_s$, where $t_s = d / V_s(\omega)$ is the arrival time of the frequency component, ω and $V_s(\omega)$ is the phase velocity of the corresponding frequency, ω. The phase difference between these two signals is:

$$\begin{aligned} \Delta\phi(\omega) &= [\phi_0(\omega) + \omega \cdot t_w] - [\phi_0(\omega) + \omega \cdot t_s] \\ &= [t_w - t_s] \cdot \omega \\ &= [\frac{d}{V_s(\omega)} - \frac{d}{V_w}] \cdot \omega \end{aligned} \tag{D.2}$$

Since phase velocity in bone sample doesn't change significantly, equation (D.2) can be approximated by:

$$\Delta\phi(\omega)=\left[\frac{d}{V_s(\omega)}-\frac{d}{V_w}\right]\cdot\omega\approx a\cdot\omega, \tag{D.3}$$

where a is a constant. Equation (D.3) shows a linear relationship of phase difference with frequency, indicating $\Delta\phi(\omega=0)=0$.

In the case of using broadband ultrasound to study bone, most of the energy is confined with a band of frequencies and outside the band there is no significant energy. The signal-to-noise ratio (SNR) is very poor and the phase difference calculated by equation (D.2) might not show linearity. Since the phase-unwrapping starts at the low frequency, the misfit thus will be carried to the effective frequency range.

To correct this misfit, we focus on the effective frequency range where SNR is high and show a linear character. The effective frequency range can be found by investigating the power spectrum of the signal through bone samples. The phase difference within this range will be fitted by a straight line in least square sense. Suppose the intercept of the least square fit is $2n\pi+\phi_0$, where n is an integer, ϕ_0 is usually a small number. We can simply shift $2n\pi$ to force the straight line passing through the origin. Thus, the corrected phase difference $\Delta\phi_c(\omega)$ is

$$\Delta\phi_c(\omega)=\Delta\phi(\omega)-2n\pi. \tag{D.4}$$